



HAL
open science

Experimental and theoretical studies of the $np\ ^1\ ^1\ u +$ and $np\ ^1\ ^1\ u + (n\ ^4, N' = 1\ ^6)$ states of D2: Energies, natural widths, absorption line intensities, and dynamics

M. Glass-Maujean, Ch. Jungen, A. Vasserot, H. Schmoranzer, A. Knie, S. Kübler, A. Ehresmann, W. Ubachs

► To cite this version:

M. Glass-Maujean, Ch. Jungen, A. Vasserot, H. Schmoranzer, A. Knie, et al.. Experimental and theoretical studies of the $np\ ^1\ ^1\ u +$ and $np\ ^1\ ^1\ u + (n\ ^4, N' = 1\ ^6)$ states of D2: Energies, natural widths, absorption line intensities, and dynamics. *Journal of Molecular Spectroscopy*, 2017, 338, pp.22 - 71. 10.1016/j.jms.2017.05.011 . hal-01537881

HAL Id: hal-01537881

<https://hal.sorbonne-universite.fr/hal-01537881>

Submitted on 13 Jun 2017

HAL is a multi-disciplinary open access archive for the deposit and dissemination of scientific research documents, whether they are published or not. The documents may come from teaching and research institutions in France or abroad, or from public or private research centers.

L'archive ouverte pluridisciplinaire **HAL**, est destinée au dépôt et à la diffusion de documents scientifiques de niveau recherche, publiés ou non, émanant des établissements d'enseignement et de recherche français ou étrangers, des laboratoires publics ou privés.

Experimental and theoretical studies of the $np\sigma^1\Sigma_u^+$ and $np\pi^1\Pi_u^+$ ($n \geq 4$, $N' = 1 - 6$) states of D_2 : energies, natural widths, absorption line intensities, and dynamics

M. Glass-Maujean^{a,*}, Ch. Jungen^{b,c}, A. M. Vasserot^a,
H. Schmoranzner^d, A. Knie^e, S. Kübler^e, A. Ehresmann^e, W. Ubachs^f

^aLaboratoire d'Etudes du Rayonnement et de la Matière en Astrophysique et Atmosphères, UMR-8112, Sorbonne Universités, UPMC Université Paris 06, 4 pl Jussieu F-75005, Paris, France

^bLaboratoire Aimé Cotton du CNRS, Bâtiment 505, Université de Paris-Sud, F-91405 Orsay, France

^cDepartment of Physics and Astronomy, University College London, London WC1E 6BT, United Kingdom

^dFachbereich Physik, Technische Universität Kaiserslautern, D-67653 Kaiserslautern, Germany

^eInstitute of Physics and CINSaT, Heinrich-Plett-Str. 40, Universität Kassel, D-34132 Kassel, Germany

^fDepartment of Physics and Astronomy, Vrije Universiteit, De Boelelaan 1081, 1081 HV Amsterdam, The Netherlands

Abstract

Over a thousand spectral lines in the photoexcitation spectrum of molecular deuterium (D_2) to $np^1\Sigma_u^+$ and $1\Pi_u^+$ Rydberg levels ($n \geq 4$) were measured for rotational levels $N' = 1 - 6$ in the $117\,000 - 137\,000\text{ cm}^{-1}$ spectral range by two different types of experiments at two synchrotron radiation sources: a vacuum ultraviolet (VUV) Fourier-transform (FT) spectrometer at SOLEIL, Paris and a 10m-normal-incidence monochromator (NIM) at BESSY II, Berlin. The experimental energies, the absorption cross sections, Einstein A -coefficients, and line widths are compared with *ab initio* multi-channel quantum defect (MQDT) calculations for these levels. More than 350 R(0) or P(2) lines were assigned, some 280 R(1) or P(3) lines, some 270 R(2) or P(4) lines, over 100 R(3) or P(5) lines, over 90 R(4) lines, and 24 R(5) lines to extract information on the $N' = 1 - 6$ excited levels. Transition energies were determined up to excitation energies of $137\,000\text{ cm}^{-1}$ above the ground state, thereby extending earlier work by various authors and considerably improving the spectral accuracy ($< 0.1\text{ cm}^{-1}$), leading to several reassignments. The absorption and the dissociation, ionization and fluorescence excitation cross sections from the NIM experiment are measured on absolute scale and are used to calibrate intensities in the VUV-FT spectra. The overall agreement between experiment and first principles calculations, without adjustable parameters, is excellent in view of the multi-state interferences treated within the MQDT-framework: For the low N' values the averaged deviations between those observed in the FT-SOLEIL spectra and those calculated with MQDT are $\sim 0.1\text{ cm}^{-1}$ with a spread of $\sim 0.5\text{ cm}^{-1}$. The line intensities in terms of Einstein coefficients are well represented in the MQDT-framework, as are the level widths representing the lifetimes associated with the sum of the three decay channels. These line intensities follow, in general, the $1/n^3$ scaling behavior as characteristic in Rydberg series, but deviations occur and those are explained by MQDT. The decay dynamics of the excited N Rydberg levels is analyzed on the basis of the measured quantum yields for ionization, dissociation and fluorescence observed in the NIM experiment in terms of absolute cross sections for the distinctive channels. In particular in the $n = 4$ manifolds dissociation is found to play a major role, where in the $n = 5$ manifolds the behavior is most erratic due to strong competition between decay channels. At $n = 6$, ionization takes over as the dominant channel. Despite the excellent agreement between observations and the outcome of the MQDT calculations for both level energies and dynamics, some pronounced deviations are found as in the splitting of the $5p\pi, v = 4 - 6, N' = 1$ levels. The shortcomings of the MQDT calculations are ascribed to the treatment of the excited states in terms of a $1snp$ single electron configuration, therewith neglecting possible interferences with $1snf$ or $2s$ core excited states. Some 27 lines remained unassigned; in view of their observation in fluorescence it is stipulated that these lines probe levels in the nf manifold.

Preprint submitted to Journal of Molecular Spectroscopy

May 15, 2017

Keywords: Molecular deuterium, Synchrotron radiation, Vacuum ultraviolet Fourier-transform spectroscopy, Normal incidence monochromator, Absolute absorption cross sections, Line widths, Autoionization, Dissociation, Fluorescence, Multi-channel quantum defect theory

1. Introduction

The dipole-allowed electronic absorption spectrum of molecular hydrogen and its isotopomers covers the vacuum ultraviolet wavelength range, with an onset at 115 nm and ranging to 70 nm. This strong absorption spectrum of the smallest neutral molecule has been investigated in many studies over the past century, starting with the pivotal work of Lyman [1] and Werner [2], after whom the lowest lying excitations to the $2p\sigma$ and $2p\pi$ states were named. Broader overview studies of the hydrogen molecule extending into the dissociation, ionization and ion-pair continuum were performed by Herzberg and Jungen [3], by Chupka and coworkers [4, 5], and by Guyon and coworkers [6, 7, 8]. Early studies on the Lyman and Werner bands, specifically focusing on the deuterium (D_2) isotopomer, and using classical grating-based spectroscopic techniques, were performed by Herzberg and co-workers [9, 10]. Later, laser-based studies of these lowest lying D_2 absorption bands were performed using tunable laser sources in the vacuum ultraviolet [11, 12]. A review of the spectroscopy of D_2 by Freund et al. [13] provides an overview of the results from classical spectroscopy, but it lacks the information of laser-based work and the synchrotron studies.

In recent years the availability of powerful synchrotron-based vacuum ultraviolet sources has made it possible to investigate the absorption and excitation spectra of molecular hydrogen and its isotopomers in much detail, while covering the entire wavelength range of the dipole-allowed spectrum. Such studies have been reported using the versatile BESSY II setup for the spectroscopy and decay dynamics of H_2 [14, 15, 16, 17, 18, 19, 20, 21, 22, 23, 24, 25] and some investigations on D_2 [26, 27], while the SOLEIL setup was used for high-resolution absorption spectroscopic studies for H_2 [28], for HD [29, 30], and for D_2 [31, 32, 33].

The present study provides an exhaustive overview study on the dipole allowed spectrum of D_2 , excit-

ing the $np\sigma^1\Sigma_u^+$ and $np\pi^1\Pi_u^+$ Rydberg series. The spectra cover energy space between the second dissociation threshold $D(n=2)+D(n=1)$ at $119\,029\text{ cm}^{-1}$ and the third dissociation threshold $D(n=3)+D(n=1)$ at $134\,266\text{ cm}^{-1}$, with the ionization threshold lying in between at $124\,745\text{ cm}^{-1}$. The experiments combine the advantageous features of both synchrotron-based instruments: high resolution and versatility for investigating decay dynamics. Some of the information, concerning the $np\pi^1\Pi_u^-$ states [34, 26] and the $np\sigma^1\Sigma_u^+, N'=0$ levels of D_2 [27, 33] were published before. Those sets of levels are subject to $\Pi-\Pi$ or $\Sigma-\Sigma$ vibronic interaction but not to rotational coupling. In contrast, the $N' \geq 1$ levels in $np^1\Sigma_u^+$ and Π_u^+ series, investigated here, are subject to rotational coupling and to vibronic coupling as well.

This study concerns the $N' = 1 - 6$ levels of both Rydberg series $np\pi$ and $np\sigma$. More than a thousand spectral lines, experimentally observed by both or by either one of the instruments, are reported in the form of extensive Tables including accurate line positions, widths, intensities, and decay rates for fluorescence, dissociation and ionization. Parts of the absorption spectrum had been assigned in an earlier study of Takezawa and Tanaka [35], while a decade before an investigation was reported by Monfils [36]. A comparison is made between the present results and those observed previously, and in particular the reassignments from a comparison with Ref. [35] will be listed.

As was recognized by Herzberg [37] the spectrum of molecular hydrogen does not exhibit the characteristic features of a molecular band spectrum, introducing a complexity which makes the line identification in terms of R, Q and P branches and rotational quantum numbers more difficult than for heavier molecular species. The rotational and vibrational energy splittings are so large that various bands of electronic absorption systems become mutually intertwined, such that inspection of the spectrum does not reveal recognizable patterns of quantum states in a band. It is a 'many-line' spectrum instead of a band spectrum. Moreover, due to the low mass of the hydrogen atoms, deviations from the Born-Oppenheimer approximation, leading to non-

*Corresponding author
 Email address: michele.glass@upmc.fr (M. Glass-Maujean)

adiabatic interactions, become most prominent in the hydrogen molecule. For these reasons, line assignments in the spectra of H₂, HD and D₂ are difficult. All this holds, *a fortiori*, for the regions in the spectrum where intensity borrowing between interfering states prevails. This prohibits the observed intensities to be used as a guiding principle. As a consequence the assignment of spectral lines very much depends on the theoretical description of the spectrum, and the present work involves such a theoretical approach to assign the wealth of experimental data obtained.

For the lowest lying electronically excited states of molecular hydrogen computational methods have been developed, based on closed-coupling calculations taking into account non-adiabatic interactions comprising the set states of $2p\sigma^1\Sigma_u^+$ and $2p\pi^1\Pi_u$ symmetry. This has led to a very good approximation of the experimental spectrum of the Lyman and Werner bands in the H₂ molecule yielding agreement at the level of 0.15 cm⁻¹, although the methods used were not fully *ab initio* and some adaptation of the potential energy curves was invoked for matching the experimental data [38, 39]. Based on this framework the large sets of spectral lines in the atlases of the Lyman bands [40] and the Werner bands [41] could be assigned and reproduced.

For the case of D₂ these methods were applied to describe the electron-excited emission spectrum [42]. Similar closed-coupling calculations were applied to assign the emission spectra in discharges of deuterium originating from the $3p\pi D^1\Pi_u$ and $4p\pi D^1\Pi_u$ excited states [43] as well as the $3p\sigma B^1\Sigma_u^+$ state [44]. The most accurate and extensive experimental study of the D₂ dipole allowed absorption spectrum, probing states below its H(*n* = 2)+H(*n* = 1) dissociation limit, was performed with the vacuum-ultraviolet (VUV) Fourier-transform (FT) spectrometer at the SOLEIL synchrotron [32], which is more precise than an older extensive study performed via classical absorption based on a spectrograph of 10m length [10]. For a limited wavelength range, covering the $B^1\Sigma_u^+$ - $X^1\Sigma_g^+$ (*v'*, 0) bands for *v'* = 9 – 11 and the $C^1\Pi_u$ - $X^1\Sigma_g^+$ (0,0) bands, extreme ultraviolet laser-based excitation was combined with collimated molecular beams to record spectra of the highest resolution and

accuracy obtained for D₂ [12].

Whereas the coupled-equations calculations are reliable and precise for the lowest excited electronic states ($B^1\Sigma_u^+$, $C^1\Pi_u$ and $B^1\Sigma_u^+$), this is less true for higher ones [45]. A detailed comparison of the spectroscopic properties of D₂ and H₂ must necessarily involve the study of non-adiabatic coupling of the electronic and nuclear degrees of freedom, a type of coupling which is strongly dependent on the nuclear mass. Multichannel quantum defect theory (MQDT) is currently the only approach yielding an accurate description for the $np, n \geq 4$ levels in molecular hydrogen. Specific molecular MQDT methods were developed in connection to the analysis of molecular hydrogen spectra over the years [3, 46, 47, 48, 49]. The calculations are based on quantum-mechanical clamped-nuclei potential energy curves and dipole transition moments available for the lowest Rydberg members of the $np\sigma$ and $np\pi$ series, which are also fully *ab initio* [50, 51, 52]. An important aspect of MQDT is that it not only yields values for level energies, but that it is superior in providing the dynamics of the excited states, which may undergo radiative, dissociative and ionization decay at the same time. In such conditions MQDT provides a full description of competing decay processes [47, 19, 18].

The present investigation aims at applying this framework of MQDT for the analysis of experimentally observed absorption spectra of D₂ probing excited states of $np\sigma^1\Sigma_u^+$ and $np\pi^1\Pi_u^+$ symmetry forming Rydberg series converging to the first ionization limit of the molecule, and beyond into the autoionization continuum. The experimental spectrum of D₂ is investigated through a combined study with a Fourier-transform (FT) setup at SOLEIL and with a 10m-normal-incidence monochromator (NIM) experiment at BESSY II. Whereas the FT measurements are superior by the very high energy resolution, the NIM experiment enables absolute measurements of the line intensities and furthermore to determine the absolute cross sections of the various decay channels: fluorescence, dissociation and ionization. Observed level energies, autoionization widths and the absorption intensities of the lines are then compared with results from *ab initio* calculations in the MQDT framework.

The manuscript is organized as follows. In the proceeding sections some details of the experimental procedures are discussed (section 2) and a description of the multi-channel quantum defect (MQDT) theoretical model (in section 3) that was used to assign the spectra. Since the MQDT methods calculates all excited state levels of a common symmetry, hence for a single angular momentum N' , the data are presented in six different sections, each pertaining to this quantum number $N' = 1 - 6$. Thereafter the study ends with a discussion and conclusion (section 10), also including a comparison with previous work.

2. Experimental

The absorption spectrum of D_2 was recorded using the FT spectrometer installed on the DESIRS beamline at the SOLEIL synchrotron radiation source [53, 54]. The continuum background provided by the undulator corresponds to a bell-shaped curve of approximately 7000 cm^{-1} width. The spectrum extending from 117000 to 137000 cm^{-1} was therefore partitioned into four overlapping sections: in one of these ($E < 120000 \text{ cm}^{-1}$), a molecular jet expansion is used, in the three others a low pressure cell at low temperature. The FT spectrometer possesses its own internal calibration derived from the spatial step-size of the interferometer, which is controlled by a frequency stabilized He-Ne laser. Nevertheless small alignment errors may induce errors in the calibration that may vary from one recording to another. De Lange et al. [32] introduced calibration corrections for the different energy intervals under investigation, which account for the small deviations in the travel of the moving mirror. These corrections were extrapolated to higher energies. This procedure induces a residual error which increases from 0.02 to 0.035 cm^{-1} as the energy increases [34]. The noise level observed in the FT spectra contains a periodic component linked to the spectral resolution and the sinc apparatus function, which imprints an additional uncertainty on the positions of weak spectral lines. The total uncertainty of the line positions is estimated by taking the sum of the uncertainty of the calibration and three times the uncertainty of the Gaussian

fit for each line. For the weakest transitions an extra contribution is added, accounting for the effect of the periodic noise (see also [53, 34]). The resulting uncertainty of the frequency scale of the FT spectra corresponds to a few 0.01 cm^{-1} . The continuum background has been fitted by a Gaussian and the Beer-Lambert law was applied to obtain a signal proportional to the absorption cross section. A section of this quantity is plotted in Fig. 1(f). The main problems encountered in applying the Beer-Lambert law are: the zero of the signal is not precisely defined, and the medium is optically thick for the more intense lines.

The second experiment was performed on the 10m-normal-incidence monochromator (NIM) at BESSY II. The experimental setup has been described in detail in numerous publications (see in particular [55, 18, 14]). Briefly, the VUV photons coming from the undulator beamline U125/2-10m-NIM of BESSY II are dispersed by a 10 m-normal-incidence monochromator equipped with a 4800-lines/mm grating giving a spectral resolution of $1\text{-}2 \text{ cm}^{-1}$ (0.001 nm) in first order; this value represents the convolution of the apparatus function with the Doppler width at room temperature. The uncertainty of the scan linearity ($\approx 1 \text{ cm}^{-1}$) is the main source of error in the frequency measurement.

For the BESSY NIM spectra the absorption column densities in a differentially pumped windowless gas cell are well defined, with an absorption path length of 39 mm , gas pressures at typical values of 13.3 or 26.7 mbar , while the experiments were performed at room temperature. Thus they allow for a measurement of absolute absorption cross sections, and henceforth enable derivation of absolute intensities of spectral lines. Experimental Einstein coefficients A were extracted from the area of the lines obtained from the Gaussian fits using the relation:

$$\int \sigma d\omega = \frac{1}{8\pi\omega^2 c} A_{v',v''=0,N',N''} \frac{2N'+1}{2N''+1} n_{N''} \quad (1)$$

with $N' = N'' + 1$ for an R(N'') line and $N' = N'' - 1$ for a P(N'') line. Here σ is the measured absorption cross section which is integrated over the profile of a given line, ω is the incident photon energy (in cm^{-1}), and $n_{N''}$ is the fraction of molecules in the rotational

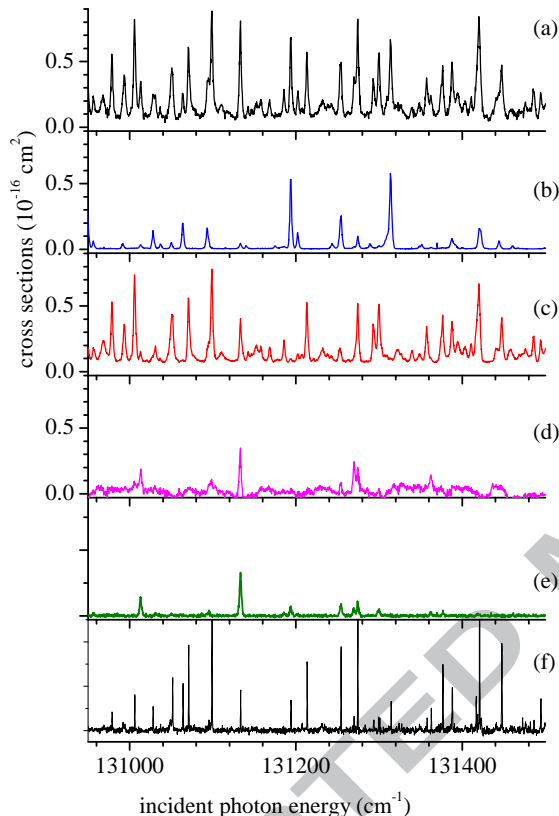


Figure 1: (Color online) A section of the D_2 absorption and photoexcitation spectra recorded at BESSY II for (a)-(e) and at SOLEIL for (f): (a) (black) absorption spectrum, σ_{abs} ; (b) (blue online) dissociation spectrum, σ_{diss} ; (c) (red online) ionization spectrum, σ_{ion} ; (d) (violet online) fluorescence signal determined indirectly via Eq. (2). (e) (green online) fluorescence spectrum from direct recording. (f) the D_2 absorption spectrum recorded with FT-VUV, showing the much higher resolution of that method. The vertical line guides the eyes along a single spectral line appearing with different intensities in the various excitation spectra.

state N'' of the vibrational ground state at 300 K : 0.18 for $N'' = 0$, 0.20 for $N'' = 1$, 0.38 for $N'' = 2$, 0.11 for $N'' = 3$, 0.10 for $N'' = 4$, 0.006 for $N'' = 5$, and 0.001 for $N'' = 6$.

The BESSY setup enables simultaneous recording of excitation spectra for photoionization, photodissociation and visible molecular fluorescence [18], which is graphically illustrated in Fig. 1. The Lyman- α fluorescence emitted from the $D(n = 2)$ fragments and visible fluorescence (380-700 nm) enables the detection of dissociation and molecular fluorescence respectively. A small dc-electric field is used to collect the photoions and to allow fluorescence from the $D(2s)$ atoms [56]. The photoionization and photodissociation spectra were intensity calibrated on the basis of absorption peaks that are known to be fully ionized or fully dissociated. In order to cross-check the various calibrations the absorption cross section was recalculated as the sum of the dissociation and ionization cross sections. The only lines for which the absorption cross section could not be reproduced correctly in this way are transitions leading to molecular fluorescence. For these lines, the experimental fluorescence cross section σ_{fluo} has been determined subsequently from the difference spectrum obtained by subtracting the sum of the dissociation and ionization cross sections σ_{diss} and σ_{ion} from the absorption cross section σ_{abs} , displayed in Fig. 1(d), via:

$$\sigma_{fluo} = \sigma_{abs} - \sigma_{diss} - \sigma_{ion} \quad (2)$$

The recorded visible fluorescence excitation spectrum, shown in Fig. 1(e), does not provide this information because this visible fluorescence populates a number of excited levels of g -symmetry, such as the $EF^1\Sigma_g^+$ or $GK^1\Sigma_g^+$ states, and does not represent the main fluorescence decay process resulting in the emission of VUV photons. The energy region investigated falls below the threshold for ion-pair formation ($\sim 139500 \text{ cm}^{-1}$), hence this decay channel may be neglected and does not contribute to Eq. (2) [57, 58, 59, 60]. Figure 1(a-e) displays a section of the experimental spectra obtained using the BESSY NIM setup. Note how a given line may appear with very different intensities in the different detection channels. It is this information which allows the decay dynamics to be quantified. The methods to

quantitatively unravel the competing decay channels of fluorescence, dissociation and ionization, in connection to the total absorption cross section, have been described previously in more detail [18].

Since the absorption measurements with the VUV-FT setup at SOLEIL were recorded from a quasi-static outflow of D_2 gas out of a windowless cell, the intensities are not measured on an absolute scale of column density. However, by comparison with the NIM values, it was possible to calibrate the intensities in the FT spectra. A preliminary estimation of cross sections in the FT-SOLEIL spectra had been made previously for the R(0) and R(1) lines probing the $3p\pi$ $D^1\Pi_u$ state [61]. In the presently performed reanalysis the different temperatures of recordings at BESSY (room temperature) and VUV-FT (liquid nitrogen cooled cell yielding effective quasi-static gas flow temperatures of 100 - 150 K) were accounted for. The effective temperatures in the VUV-FT spectra were verified from the observed Doppler widths: 0.50 ± 0.05 cm^{-1} and 0.40 ± 0.05 cm^{-1} . For a number of Q(N''), R(N'') and P(N'') lines observed both in BESSY and VUV-FT spectra, the statistical mean values of the product $An_{N''}$ was derived and compared. From these comparisons the relative populations of the $n_{N''}$ ground state levels were derived adopting theoretical values for the Einstein coefficients A , which were found to agree with the values from BESSY spectra, and assuming a Boltzmann partition for $n_{N''}$. This procedure allows for deducing line intensities from the FT-spectra with an uncertainty estimated to be at least 30%.

Large sets of data have been recorded in both experiments which are complementary to each other. The FT-VUV experiment provides a much higher resolution due to the Fourier-transform technique, but the sensitivity is not as high in view of the fact that (i) the measurements are not background free, and (ii) the continuum exhibits a periodic noise character associated with the Fourier-transforms produced from the measured interferograms. The NIM-BESSY experiments combine the advantage of a better sensitivity with the advantage of the action spectroscopies delivering information in the competing decay processes.

Figure 2 presents a detailed portion of the

recorded spectrum illustrating further its characteristics. Clearly is shown that the FT-VUV spectrum exhibits a higher resolution; the Q(2) $7p\pi, v = 8$ line near 133338 cm^{-1} appears as a sharp spike whereas in the NIM spectrum it is much broader. The R(1) $6p\sigma, v = 9$ transition near 133362 cm^{-1} affords an example of an intrinsically broad transition with $\Gamma = 2.4 \pm 0.3$ cm^{-1} , which is only moderately further broadened in the NIM spectrum. R(2) $6p\sigma, v = 9$ near 133284 cm^{-1} on the other hand is an example of a ‘complex’ resonance with a high- n fine structure due to its mixing with the $np4, v = 6$ series for $54 < n < 65$. The central peak has $\Gamma < 0.3$ cm^{-1} . The fine structure appears resolved in the FT spectrum but coalesces into an (apparently) broad peak in the NIM spectrum. This part of the spectrum also illustrates that the ionization channel is much stronger than the dissociation channel, which is a general trend found in the present study.

The data will be presented in different sections following, each focusing on one of the states of rotational quantum number N' . Information from R($N' - 1$) and P($N' + 1$) lines, probing the same excited levels N' , will be connected in the analysis. Assignments of the lines are based on the theoretical framework of MQDT, presented in the next section, and on combination differences $\Delta_{N'', N''+2}$ in the ground states that probe the same excited level $N' = N'' + 1$. The combination differences, $\Delta_{0,2} = 179.067$ cm^{-1} , $\Delta_{1,3} = 297.534$ cm^{-1} , $\Delta_{2,4} = 414.649$ cm^{-1} , and $\Delta_{3,5} = 529.900$ cm^{-1} , are derived from the highly accurate calculations for the ground state of D_2 [62], the lowest three of which were experimentally verified in the highly accurate study of the Lyman and Werner bands [32].

3. Theoretical approach

The singlet np Rydberg levels of D_2 , like those of H_2 , correspond to a $np\sigma$ and a $np\pi$ molecular orbital, yielding for each n a $^1\Sigma_u^+$ and a $^1\Pi_u^\pm$ molecular state (right side of Fig. 3). Built on the $^1\Pi_u^-$ component, rotational levels N' of total parity $-(-1)^{N'}$ - so-called d -symmetry levels - arise, whereas the $^1\Sigma_u^+$ and $^1\Pi_u^+$ components produce pairs of levels of total parity $+(-1)^{N'}$ - so called c - symmetry levels. The

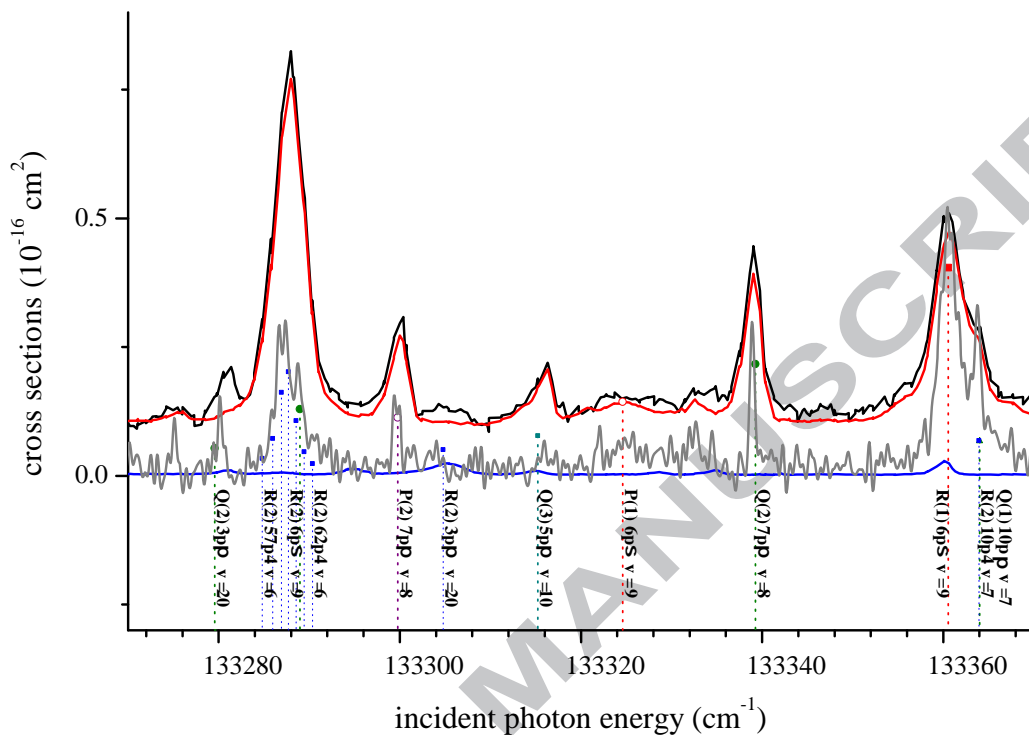


Figure 2: (Color online) Part of the spectrum in range $133270 - 133370 \text{ cm}^{-1}$ showing some characteristics as discussed in the main text. Full lines display absorption (black), ionization (red) and dissociation (blue), all from the NIM setup. The FT absorption spectrum is displayed by the grey full line. The points with drop lines correspond to calculated lines.

labels c and d coincide in our case with the commonly used designations e and f [63] which had been utilized in Ref. [35]. Watson [64] re-introduced the historical c/d symmetry classification scheme for linear Hund's case (b) and (d) molecules, showing that it is related to a residual plane of symmetry normal to the axis of rotation which remains defined even when Coriolis forces dominate. Indeed, in the present situation the $c-$ levels correspond to the $p\sigma$ and $p\pi$ orbital components which lie in the plane of rotation and become mixed by it, see just below, whereas the $d-$ levels correspond to the $p\pi$ component oriented perpendicular to the plane. The c/d parity classification thus provides immediate insight as to why $d-$ type levels are subject only to very weak rovibronic interactions in diatomic hydrogen, in sharp contrast with the $c-$

type levels which carry most of the decay dynamics.

As the Rydberg series evolve towards higher n , the two c level series interact more and more strongly. As recognized in [3], the two series converge towards two distinct rotational levels of the molecular ion, $N^+ = N' - 1$ and $N^+ = N' + 1$ respectively. As a result a transformation of the level pattern occurs, whereby the electronic ${}^1\Pi_u - {}^1\Sigma_u^+$ splitting dominating the low- n Rydberg structure is replaced by the rotational $(N^+ = N' + 1) - (N^+ = N' - 1)$ splitting dominating the level structure for high n (left side of Fig. 3). This latter situation no longer corresponds to the assumption underlying the Born-Oppenheimer approximation, but instead to its inverse, as now the nuclear (rotational) motion is fast compared to the motion of the distant slowly moving

high- n Rydberg electron. Figure 3 is a schematic diagram representing the correlation between the two limiting situations. The observation of these series for H_2 in Ref. [3] led Fano to write his seminal paper on molecular frame transformations and their use in multichannel quantum defect theory [65].

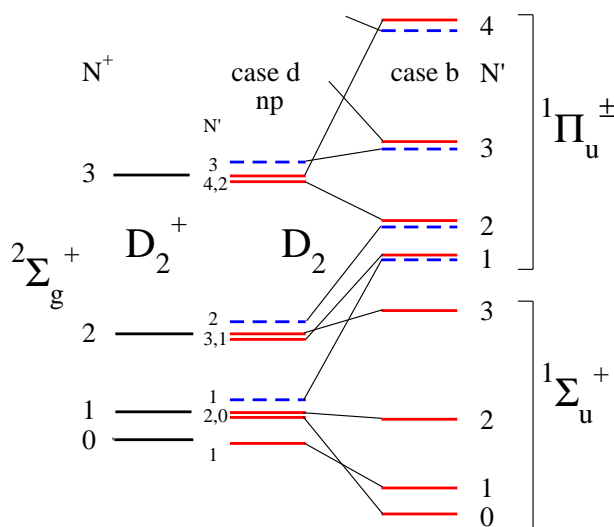


Figure 3: (Color online) Correlation of rotational levels between D_2^+ and D_2 (adapted from Fig. 6 of Ref. [3]). At the left are the rotational levels of D_2^+ , in the center those resulting from them in D_2 by the addition of an np electron with high n (case (d)), and at the right those corresponding to low n (case (b)). Full lines (red): c -symmetry levels with total parity $+(-1)^{N'}$; Broken lines (blue): d -symmetry levels with total parity $-(-1)^{N'}$.

The transition between the two coupling regimes, termed Hund's coupling case (b) and Hund's coupling case (d), respectively, takes place when the two energies are about equal; this happens for $n \approx 10$ in D_2 when $N' = 2$. In addition to the transformation from one coupling case to another, local perturbations between the two series occur, namely when for given N' a level corresponding to $N^+ = N' + 1$ with lower n falls amongst the higher- n levels converging toward the lower limit $N^+ = N' - 1$. When the higher- n manifold is very dense, just below the $N^+ = N' - 1$ threshold, a cluster of perturbed levels arises - a 'complex' resonance pattern - whereas above the threshold

the lower- n level lies in the true ionization continuum and is broadened by rotational autoionization.

The situations just described are ideally suited for a unified description in terms of multichannel quantum defect theory combined with a frame transformation [65]. The theoretical formalism has two key elements. First, multichannel quantum defect theory is an extension of the scattering theory as applied to ion-electron collisions into the discrete range, where bound or quasi-bound Rydberg states are present [66]. The unifying key element is the quantum defect μ - in a multichannel situation a matrix - which in the discrete range provides the Rydberg energies $-\mathcal{R}/(n-\mu)^2$ for the Rydberg levels n , whereas in the adjoining ionization continuum the quantity $\pi\mu$ adds to the Coulomb phase as a system-specific scattering phase shift. The quantum defect generally varies slowly with the excitation energy, so that extrapolation methods may be used to infer scattering dynamics from bound level measurements or vice versa. This is why, for instance, rotational autoionization can be predicted on the basis of bound state quantum defects. The second element is the frame transformation which describes the uncoupling of the Rydberg electron from the molecular frame as it roams farther and farther away from the residual ion. In many situations the transformation is analytically known - for instance in terms of vector coupling coefficients in the case of the rotation-electron coupling discussed here, and thereby the number of unknown parameters in a given problem may be reduced substantially. The latter aspect adds considerably to the power of the method.

These concepts have been developed and applied extensively in Refs. [46, 67] where the formalism is described in detail. Review papers have also been published [48, 68]. Refs. [21, 22, 69] provide the tools necessary for calculations of absolute absorption and photoionization cross sections. In those papers vibration-electron coupling was included in addition to the rotation-electron coupling, with the result that nearly all of the dipole-allowed absorption spectrum of H_2 became accessible to a quantitative theoretical interpretation. In Refs. [21, 22, 69], as in more recent papers [26], the quantum defect functions $\mu_\Lambda(R)$ and electronic absorption transition moments $d_\Lambda(R)$

for $\ell = 1$ channels have been extracted from state-of-the-art first-principles computations [50, 51, 52] without any adjustment, so that the theoretical formalism used has *ab initio* character. This is also true for the present application to the c -symmetry levels in D_2 .

As was done in the early papers, the present calculations include only $\ell = 1$ channels associated with the rovibrational levels of the $X^+ 2\Sigma_g^+$ ground state of D_2^+ , and they also disregard electron and nuclear spins as well as dissociation processes. This approach corresponds to a streamlined version of the available MQDT theoretical machinery, adapted to the initial analysis of the large data set at hand. Since the 1970's molecular MQDT has been extended both conceptually and technically, to allow for additional partial wave components $\ell > 1$ of the excited Rydberg electron [70], to include electronically excited ion core channels [71], and to account for hyperfine interactions, as was done for the case of H_2 [72, 73] and D_2 [74, 75]. Molecular dissociation processes have been incorporated in the MQDT formalism, allowing partial ionization and dissociation cross sections to be evaluated in a framework equivalent to a reactive scattering scenario [49], and where it is also possible to allow for electronically excited ion core states [76]. These refinements are not included in the present analysis but are left to a forthcoming paper dealing with the interpretation of the finer details of the data set obtained here.

The Rydberg np absorption spectra of diatomic hydrogen display striking examples of propensity rules. One example concerns the rotational line intensities within each pair of interacting c -symmetry np series. Experimentally it is observed that the transition of the two coupled series from Hund's case (b) toward case (d) not only corresponds to a rearrangement of the Rydberg state level energies, but is also accompanied by a profound modification of the rotational line intensities. As n increases along the series, each quadruplet of R - and P -transitions converging towards the $N^+ = N' - 1$ and $N^+ = N' + 1$ limits respectively, is effectively reduced to a doublet. It turns out that the R -transition belonging to the $N^+ = N' - 1$ series and the P -transition belonging to the $N^+ = N' + 1$ series are strong, whereas the two

other series become very weak and essentially vanish. In other words, only transitions to case (d) levels corresponding to $N^+ = N''$ have appreciable intensity. It will be seen in the result sections below that this propensity rule is naturally accounted for by MQDT when the parameters derived from the *ab initio* computations of Refs. [50, 51, 52] are used. The physical explanation for this striking phenomenon derives from the fact that the electronic transition at hand corresponds in a good approximation to an atomic $s \rightarrow p$ transition. As the angular momentum of the photon provides the angular momentum of the excited or outgoing final state electron, the nuclei do not move during the process, and hence $N^+ = N''$. This propensity rule may be viewed as a rotational analog of the Franck-Condon principle. Formally it arises via the 6- j symbol

$$\left\{ \begin{array}{ccc} N^+ & N'' & \ell'' \\ 1 & N' & \ell \end{array} \right\} \quad (3)$$

which governs the Hund's case (b) to (d) absorption transition in the united-atom limit [77, 78], and which in order not to vanish requires $N^+ = N''$ when $\ell'' = 0$. In the Rydberg spectrum the selection rule implied by Eq. (3) is reduced to the status of a propensity rule because the united-atom approximation is not exact in the molecule, and also because interchannel couplings are active which prevent a pure case (d) situation to occur [65].

Vibrational autoionization in diatomic hydrogen provides another example of a propensity rule. This process involves the conversion of vibrational energy of the ion core into electronic energy, which enables the initially bound Rydberg electron to depart in the continuum. This vibronic process is governed by the R -dependence of the quantum defect via a vibrational integral of the type $\langle v_f^+ | \mu(R) | v_i \rangle$, where v_i is the vibrational quantum number of the quasibound Rydberg level and v_f^+ is the final vibrational state of the ion core left behind by the escaping electron. To the extent that the vibrational motion is harmonic and the quantum defect varies linearly with R , the selection rule $\Delta v^+ = v_f^+ - v_i = -1$ must be obeyed [3]. Again, this rule is not strict because the assumptions underlying it are only approximately valid in

the real molecule. Table 1 summarizes the propensity rules which apply to the rovibronic predissociation, autoionization and fluorescence decay processes discussed here. Also given are approximate quantum number dependences expected for these processes inasmuch as they can be formulated. We stress again that these rules provide overall estimates, but do in no way account for the complex details of the channel interactions present in the Rydberg series.

The systematic study of the absorption spectra of H_2 and D_2 provides a unique opportunity to study isotope effects in strongly coupled multichannel systems that are electronically identical, but whose nuclear masses differ by a factor of two. Some facets of the mass effects that occur in the d -symmetry Rydberg series have been discussed in Ref. [26]. The previous applications of MQDT to c -symmetry levels of H_2 and here to D_2 , demonstrate that the MQDT approach successfully accounts for the vast mass difference between the two isotopomers, from low n -values up into the ionization continuum. In the calculations this is achieved simply (i) by using the calculated values for $\text{H}_2^+/\text{D}_2^+$ rovibrational ionization levels v^+N^+ - the rovibrational ion thresholds - and calculating the associated wave functions, with the appropriate nuclear reduced mass in each case, and (ii) by using the appropriate mass-corrected Rydberg constant \mathcal{R}_M in the multichannel calculations for each isotopomer. As our results discussed below will show, these changes account for the great diversity of mass-effects as they occur throughout the Rydberg spectrum.

For instance in the c -symmetry levels rotational-electronic predissociation at low n proceeds with rates that are proportional to the square of the inverse of the reduced mass, i.e. $\propto M^{-2}$. This mass-dependent scaling law for predissociation was derived and measured in the early work in the hydrogen molecule [79, 80]; this mass-scaling was further experimentally verified in accurate measurements of predissociation widths for a series of vibrational levels pertaining to the $\text{D}^1\Pi_u$ state in H_2 , D_2 and HD [30]. On the other hand, rotational autoionization processes that occur at high n have no mass dependence at all, but instead are proportional to the squared difference, $(\mu_{p\sigma} - \mu_{p\pi})^2$, of the spatial

components the molecule-fixed quantum defects [3]. The mass-dependences of vibronic interactions appear via a different mechanism. At low n , where the Born-Oppenheimer picture constitutes the natural zero-order approximation, vibronic interactions are mediated by matrix elements that scale as $M^{-3/4}$ [26], whereas in the inverse limit the preferred $\Delta v^+ = -1$ vibrational autoionization processes proceed with rates $\propto M^{-1/2}$ [26]. These limiting dependences are further modified by multichannel effects and the very way the Rydberg series are arranged. As already mentioned above, for vibrational autoionization to occur, a given level nv must lie higher than the threshold $v^+ = v - 1$. The ionization thresholds are spaced more closely in the heavier isotope - approximately by a factor $\sqrt{2}$ in D_2 as compared to H_2 . Therefore the first level of a series that can autoionize via the preferred $\Delta v^+ = -1$ process has a higher n value in D_2 than in H_2 . This ‘visibility’ criterion - namely the energetics allowing or not allowing autoionization to occur [68] - further reduces the vibrational autoionization rate, beyond the $M^{-1/2}$ scaling rule mentioned above. The approximate mass dependences expected for the rovibronic predissociation and autoionization processes are collected in Table 1.

4. Results for $N' = 1$ levels

More than 200 R(0) lines and nearly 100 P(2) lines of np ($n \geq 4$) character were recorded and their transition frequencies measured on the VUV-FT spectra. Most of the R(0) and P(2) lines observed in the NIM BESSY spectra are found in the FT SOLEIL spectrum as well. However, due to the higher temperature (room temperature) of the gas used at BESSY and as a result of the higher sensitivity, an additional 33 P(2) lines and 36 R(0) lines were found in the NIM BESSY measurements. The assignments were made on the basis of the MQDT calculations, added by verification via the combination differences. The results for all transitions probing $N' = 1$ levels, including all experimental and theoretical information on level energies, widths, line strengths, and competitive decay channels, are collected in Table 2.

4.1. Level energies $N' = 1$

The internal consistency of measurements of R(0) and P(2) lines, restricted to the observations at FT-SOLEIL, was tested by evaluating the combination difference of pairs yielding an averaged value of $179.063 \pm 0.010 \text{ cm}^{-1}$ in agreement with the accurate value for the ground state splitting [62].

Further, a comparison can be made with the results of the MQDT-calculation, which is the essential basis for assigning the transitions. For the more than 200 lines measured on the FT spectra, a difference in transition frequencies (obs.-calc.) was determined yielding an average value of -0.09 cm^{-1} and a spread of 0.25 cm^{-1} . Such a deviation can be seen as good agreement in view of the fact that calculations are fully *ab initio* and that the relative accuracy on the transition frequencies is $\Delta\nu/\nu \leq 2 \times 10^{-6}$, but is somewhat larger than the mean estimated absolute measurement uncertainties of 0.05 cm^{-1} .

In some special cases, the observed level energies or transition frequencies differ even more from the values calculated by MQDT, as is illustrated in Fig. 4. The $5p\pi, v = 4 - 6$ levels (for $N' = 1$) are observed as doublet lines with the calculated value being in the middle of the two observed lines. A similar feature of split lines had been observed previously in the H_2 spectrum, also in the $5p\pi$ manifold [23]. This situation is probably due to the coupling with the $1snf$ configurations not taken into account here [70]. Even larger discrepancies are observed for $4p\pi, v = 13 - 14$, $4p\sigma, v = 14$, $6p\sigma, v = 10$ and $6p\pi, v = 10$. These levels are located at high energies and explore large internuclear distances; at such large values of $R > 5 a_0$, the $1snp$ configurations interact with the $2snp$ configurations and specially the $B''^1\Sigma_u^+ 4p\sigma$ state becomes $2s2p\bar{B}^1\Sigma_u^+$, the $B''\bar{B}$ forming a double-well potential [81, 82, 83, 84, 14]; the approximation of np isolated configurations is, again, not valid anymore.

The discrepancies between observed and calculated values for the $^1\Pi_u^+, N' = 1$ ortho levels may be compared to the discrepancies observed in the $^1\Pi_u^-, N' = 1$ para levels, previously reported [34, 26] (see Fig. 4 left panel). The latter are sensitive to vibronic interactions only while the former are sensitive to both vibronic and rotational interactions. The right panel

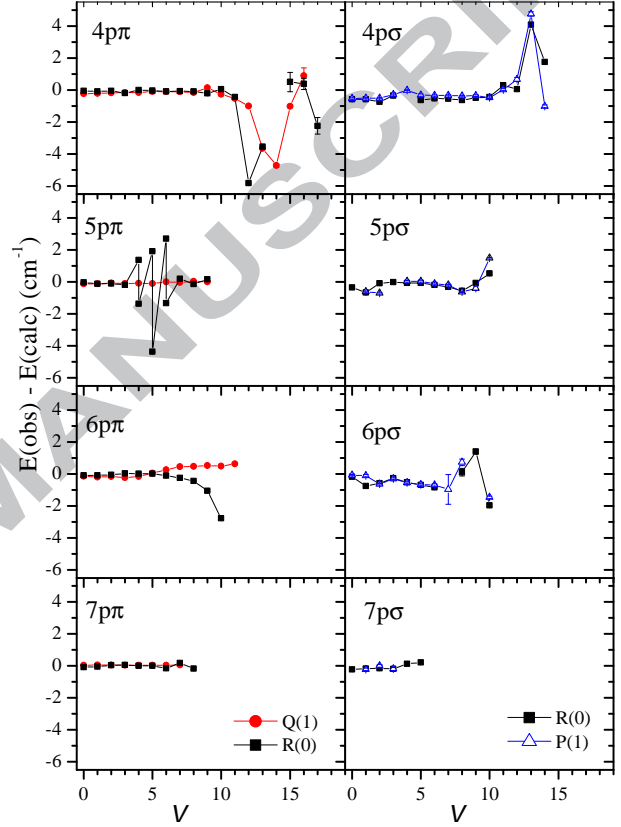


Figure 4: (color online) Graphical representation of the deviations between observed $N' = 1$ level energies (as obtained via R(0) transitions) and MQDT-calculated values, for $np\pi, v$ (left) and for $np\sigma, v$ (right), represented by (black) square data points. For the $np\pi \ ^1\Pi_u^+$ levels a comparison is made with the opposite parity Λ -doublet components $np\pi \ ^1\Pi_u^-$ as measured in Q(1) transitions, represented by (red) circular data points. For the $np\sigma \ ^1\Sigma_u^+$ $N' = 1$ levels a comparison is made with $N' = 0$ levels, as measured in P(1) transitions, represented by (blue) triangular data points.

of Fig. 4 shows a comparison with the deviations between observation and calculation for the $N' = 1$ levels and the deviations for $N' = 0$, observed in P(1) lines [27, 33]. In some examples the comparisons show that the deviations from theory are independent of rotational quantum number, holding both for $N' = 0$ and 1. This is the case for the deviation resonance in $4p\sigma$ (at $v = 13$), and the onset of deviation at high v quantum number in $5p\sigma$ and $6p\sigma$. The origin of the discrepancies lies outside the np configuration treatment.

In the examples of the $np\pi$ vibrational series displayed in Fig. 4 a comparison is made between Λ -doublet levels of the same $N' = 1$ levels. In the $4p\pi$ vibrational series the deviation resonance is found in both Λ -components, although shifted by two vibrational quanta (from $v = 12$ to $v = 14$). In contrast, for the $5p\pi$ levels the splitting is observed only for the $^1\Pi_u^+$ component. Similarly, the onset of deviation for $6p\pi$ at high v is only observed for the $^1\Pi_u^+$ component.

For the lines observed in the NIM spectra only, the deviations between observed and calculation remain within the order of the calibration uncertainty of 1 cm^{-1} (Table 2). Takezawa and Tanaka [35] had published a set of energy values for $N' = 1$ levels, that were mostly consistent with the quoted uncertainty of 0.6 cm^{-1} , although for some levels the assignments had to be changed based on the present MQDT-calculations.

4.2. Widths of $N' = 1$ levels

The natural decay widths of the upper levels of the R(0) and P(2) transitions observed in the FT-SOLEIL spectra have been determined from the observed widths of the lines through a deconvolution procedure (see [34] for details). Values and uncertainties are listed in Table 2 and compared with the ionization widths as calculated from MQDT. This comparison on the line widths is further illustrated in Fig. 5 for the $np0$ series and in Fig. 6 for the $np2$ series. In the figures also a comparison is made with results from H₂ [21]. Only above the ionization threshold were line broadening phenomena clearly observed. A comparison is made with the calculated ionization widths in the entire range below the

third dissociation limit, covering the observational window of the present study. The dissociation to D($n = 1$)+D($n = 3$) opens above 134266 cm^{-1} .

No level (np with $n \geq 4$) located below the ionization limit presents a measurable natural width; the determined width is less than the uncertainty of the measurement, which therefore provides an upper limit for the natural width. No broadening was found in the levels associated with $4p\sigma$. The dissociation widths in the $4p\sigma$ levels in D₂ are found to be less than 0.15 cm^{-1} , in sharp contrast to the values obtained for H₂ [14], where the $4p\sigma$ dissociation widths were found to be around 1 or 2 cm^{-1} . This is somewhat surprising since for the $3p\pi$ D¹ Π_u vibrational levels rather strong predissociation broadening was found for all three isotopes H₂ [85, 28, 86], HD and D₂ [31], results of which are represented by a mass-scaling law [30].

The largest widths for H₂ had been found for $n = 8$ [21, 22], whereas the largest widths in D₂ occur at $n = 10$ (see Figs. 5 and 6). This may be attributed to the relative location of the ionic level $v^+, N^+ = 0$ with respect to the excited states in the neutral, falling in between $8p0$ and $9p0, v' = v^+ - 1$ levels for H₂ and in between the $10p0$ and $11p0$ levels for D₂, written in Hund's coupling case (d). This phenomenon is entirely due to the location of the ionization potential and governed by the propensity rule for strong ionization as discussed in the theoretical Section. It underlines that the decay and line broadening is mainly associated with ionization.

Overall, the widths of $np0$ levels exceed that of $np2$ levels, as is illustrated by comparing Figs. 5 and 6. Even if for $n = 10$ the coupling case (b) is no longer applicable, the transition to coupling case (d) is not yet completed and the vibronic coupling for the $np\sigma$ levels is far stronger than for the $np\pi$ levels. This remains partly in effect for the $np0$ and $np2$ levels at moderate n values, too. On the other hand, more $np0$ levels could be observed than $np2$ levels, because in coupling case (d), the $np2$ levels can only be detected through P(2) lines, and those tend to become weaker in the transition to Hund's case (d) as discussed in the theoretical section. Far fewer P(2) lines were detected than R(0) lines, even on the NIM spectra.

In Figs. 5 and 6 the calculated values for H₂ are

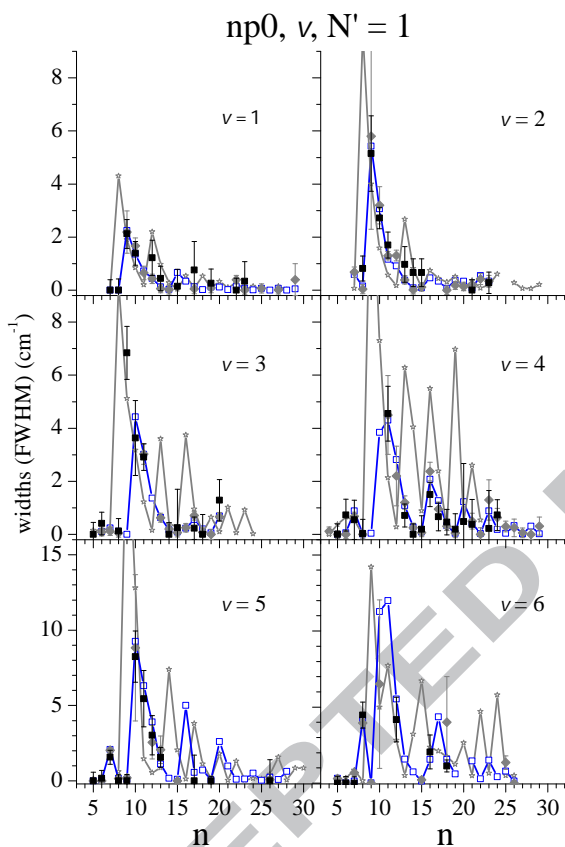


Figure 5: (Color online) Calculated and measured widths of the $np0, N' = 1, v = 1 - 6$ levels of D_2 . Open (blue) connected squares: calculated MQDT values; (grey) diamonds: experimental FT values; (black) squares: experimental NIM values. For comparison the MQDT values for H_2 are included as well, with open (grey) connected stars.

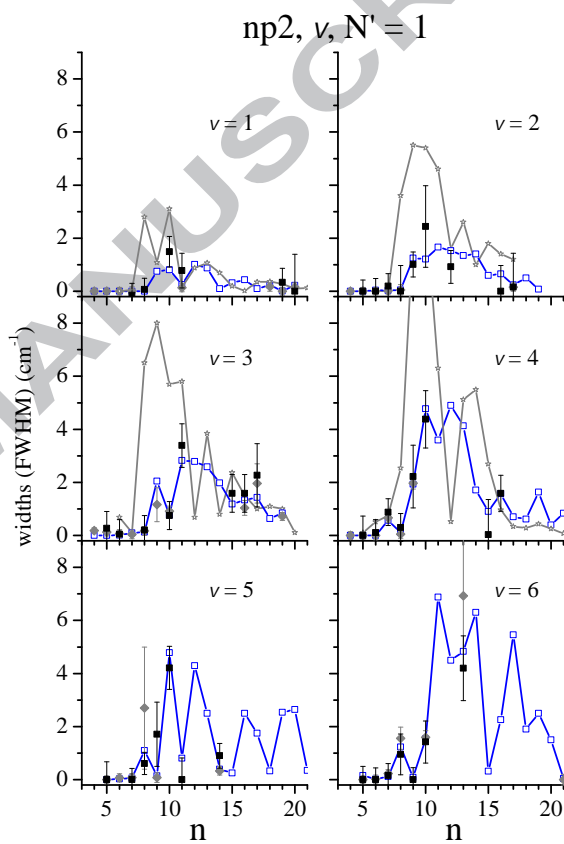


Figure 6: (Color online) Same as Fig. 5 for the $np2, N' = 1, v = 1 - 6$ levels.

displayed alongside with results for D₂. For both isotopomers, the values for the widths are somewhat erratic, indicating that ionization depends strongly on local perturbations. Generally, the ionization widths for H₂ are broader than those for D₂, in line with the rules given for vibrational autoionization in Table 1.

Values for the line widths are more difficult to extract from the NIM spectra as the resolution is lower, and lines are more often blended within the line profile. The values of the line widths measured in the NIM spectra agree with those obtained from the FT spectrum (see Figs. 5 and 6), insofar they exceed the instrument width. They also agree with the calculated ones except for one case: the $9p\sigma, v = 3, N' = 1$ level. For this resonance, the measured width corresponds to the envelope of a complex resonance: the $9p\sigma, v = 3, N' = 1$ level interacts with the Rydberg $np2, v = 2, N' = 1$ series, for n around 65. This apparent width of $6.8 \pm 1.0 \text{ cm}^{-1}$ can be compared to the calculated envelope width of 6.3 cm^{-1} .

4.3. Line intensities for $N' = 1$ levels

The absolute intensities of some 350 R(0) or P(2) lines were measured, extending over more than two orders of magnitude as is graphically displayed in Fig. 7a. The calculations cover more than 400 pairs of R(0) and P(2) lines to be compared with the measured values. Figure 7b displays a histogram of ratios of measured values A_{meas} over calculated values A_{calc} , defined as $\rho_A = A_{\text{meas}}/A_{\text{calc}}$, for the R(0) and P(2) lines. The result shows a fair agreement with values $\rho_A = 1.1$ for R(0) and $\rho_A = 1.2$ for P(2), respectively, with a FWHM of 0.7. As noted previously [26, 33], the uncertainty of the A_{calc} values can be estimated at 10 to 20%, depending on the importance of the influence of the dissociation continuum. For a large majority of the observed lines, the value of $\rho_A = 1$ (with a 20% uncertainty) is compatible within the error bars to these ratios. Nevertheless in some cases a clear disagreement is found.

There are a few cases for which the ratio is $\rho_A < 1$: the R(0) and P(2) lines exciting $5p\pi, v = 4, 5$ and 6 levels with $N' = 1$. In section 4.1, it was noted that these lines are split. Clearly, an unknown state strongly interacts with the $5p\pi$ state causing the line strengths and emission probabilities of the $5p\pi$ levels

to be shared with the interacting levels. The sums of the measured line strengths agree with the calculated ones, demonstrating that this is a case of intensity borrowing to a perturber state. The unknown perturber state does not belong to the np configuration because it is absent in the calculations; it probably belongs to the nf configuration. The $4p\pi, v = 15$, R(0) line presents also a ratio $\rho_A < 1$. This line is measured in the dissociation excitation spectrum only, and cannot be extracted in the other spectra being blended. Thus, the measured value is only a partial one and corresponds mainly to the dissociation cross section.

In a number of cases $\rho_A > 1$ is found. This may be due simply to an artifact of line blending, but some examples appear to have a physical cause pointing at shortcomings in the theoretical framework, based on an isolated np configuration. The $14p0, v = 2$, R(0) line, located at $127\,280 \text{ cm}^{-1}$, and appearing as isolated in the spectrum, has $\rho_A = 3.9 \pm 0.7$, while the corresponding P(2) line exhibits a ratio of $\rho_A = 1 \pm 1$. Also the $8p\pi, v = 1$, P(2) line, without any coincidence predicted and exhibiting a ratio of $\rho_A = 1.7 \pm 0.2$, is far off from the MQDT-prediction. Possibly, these lines are blended with extra lines which do not belong to the np configuration but to an nf configuration. The situation is similar to that of the $9p\pi, v = 2$, Q(1), $14p\pi, v = 4$, Q(1) and $11p\pi, v = 0$ Q(3) lines as previously reported [26].

The $4p\sigma, v = 9$ and 11 R(0) and P(2) lines are twice more intense than predicted. In this example the corresponding excited levels are dissociated. To calculate their energies, the position of the quasi-continuum levels must be varied in order to maximize their distances from the $4p\sigma$ level [18]. Using this procedure, the resulting accuracy of the energies is rather good but the uncertainty of the intensities is rather large [87]. For the $5p\sigma$ levels, the measured intensities are too high by 30 to 40% in comparison with the calculations. These levels are strongly coupled to those of $4p\sigma$ character, which are not well reproduced in the calculations.

The results of the line intensities for the $np\sigma$ and $np0, v = 0 - 7$ R(0) and P(2) lines are collected in Fig. 8 and those for the transitions to the $np\pi$ and $np2, v = 0 - 6$ levels in Fig. 9. In the special case of

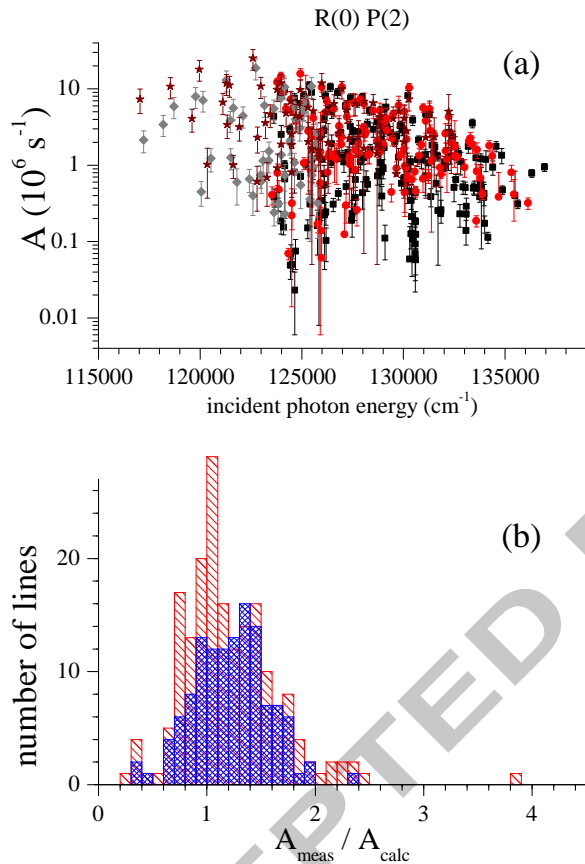


Figure 7: (Color online) (a) Einstein coefficients A for transitions involving $N' = 1$ excited levels in D_2 as measured. The A values in the FT-VUV spectra are in (grey) diamonds for R(0) and in dark (brown) stars for P(2). The measured NIM-BESSY values are in solid (black) squares for R(0) and solid (red) circles for P(2). (b) Comparison with theory: Ratios of Einstein coefficients $\rho_A = A_{\text{meas}}/A_{\text{calc}}$ for the R(0) lines (red sparsely hatched pattern) and P(2) lines (blue densely hatched pattern).

the $9p\sigma, v = 3$ lines, the calculated values correspond to the sum over the complex resonance. Altogether intensities are listed for 221 R(0) and 134 P(2) lines. For 126 of these lines the intensities were measured on both the NIM and the FT spectra and may be compared with each other within the error bars (see Figs. 8 and 9). For 51 R(0) and 26 P(2) lines, the FT values are the only ones because either the lines are located at low energy (below the limit of the NIM recordings) or they were resolved at the higher resolution of the FT and not in the NIM spectra. For 16 R(0) and 1 P(2) lines, the intensity values from the FT have lower uncertainties than the NIM values due to the better resolution; these intensities are listed in Table 2. Altogether 67 R(0) and 27 P(2) line intensities could be added to the NIM values due to this procedure. In all cases, the lines for which the calculations gave weak intensities were not observed in the spectrum. All the lines with reasonable calculated A values were seen in the spectrum, but many of them could not be quantitatively evaluated because they were not resolved.

4.4. Decay dynamics $N' = 1$ levels

Below the ionization threshold, lying at 124745 cm^{-1} , the only open de-excitation channels are fluorescence and dissociation. Fluorescence was observed from all these levels except from $3p\pi D^1\Pi_u^+$ levels [31, 87]; fluorescence was observed even from the $4p\sigma B''^1\Sigma_u^+, v = 5$ level which was not the case for H_2 [14]. The dissociation yields of these levels vary from 21% (for the $5p\pi, v = 2$ level) to 91% (for the $4p\sigma, v = 5$ level). The dissociation of the $4p\sigma, v = 5, N' = 1$ level must therefore be quite slow, much slower than the dissociation observed for the corresponding level of H_2 . and in fact slower by more than the factor of 4 predicted by the approximate isotope rules (cf. Table 1). The measured fluorescence yield is $(9 \pm 4)\%$; the fluorescence lifetime of this state can be estimated from H_2 measurements [85] at 7 ns corresponding to a fluorescence width of $7 \times 10^{-4} \text{ cm}^{-1}$. The dissociation width can then be estimated at about 10^{-2} cm^{-1} , consistent with the observed width in the FT spectrum ($< 0.15 \text{ cm}^{-1}$) [33] but quite different from the value of $(2.5 \pm 0.2) \text{ cm}^{-1}$ measured for H_2 [14]. For the $10p0, v = 0$ level,

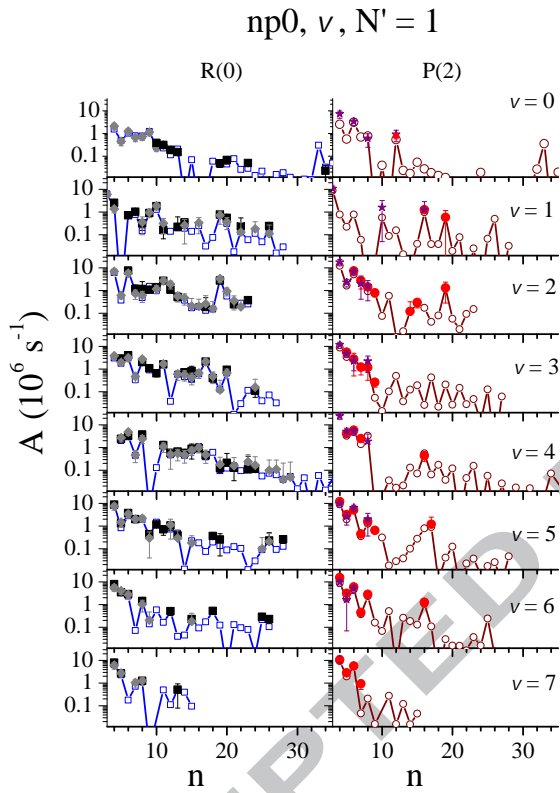


Figure 8: (Color online) Einstein coefficients A for the R(0) lines (left panel) and for the P(2) lines (right panel) for transitions to $np0, v = 0$ to 7 levels. Full black squares: measured R(0) NIM values; full grey diamonds: measured R(0) FT values; open blue squares: calculated R(0) values. Full red circles: measured P(2) NIM values; full purple stars: measured P(2) FT values; open dark red circles: calculated P(2) values.

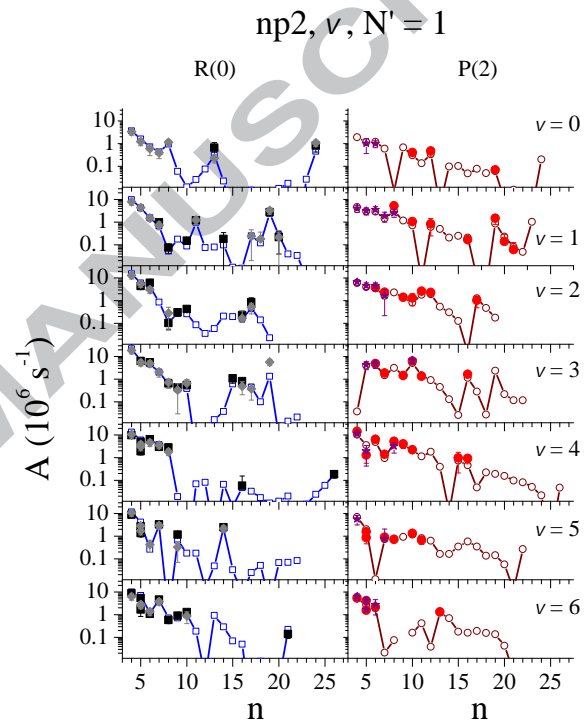


Figure 9: (Color online) Same as Fig. 8 for Einstein coefficients A for R(0) and P(2) lines in transition to $np2, v$ levels.

the fluorescence width can be estimated at $5 \times 10^{-5} \text{ cm}^{-1}$ according to the $1/n^3$ scaling law of the fluorescence lifetimes. The value of its dissociation width can be deduced from the dissociation yield of 23%, and is $1 \times 10^{-5} \text{ cm}^{-1}$, which is a very small value. This type of experiment, as performed in the versatile spectrometer at BESSY, demonstrates its sensitivity for monitoring the various decay processes.

Even above the ionization threshold several levels are observed in the fluorescence excitation spectrum. In H_2 , three $N' = 1$ ${}^1\Pi_u^+$ levels had been observed to fluoresce: the $4p\pi$ $D^1\Pi_u$, $v = 5$ and 9, and the $5p\pi$ $D^{11}\Pi_u^+$, $v = 3$ levels [18]. In D_2 , the fluorescing levels are far more numerous, not only due to the higher density of vibrational levels but also other electronic states are observed to fluoresce: $6p\pi$ and $5p\sigma$. For $5p\sigma$ this is particularly unexpected as no state of $np\sigma$ character above the ionization threshold had been seen to fluoresce in H_2 [18]. All the levels observed here in the fluorescence excitation spectrum are observed in the FT spectrum, in absorption, and exhibit a width smaller than 0.15 cm^{-1} , which is the limit of the FT measurement; all of them need a $|\Delta v \geq 2|$ change to ionize, in view of their energy with respect to threshold, and have calculated ionization widths lying in the range of 10^{-3} cm^{-1} , except for the $6p\pi$, $v = 2$ level with an ionization width of $4 \times 10^{-2} \text{ cm}^{-1}$.

Figure 10 displays the competing decay behavior of the $np\pi$ ${}^1\Pi_u^+$ and $np\sigma$ ${}^1\Sigma_u^+$ levels with $4 \leq n \leq 6$. The general trend is primarily dissociation at $n = 4$, going through a transition regime at $n = 5$, to $n = 6$ where ionization becomes fully dominant. Above the ionization threshold, ionization may compete with dissociation. Dissociation is very efficient indeed for the $D^1\Pi_u^+$ levels [31, 87] but also for the $4p\sigma$ $B^{11}\Sigma_u^+$, $v \geq 5$ levels, to the extent that none of them were seen in the ionization excitation spectrum, except for the $4p\sigma$, $v = 14$ level. Their calculated ionization widths are very small, much smaller than the estimated dissociation width at 10^{-2} cm^{-1} , except for the $4p\sigma$, $v = 10$ level located at $128\,889 \text{ cm}^{-1}$ for which an ionization width of $1.1 \times 10^{-2} \text{ cm}^{-1}$ was calculated. However, a suspected weak ionization from the $4p\sigma$, $v = 10$ level cannot be proven: the R(0) line is blended with many other lines and no relevant information can be extracted from it; the

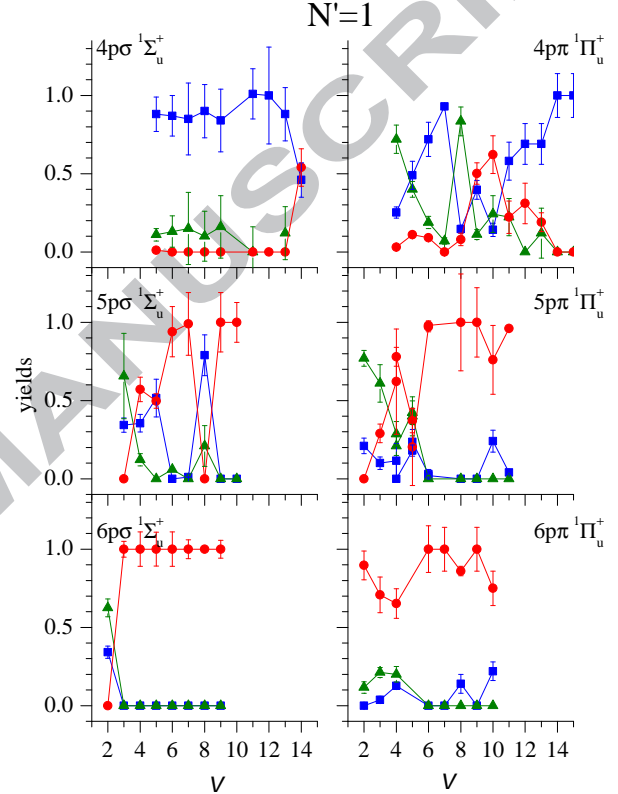


Figure 10: (Color online) Competition between decay channels with measured yield values plotted for the $N' = 1$, $4p\sigma$, $5p\sigma$, $6p\sigma$ and $4p\pi$, $5p\pi$ and $6p\pi$ levels of D_2 , as function of the excited-state vibrational quantum number v . Dissociation: blue squares; fluorescence: green triangles; and ionization: red circles.

P(2) line is blended, too, with a line connected with a fully ionized level. The $4p\pi$, $5p\pi$, $6p\pi$ and $6p\sigma$ levels (including the $5p\pi$ doubled lines) were seen in the dissociation spectrum, as was also the case for H_2 [23, 24, 25, 16]. On the contrary, the $8p\sigma, v = 4$ level, which ionizes very rapidly in H_2 with a measured width of 20 cm^{-1} [4, 21] was seen in the dissociation excitation spectrum of D_2 with a dissociation yield of $(16 \pm 4)\%$; its calculated ionization width is 10^{-2} cm^{-1} , much smaller than 20 cm^{-1} . This level is located in D_2 by 4.1 cm^{-1} higher than the $4p\sigma, v = 10$ level; their coupling induces an abnormal dissociation width to the $8p\sigma, v = 4$ level and an abnormal ionization width to the $4p\sigma, v = 10$ one.

5. Results for $N' = 2$ levels

The experimental results on level energies, widths and line intensities for excitation to the $N' = 2$ excited levels are listed in Table 3, alongside with values derived from the MQDT calculations.

5.1. Level energies $N' = 2$

The FT spectra cover 174 R(1) lines and 20 P(3) lines in the $117\,000 - 135\,500 \text{ cm}^{-1}$ spectral range. Out of these, 19 R(1) and P(3) lines have a common upper level so that the energies of 175 levels have been determined. The combination difference Δ_{13} is satisfied in all cases to within the accuracy of the present experiments. At the low temperature used in the FT experiment, there are twice less molecules in the $N'' = 3$ level than in the $N'' = 1$ level, with the result that the P(3) transitions are correspondingly weaker and their accuracy lower. Results are listed in Table 3.

In the NIM spectra, 164 R(1) and 83 P(3) lines were measured in the range of $123\,500 - 137\,000 \text{ cm}^{-1}$. Of these 122 R(1) and 7 P(3) lines were seen on both the NIM and FT spectra. Their energies were found to agree within the larger NIM uncertainty of 1 cm^{-1} . Due to the higher sensitivity and to the use of the dynamics investigated in parallel, 57 new levels could be measured on the NIM spectra: 6 of them by both the R(1) and P(3) lines, 33 by R(1) lines only and 18 by the P(3) lines. Of the 233 $N' = 2$ (+) para np levels with $n \geq 4$ in D_2 , Takezawa and Tanaka [35] had

published the energy values of 54 levels, within an uncertainty of 0.6 cm^{-1} ; for these levels the assignments were changed based on the MQDT-calculations.

The observed transition frequencies in the FT spectra can be compared with calculated values from the MQDT yielding discrepancies obs.-calc. with an average of $-0.100 \pm 0.015 \text{ cm}^{-1}$ and a spread of 0.42 cm^{-1} . Such values reflect the quality of the calculations despite the presence of some large discrepancies, as it had been observed previously, for the Q(N) and R(0) lines [34, 26] corresponding to the $4p\sigma$ or $4p\pi$ levels. For the $4p\pi, v = 11$ level, two R(1) lines were observed at $132\,228.62$ and $132\,222.02 \text{ cm}^{-1}$, both corresponding to levels which are subject to strong predissociation, while one P(3) line was observed corresponding to the first R(1) line. Additional lines had been observed previously in H_2 [25] and in D_2 [34, 26]. This is also the case for the $5p\sigma, v = 10$ R(1) line calculated at $132\,384.54 \text{ cm}^{-1}$ and for which two lines are observed at $132\,380.78 \pm 0.09$ and $132\,388.61 \pm 0.11 \text{ cm}^{-1}$. Large discrepancies were also noted for the $4p\sigma, v = 13$ and $4p\pi, v = 13$ levels. All these levels have $n = 4$ and high v values, exploring large internuclear distances where the configurations defined at short distances are not valid anymore; the $1snp$ configuration may be mixed with $1snf$ or/and $2snp$ configurations, not taken into account in the MQDT calculations.

For the 57 levels measured on the NIM spectra only, the energy discrepancies obs.-calc. are less than the experimental uncertainty of 1 cm^{-1} , except for two of them: the $40p3, v = 2$ and the $15p1, v = 6$ levels, for which the experimental uncertainties may be underestimated because these lines have very low intensities.

5.2. Line widths $N' = 2$

Natural line widths were determined from the observed spectra via deconvolution of the Doppler width and apparatus function resulting in values as listed in Table 3 and graphically displayed in Fig. 11 for the $np1$ and $np3, v = 1$ to 5 levels. Values obtained from both spectra are in agreement, with those obtained from the FT spectra being generally more precise than those from the NIM-BESSY spectra.

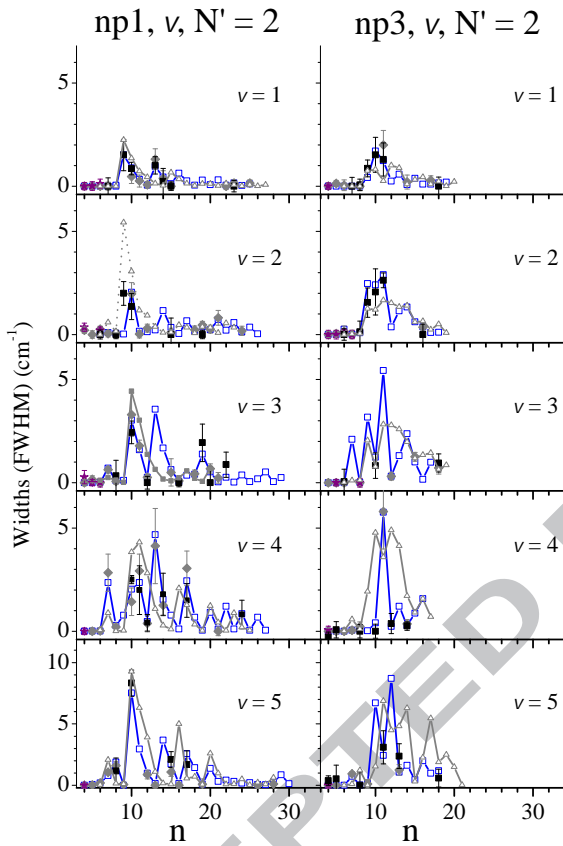


Figure 11: (Color online) Calculated and measured widths of the $np1$ (left) and $np3, v = 1$ to $5, N' = 2$ levels (right). Open (blue) connected squares: calculated MQDT values; (grey) diamonds: experimental FT values for the R(1) lines; (purple) stars: experimental FT values for the P(3) lines; (black) squares: experimental NIM values from the R(1) lines. For comparison the MQDT calculated values for the $N' = 1$ levels are shown as open (grey) connected triangles.

The levels under study with $n \geq 4, N' = 2$ exhibit small dissociation widths if any. The natural widths observed ($> 0.15 \text{ cm}^{-1}$) are mainly due to ionization, so that the experimental widths can be compared with calculated autoionization widths. Good agreement was found for all levels except for the $9p1, v = 2$ level, with a measured width of $2.0 \pm 0.6 \text{ cm}^{-1}$ on the NIM spectra and a calculated width of 0.02 cm^{-1} . However, this is explained by the fact that the $9p1, v = 2$ level is a part of a complex resonance interfering with the Rydberg $np3, v = 1$ series with $n \sim 120 - 130$.

Figure 11 also shows the calculated values for the $N' = 1$ levels corresponding to $np0$ and $np2$ states, in order to make a comparison between $N' = 2$ and $N' = 1$; their variations with n and v are largely similar with one major difference: the $9p1, v = 2$ level compared to the $9p0, v = 2$ level, where the former has an individual ionization width of 0.2 cm^{-1} and the latter a calculated width of 5.4 cm^{-1} , measured at $5.1 \pm 1.5 \text{ cm}^{-1}$; the $9p1$ level is located in the quasi continuum of the Rydberg $v = 1$ levels and the $9p0$ level is in the real continuum of the $v = 1$ levels. The ionization widths are essentially dominated by the local perturbations and follow the well-known $\Delta v = 1$ propensity rule.

The $np1$ Rydberg levels are presented in Fig. 11 up to $n = 25 - 30$, whereas for the $np3$ levels, there are very few observations beyond $n = 20$. In the coupling case (d), the dominant decay of the $np3$ levels occurs through the P(3) lines, since in a pure (d) case, the intensity of the R(1) lines is zero, while the $N'' = 3$ levels are twice less populated than the $N'' = 1$ levels.

5.3. Line intensities $N' = 2$

Among the observed 162 R(1) and 83 P(3) lines on the NIM spectra, due to blending, the intensities of 135 R(1) lines and 75 P(3) lines could be measured. The derived values for the Einstein coefficients A , as introduced in Eq. (1), extend over two orders of magnitude ($1.0 \times 10^5 - 1.6 \times 10^7 \text{ s}^{-1}$).

As for the Einstein A -coefficients the MQDT-calculations cover more than 420 pairs of R(1) and P(3) lines to be compared with measured values. Results from the NIM-BESSY and the FT-SOLEIL

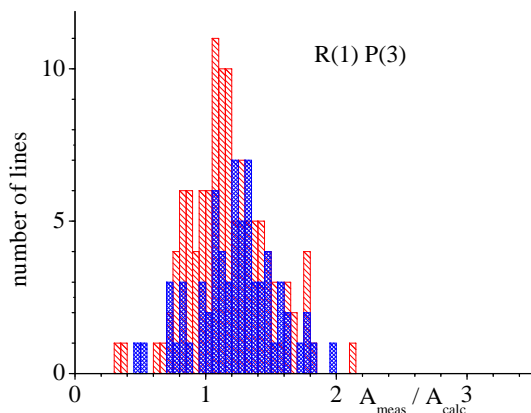


Figure 12: (Color online) Ratios of Einstein coefficients $\rho_A = A_{\text{meas}}/A_{\text{calc}}$ for the R(1) lines (red sparsely hatched pattern) and P(3) lines (blue densely hatched pattern).

experiment are compared with results from calculations in the histogram displayed in Fig. 12. After scaling the intensities in the FT-SOLEIL experiment the intensities of 35 R(1) and 12 P(3) lines could thus be included. The histogram of the ratios $\rho_A = A_{\text{meas}}/A_{\text{calc}}$ can be fitted by a Gaussian function centered at 1.13 ± 0.02 for the R(1) lines and 1.24 ± 0.02 for the P(3) lines with widths around 0.5 cm^{-1} . This demonstrates that the measurements reproduce the calculated values to within 20%, as shown in Fig. 12.

While in most cases the experimental and calculated values are in agreement within the experimental error bars and an estimated uncertainty of 20% for the calculations, there are a few exceptions. For most cases the deviation may be ascribed to blending of lines, but in some specific cases it is related to perturbation effects in the molecular structure. For the $4p\sigma, v = 5, N' = 2$ level the exciting R(1) and P(3) lines are stronger than predicted, with $\rho_A = 1.40 \pm 0.17$ and $\rho_A = 1.75 \pm 0.24$ respectively. The situation is similar for $v = 6$ and $v = 7$ levels.

In excitation to the $5p\sigma, v = 10$ level two lines are observed, both in case of R(1) and P(3) with a fitting combination difference. The summed A values compare very well with the calculated one:

$\rho_A = 1.01 \pm 0.16$ for the R(1) lines and $\rho_A = 1.8 \pm 0.8$ for the P(3) lines. The same holds for excitation of $4p\pi, v = 11$, where two R(1) lines were observed. The summed A values yield $\rho_A = 0.96 \pm 0.14$ for the R(1) lines and for the single P(3) line $\rho_A = 1.2 \pm 0.5$. These examples are similar as those observed for the $5p\pi, v = 4 - 6$ levels in case of $N' = 1$ (see Fig. 4 and section 4.1). This again is associated with a phenomenon beyond the single electron configuration for the Rydberg states. The $6p\sigma, v = 10$ level corresponds to a complex resonance, unresolved in the NIM spectra (but resolved in the FT spectrum). When summing the calculated values of the components one obtains $\rho_A = 1.4 \pm 0.8$ showing rather good agreement. For the ten other lines, for which $\rho_A > 1$ is found outside the error limits, the deviations are mainly due to line blending.

Results on line intensities of R(1) and P(3) lines probing $N' = 2$ excited states are displayed for the $np1, v = 1$ to 7 levels in Fig. 13. Similarly the line intensities probing $np3, v = 1$ to 6 levels are displayed in Fig. 14. The experimental data are compared with line intensity values obtained from MQDT, while also adiabatic values are displayed for comparison, obtained using a $1/n^3$ scaling rule from the $5p\sigma$ and $3p\pi$ lines. Overall, the A values of 189 R(1) and 87 P(3) lines could be determined, among them 44 R(1) and 12 P(3) values from the calibrated FT spectra.

The experimental data show that strong variations occur (up to two orders of magnitude) with respect to the smooth adiabatic decrease. These effects, due to local non-adiabatic perturbations, are well reproduced in the MQDT-calculations. Moreover, the A values of the R(1) lines are larger than the adiabatic values for the $np1$ levels whereas the opposite holds for the P(3) lines. Such a behavior is expected for the change from coupling case (b) to coupling case (d). The opposite is the case for the $np3$ levels shown in Fig. 14.

5.4. Decay dynamics $N' = 2$

Analysis of the NIM-Bessy spectra reveals quantitative information on the decay channels of the $N' = 2$ excited states, with resulting yields plotted in Fig. 15 and values listed in Table 3. Above the ionization limit, ionization does compete not only with

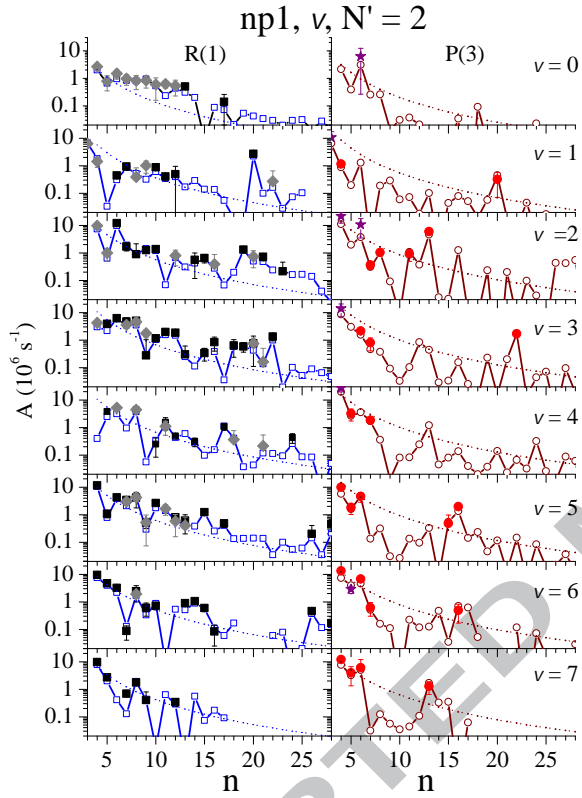


Figure 13: (Color online) Einstein coefficients A for the R(1) lines (left panel) and for the P(3) lines (right panel) for the transitions probing $np1, v = 0$ to 7 levels. Left panel: Open blue squares: calculated value; black squares: measured values from BESSY (NIM); grey diamonds: measured values from SOLEIL (FT). Right panel: Open dark red circles: calculated values; red circles: measured values from BESSY; purple stars: measured values from SOLEIL. The dotted lines refer to adiabatic values.

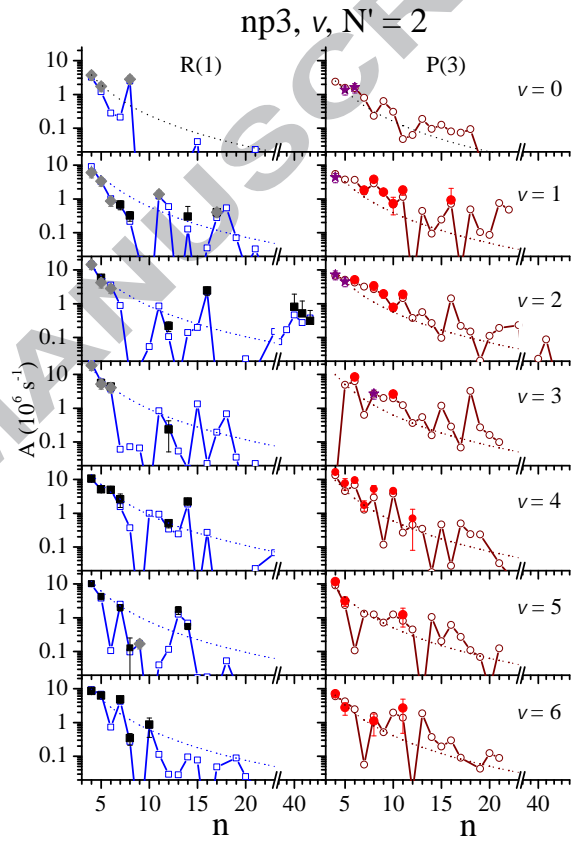


Figure 14: (Color online) Similar as Fig. 13: Einstein coefficients for the transitions probing $np3, v = 0, N' = 2$ levels.

dissociation but also with fluorescence; many more of such occurrences were found in D_2 than in H_2 . In H_2 , seven $N' = 2$ levels had been seen to partly fluoresce, all with $4p\pi$ or $5p\pi$ configuration except one: the $7p\sigma, v = 2$ level [18].

It appears that the dynamics of the $4p\sigma$ levels is more varied than in H_2 [14], where dissociation was the only decay channel. As it is observed for the $N' = 1, 4p\sigma$ levels, also for $N' = 2$ ionization may compete, which is the case for the $v = 8, 10$, and 12 levels in a pronounced manner. For these levels calculated ionization widths were found to be $0.15, 0.11$, and 0.036 cm^{-1} , respectively, contrary to the other $4p\sigma, v$ levels for which the ionization widths lie in the $10^{-6} - 10^{-3} \text{ cm}^{-1}$ range.

For the $4p\pi$ levels, again large variations in the various yields with v are observed, while fluorescence is stronger, indicating that dissociation must be slower. For the $v = 9, 12, 13$ and 14 levels, the calculated ionization widths are particularly high: 5.7×10^{-2} , 2.5×10^{-2} , 2.2×10^{-2} and 0.17 cm^{-1} , respectively. These values are completely correlated to the observed high values of the ionization yield. The $v = 11$ level is seen to be completely dissociated in spite of a large calculated ionization width, but this level is split into two components, indicating that this level may be perturbed outside the single-electron configuration which MQDT approach fails to reproduce. The dissociation of the $4p\pi$ levels proceeds through an indirect coupling: the $4p\pi$ levels are coupled to the predissociated $4p\sigma$ levels through rotational coupling and to the predissociated $3p\pi$ levels through vibrational coupling. Both the $4p\sigma$ and $3p\pi$ levels are predissociated by the same continuum, namely $3p\sigma B^1\Sigma_u^+$, with a possible interference between the two dissociation channels occurring [88].

For the $5p\sigma, N' = 2$ levels, dissociation, fluorescence and ionization compete as was observed for the $N' = 1$ levels as well (see Fig. 10). The radiative lifetime may be estimated from an H_2 measurement at $\approx 8 \text{ ns}$ [89] giving a radiative width of $\approx 7 \times 10^{-4} \text{ cm}^{-1}$. The estimated dissociation widths due to the direct coupling of the $5p\sigma$ state to the $3p\sigma$ continuum are of the order of a few 10^{-5} cm^{-1} , far too small to explain the observed dissociation yields; the dissociation widths must amount to a few 10^{-3} cm^{-1} .

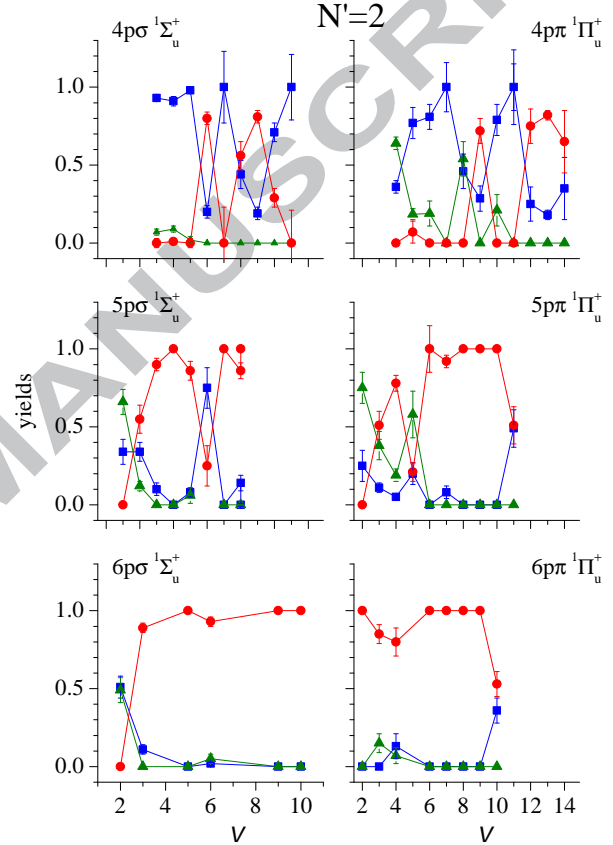


Figure 15: (Color online) Measured yield values for the decay channels of the $4p\sigma$, $5p\sigma$, $6p\sigma$ and $4p\pi$, $5p\pi$, and $6p\pi$ levels of D_2 (all $N' = 2$), plotted as functions of the excited-state vibrational quantum number v . Dissociation: squares (blue); fluorescence: triangles (green); and ionization: circles (red).

Therefore, dissociation must be due to an indirect mechanism, most likely via coupling to the $4p\sigma$ dissociated levels. For the $v = 10$ levels split in two components, the dynamics is not the same for both of them; at 132083.9 cm^{-1} , the dissociation yield is $14 \pm 5 \%$ and at 132088.8 cm^{-1} it is zero. For the $v = 8$ level, the calculated ionization width is particularly small, namely $4 \times 10^{-3} \text{ cm}^{-1}$, explaining that dissociation could compete; even fluorescence was detected but not quantified on the difference spectrum.

For the $5p\pi, N' = 2$ levels, the three decay channels compete as it had been observed for the $N' = 1$ levels, showing that ionization and dissociation are particularly slow.

For the $6p\sigma$ and $6p\pi$ levels located above the ionization threshold, ionization dominates. The values observed for the dissociation yields are correlated to the calculated ionization widths. For the levels with $n > 6$, the $7p\pi, v = 2$ is the only one to partly fluoresce, and the $9p1, v = 5$ level is the only one to be partly dissociated. It is quite surprising that this latter level with such a high n value is not rapidly ionized, since the ionization width of the corresponding $N' = 1$ level in H_2 being 15 cm^{-1} [28]; here a value for $N' = 2$ of H_2 has not been reported. As mentioned before, this level is involved in a complex resonance in the quasi continuum of the $np1, v = 4$ levels and also mixed with the $5p\sigma, v = 8$ and the $3p\pi, v = 15$ levels which are predissociated. This example shows clearly that the interactions are of the multichannel type and not only of the two-channel type. For all the other levels with $n \geq 7$, ionization is the only detected decay channel.

6. Results for $N' = 3$ levels

The experimental results on level energies, widths and line intensities for excitation to the $N' = 3$ excited levels are listed in Table 4, alongside with values derived from the MQDT calculations.

6.1. Level energies $N' = 3$

As many as 134 R(2) lines but only 6 P(4) lines have been identified in the FT spectrum. This disparity reflects the ground state Boltzmann rotational

distribution present in the gas samples used in the FT experiment [27] (150 K and 100 K, respectively). The fractions of the D_2 molecules in the $N'' = 4$ ground state levels are 1% and 10^{-3} , at these temperatures, as compared to 32% and 18%, respectively, for the $N'' = 2$ levels. Only four couples of R(2) and P(4) lines having a common upper level have been observed, and their energy differences agree with the known ground state difference $\Delta_{2,4} = 414.65 \text{ cm}^{-1}$ [62].

A systematic comparison of the 136 $N' = 3$ level energies, measured and assigned in the FT spectra from those predicted by the MQDT calculations, yields: the averaged value for obs.-calc. corresponds to $0.12 \pm 0.01 \text{ cm}^{-1}$ with a spread of 0.58 cm^{-1} .

The differences obs.-calc. are all smaller than 1 cm^{-1} (in absolute values) except for six levels. The $4p\sigma, v = 11$ and the $5p\pi, v = 9$ levels present discrepancies between 1 and 2 cm^{-1} but, for four levels, the discrepancies lie between 5 and 9 cm^{-1} ; they are: the $4p\sigma, v = 13$, the $4p\pi, v = 12$ and 13 and the $5p\pi, v = 10$ levels. All these levels lie above 131000 cm^{-1} , corresponding to low n and high v values exploring large internuclear distances. We postulate that again in this parameter range, the approximation based on the assumption of an isolated $1snp$ configuration is not valid anymore.

Some 165 R(2) and 61 P(4) lines have been identified in the NIM spectra, with 46 pairs of R(2) and P(4) lines exciting the same $N' = 3$ level. Among these 66 R(2) and 60 P(4) lines (with 45 pairs) were not seen in the FT spectrum. Due to a higher sensitivity and higher gas temperature, 81 additional level energies have been determined with the uncertainty of the NIM measurements (1 cm^{-1}). Only a larger discrepancy was found for the $5p\sigma, v = 11$ level (obs.-calc. = 1.9 cm^{-1}) which is located near the dissociation limit.

Due to increasing rotation, the manifold of $N' = 3$ Rydberg levels is more strongly affected by rotational-electronic non-adiabatic interaction than the $N' = 1$ and 2 manifolds presented above. The multichannel perturbations are more and more numerous. As a consequence, more 'complex' resonances occur, where a relatively low- n Rydberg level overlaps with a quasi-continuum of high- n levels. For

$N' = 3$, the $9p2, v = 2$ level lies in the midst of the $np4, v = 1$ manifold with $n \sim 45$. This resonance appears resolved in the FT spectrum, but remains unresolved in the NIM spectrum, as is graphically shown in Fig. 2. Other examples of complex resonances are $7p\sigma, v = 6$ embedded in $np4, v = 4$ with $n \sim 35$, and $6p\sigma, v = 10$ embedded in $np4, v = 6$ with $n = 60$.

The assignment of excited levels based on the MQDT calculations prompted a re-assignment of several lines previously identified by Takezawa and Tanaka [35], who had measured the energies of 41 $N' = 3$ levels.

6.2. Widths of $N' = 3$ levels

The level widths have been determined from the FT and the NIM spectra using deconvolution procedures. The values for the line widths deduced from the two sets of spectra, listed in Table 4, are found in agreement with those of the MQDT-calculations, except in the special cases of complex resonances (see, e.g., the $9p2, v = 2$, R(2) line for which the width measured on the NIM ionization excitation spectrum corresponds to the envelope of the complex resonance). Dissociation and fluorescence may be in competition with ionization. In the case where this competition may be observed, the natural width is of the order of $10^{-3} - 10^{-4} \text{ cm}^{-1}$, smaller even than the instrument width of the FT-measurements. Exceptions are the $3p\pi$ vibration-rotation levels previously studied in [31, 87]. The only natural widths that can presently be experimentally accessed for $n \geq 4$ are due to fast ionization.

Figure 16 compares measured widths with the calculated ionization widths for the $np2$ and $np4, v = 1$ to 5 levels ($v = 0$ levels cannot be ionized) and show very good agreement except for the complex resonance mentioned above. As it was already observed for the case of $N' = 1-2$ (see above), the level widths do not present smooth variations with n ; a sudden increase is found at the $v^+ = v - 1$ threshold, following the propensity rule for vibrational autoionization (cf. Table 1). However, for higher n values, the variations depend mainly on the local perturbations giving rise to a quasi oscillating behavior versus n for the $np2, v \geq 4$ levels. The interactions between the

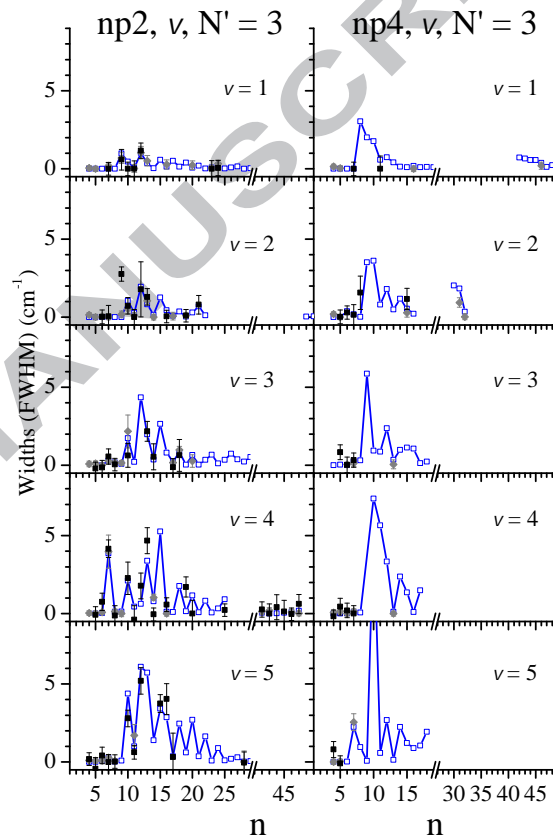


Figure 16: (Color online) Calculated and measured widths of transitions to $np2$ and $np4, N' = 3, v = 1$ to 5 levels. Open blue connected squares: calculated MQDT values; grey diamonds: experimental FT values; black squares: experimental NIM values.

$np2$ and $np4$ series are partly responsible for these variations.

6.3. Line intensities for $N' = 3$

The line intensities for R(2) and P(4) lines have been deduced from the area of the peaks similarly as in the above cases for $N' = 1 - 2$. For deriving the intensities in terms of Einstein A coefficients the Boltzmann populations for $N'' = 2$ and 4 levels, have been accounted for at the prevailing temperatures for the NIM spectra (300 K) and the FT-spectra (100 K and 150 K).

The line intensities, in terms of the corresponding Einstein A coefficients, were calculated for R(2) and P(4) lines in the $117\,000 - 137\,000\text{ cm}^{-1}$ energy range and listed in Table 4. The intensities of 154 R(2) and 50 P(4) lines have been extracted from the NIM spectra, while the calibration of the intensity scale in the FT spectra allowed for the extraction of intensities of 100 R(2) and 4 P(4) lines, among them 21 R(2) and 3 P(4) lines at low energy ($E < 123\,500\text{ cm}^{-1}$), *i.e.* below the NIM recording range. At higher energies, most of the lines were observed in both spectra and the intensities were found to agree within error margins, the uncertainties in the FT spectra being generally larger than those in the NIM spectra. Due to the higher resolution, in a few cases, the FT spectra had a lower uncertainty for lines blended in the NIM spectra, and allowed to measure the intensity for 8 additional R(2) lines.

The measured values of the Einstein A coefficients, graphically displayed in Fig. 17 for the $np2$ levels and in Fig. 18 for the $np4$ levels, cover more than two orders of magnitude: between 3×10^4 and $1.5 \times 10^7\text{ s}^{-1}$. A comparison between measured and calculated values of the A coefficients is presented in Fig. 19 in the form of a histogram. A distribution of relative values of $\rho_A = A_{\text{meas}}/A_{\text{calc}}$ is centered at 1.06 ± 0.03 and a distribution width 0.48. This width is due to the measurement uncertainties (≈ 15 to 20%) as well as to the uncertainties of the calculations (of similar order). A ratio higher than 1 may be due to blended lines; in the case of blending between R(2) lines, as in the case of a complex resonance, the measured value is compared with the sum of the calculated values of the complex resonance (see Table 4).

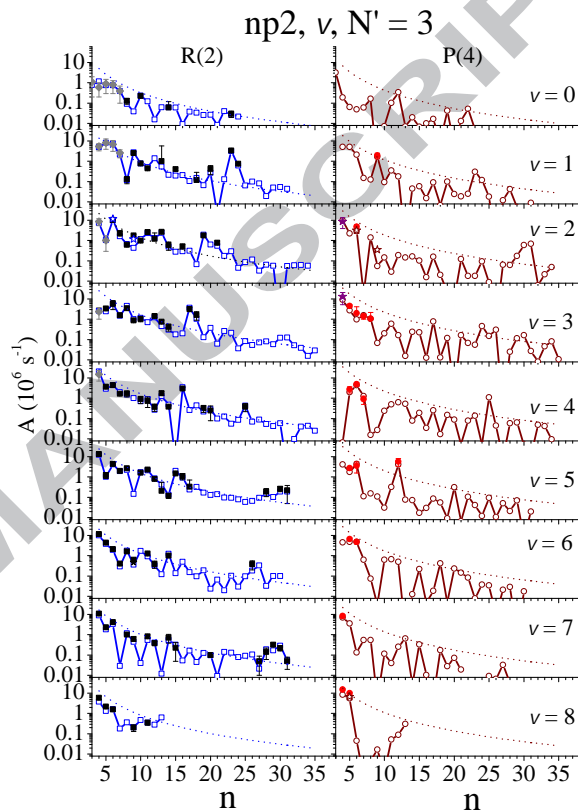


Figure 17: (Color online) Einstein coefficients A for the R(2) lines (right panel) and for the P(4) lines (left panel) for transitions to $np2, v = 0$ levels. Open blue connected squares: calculated R(2) values; grey diamonds: measured values from FT spectrum; black squares: measured R(2) values from NIM spectra; open connected dark (red) circles: calculated P(4) values; red circles: measured P(4) NIM values; full purple stars: measured P(4) FT values. The open stars refer to calculated values summed over a complex resonance ($v = 2$ graphs). The dotted lines refer to adiabatic values.

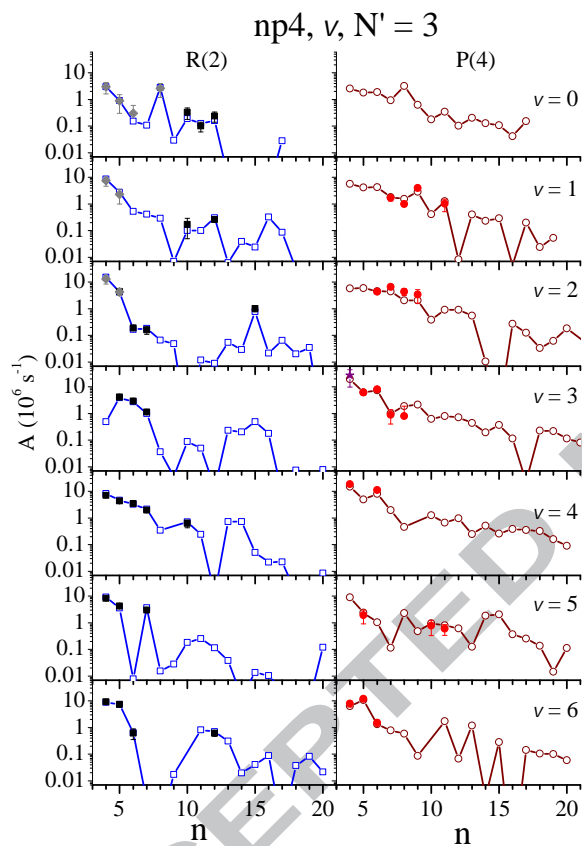


Figure 18: (Color online) Same as Fig. 17: Einstein coefficients for transitions to $np4, v = 0$ to 8 levels.

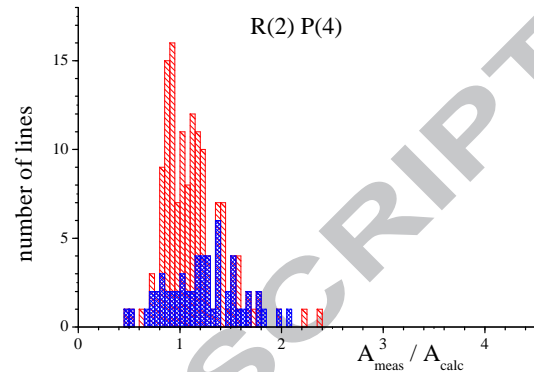


Figure 19: (Color online) Ratios of Einstein coefficients $\rho_A = A_{\text{meas}}/A_{\text{calc}}$ for the R(2) lines (red sparsely hatched pattern) and P(4) lines (blue densely hatched pattern).

An instance of major disagreement concerns the R(2) transition to $4p\sigma, v = 12$. A similar disagreement has been noted previously for the R(1) transition to the same upper state and has been interpreted as being due to shortcomings of the MQDT approach.

Some measured A values are clearly lower than their calculated counterparts, e.g., the A values for the $4p\pi, v = 14$ to 17, R(2) absorption lines. However, the measured values stem from the dissociation excitation spectrum which is monitored by Lyman- α photon detection. The respective upper levels are located above the $D(n = 3)+D(n = 1)$ dissociation threshold and are expected to undergo rapid pre-dissociation. The most probable dissociation channel is through the $B''\bar{B}$ continuum which leads to $D(3s)$ atoms. The $D(3s)$ lifetime is very long (158 ns). During this lifetime, the atoms may collide with molecules and, being placed in the weak electric field used for the ion detection, a fraction of the $D(3s)$ atoms will mix into $D(3p)$ emitting a H_α photon, and then the $D(2s)$ atoms mix again to $D(2p)$ and emit a Lyman- α photon in decay to the ground state; it is this fraction that is detected in the signal channel for dissociation.

Fig. 17 summarizes the results obtained for the $np2, v = 0$ to 8 levels and Fig. 18 for the $np4, v = 0$ to 6 levels. The calculated values reproduce the strong

erratic variations of the measured A coefficients versus n (note the log scale). In the figures the values calculated in the adiabatic approximation are plotted along with the MQDT calculated values and the experimental ones. Globally, the A values decrease with n according to the well-known $1/n^3$ Rydberg scaling rule following the adiabatic predictions. However, several strong variations up to two orders of magnitude are observed on the global decrease, and are due to strong local perturbations. It may be seen that, the MQDT calculated values for the P(4) lines are systematically lower than the adiabatic ones, which is expected for the transition from Hund's coupling case (b) (in the adiabatic approximation) to the coupling case (d) [3].

6.4. Dynamics for $N' = 3$

As seen previously for the $N' = 1$ and 2 levels, the $N' = 3$ levels in D_2 present a more diverse dynamical behavior than in H_2 . Predissociation and autoionization occur through nonadiabatic couplings, which are mass dependent and much slower than in H_2 . On the contrary, fluorescence, which is basically independent of mass, is more often observed to compete in D_2 . Whereas only one H_2 $N' = 3$ level lying above the ionization threshold had been observed to fluoresce [18], 28 $N' = 3$ levels were observed in the fluorescence excitation spectrum of D_2 at the same detection sensitivity. For nearly half of them, the signal is very low; the fluorescence rate could not be determined from the difference spectrum. All these levels correspond to np states with $n \leq 6$, that can be ionized with a $\Delta v \geq 2$ change; consequently, their ionization widths are rather low. The measured dissociation, radiative and ionization decay rates are displayed in Fig. 20 for the $np\sigma$ and $np\pi$, $n = 4$ to 6 levels.

Dissociation is the main decay channel for the $4p\sigma$ levels directly coupled to the $3p\sigma$ B' continuum, and for the $4p\pi$ levels which are coupled to predissociated levels [88]. The $5p\sigma$, $v = 5$ and $5p\pi$, $v = 8$ levels exhibit efficient dissociation, attributed to the fact that these are accidentally coupled to the predissociated $4p\sigma$, $v = 8$ and $4p\pi$, $v = 10$ nearby levels. For the $6p\sigma$ and $6p\pi$ levels, ionization is the main decay channel; some fluorescence may survive. For

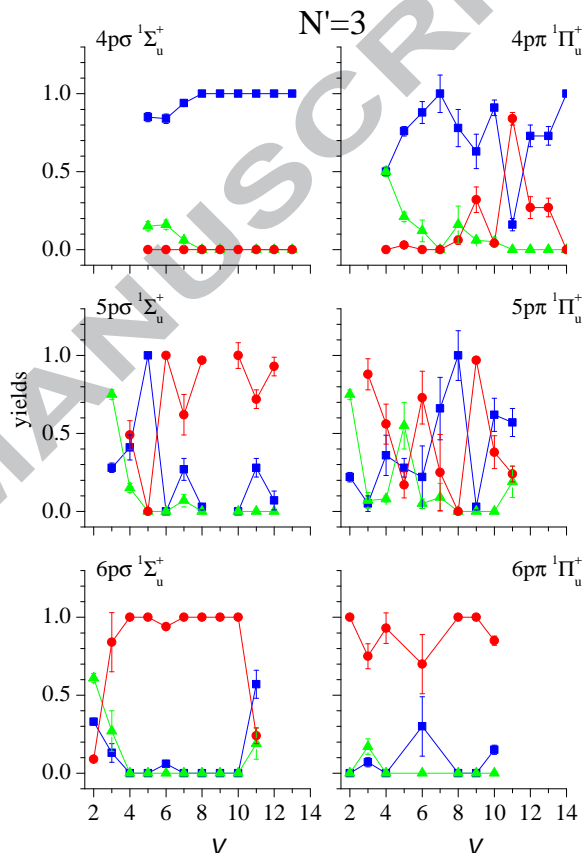


Figure 20: (Color online) Measured yield values for the $4p\sigma$, $5p\sigma$, $6p\sigma$, and $4p\pi$, $5p\pi$, and $6p\pi$ levels of D_2 (all $N' = 3$), plotted as function of the excited-state vibrational quantum number v . Dissociation: blue squares; fluorescence: green triangles; and ionization: red circles.

higher Rydberg levels, ionization is the only observable decay channel. The fluorescence observed for the $5p\pi, v = 11$ and $6p\sigma, v = 11$ levels is probably not molecular but H_α fluorescence, i.e. following dissociation to $D(n = 3)+D(n = 1)$; these levels lie above the dissociation threshold. Overall, the observed large variations in the decay rates are due to local perturbations: the $6p\pi, v = 6$ level is contaminated by the nearby dissociated $4p\sigma, v = 12$ level, as confirmed by the calculated eigenfunctions; this explains the dissociation rate observed for that level. The $4p\pi, v = 11$ level is very weakly coupled to the nearby $10p2, v = 6$ level which has a very large ionization width.

7. Results for $N' = 4$ levels

The experimental results on level energies, widths and line intensities for excitation to the $N' = 4$ excited levels are listed in Table 5, alongside with values derived from the MQDT calculations.

7.1. Level energies for $N' = 4$

On the FT spectra, 43 R(3) lines but not a single P(5) line corresponding to $n \geq 4$ could be identified. The relative population of the $N'' = 3$ level is only 1% and 4% at 100 K and 150 K, respectively, and lower than 10^{-3} for the $N'' = 5$ level. The assignment of excited levels based on the MQDT-calculations prompted a re-assignment of several lines previously identified by Takezawa and Tanaka [35], who had measured the energies of 30 $N' = 4$ levels.

The NIM excitation spectra are measured against a zero (or a small) background, while the FT-spectra are measured against a large continuum. This and the fact that the NIM spectra were recorded for higher gas temperature, these recordings are favorable for the study of weak lines pertaining to higher rotational quantum number. Altogether, on both spectra, a total 76 R(3) lines and 28 P(5) lines were measured in the 123 500 – 133 500 cm^{-1} range. Some 24 R(3) and 13 P(5) lines were observed on both spectra.

The comparison of deviations between observed and calculated values (obs.-calc. listed in Table 5)

were derived for the two types of measurements, yielding good agreement and a spread of 0.4 cm^{-1} (for the FT data) and 1 cm^{-1} (for the NIM data). From these values, the uncertainty of the calculations for $N' = 4$ levels can be estimated at 0.4 cm^{-1} .

7.2. Widths for $N' = 4$

Figure 21 displays the widths for the $N' = 4$ levels in $np3$ and $np5, v = 1$ to 5, accompanied by a comparison with MQDT calculated values. The only R(3) lines that could be observed on the FT spectra are narrow lines for which an upper limit of the width could be derived, except for the $4p\sigma, v = 5$ R(3) line exhibiting a width of $0.5 \pm 0.2 \text{ cm}^{-1}$. This resonance derives its width from dissociation. Generally, because the R(3) or P(5) lines are quite faint, they become observable even in the sensitive NIM experiment only when they are quite sharp so that their peak intensity is high. None of the transitions calculated to have a large width was actually observed, which constitutes an indirect proof of the validity of our calculations.

7.3. Intensities for $N' = 4$

The line intensities have been calculated for nearly 500 pairs of R(3) and P(5) lines in the 117 000 – 137 000 cm^{-1} energy range. For the NIM spectra, the intensities of 74 R(3) and 25 P(5) lines could be measured, and 21 R(3) line intensities were estimated from the FT spectra. The measured values, extending over two orders of magnitude are included in Table 5, and are graphically displayed in Fig. 22 for the $np3, v = 1$ to 7 levels and in Fig. 23 for the $np5, v = 1$ to 7 levels. In the latter figure, for the $6p5, v = 4$ lines, two calculated values are displayed: the individual values for the R(3) and P(5) lines and the values summed over the complex resonance.

The ratios $\rho_A = A_{\text{meas}}/A_{\text{calc}}$ were derived for the case of $N' = 4$ yielding an average value of $\rho_A = 1.14$ with a spread of 0.66. Thus overall, the agreement is good considering experimental uncertainties. However, there are a few specific disagreements where the calculated values lie outside the error margins, i.e. $\rho_A > 1.15$. For the R(3) lines reaching the $5p\sigma, v = 3$, $6p\pi, v = 4$ and $14p3, v = 5$, $N' = 4$ levels, this is due

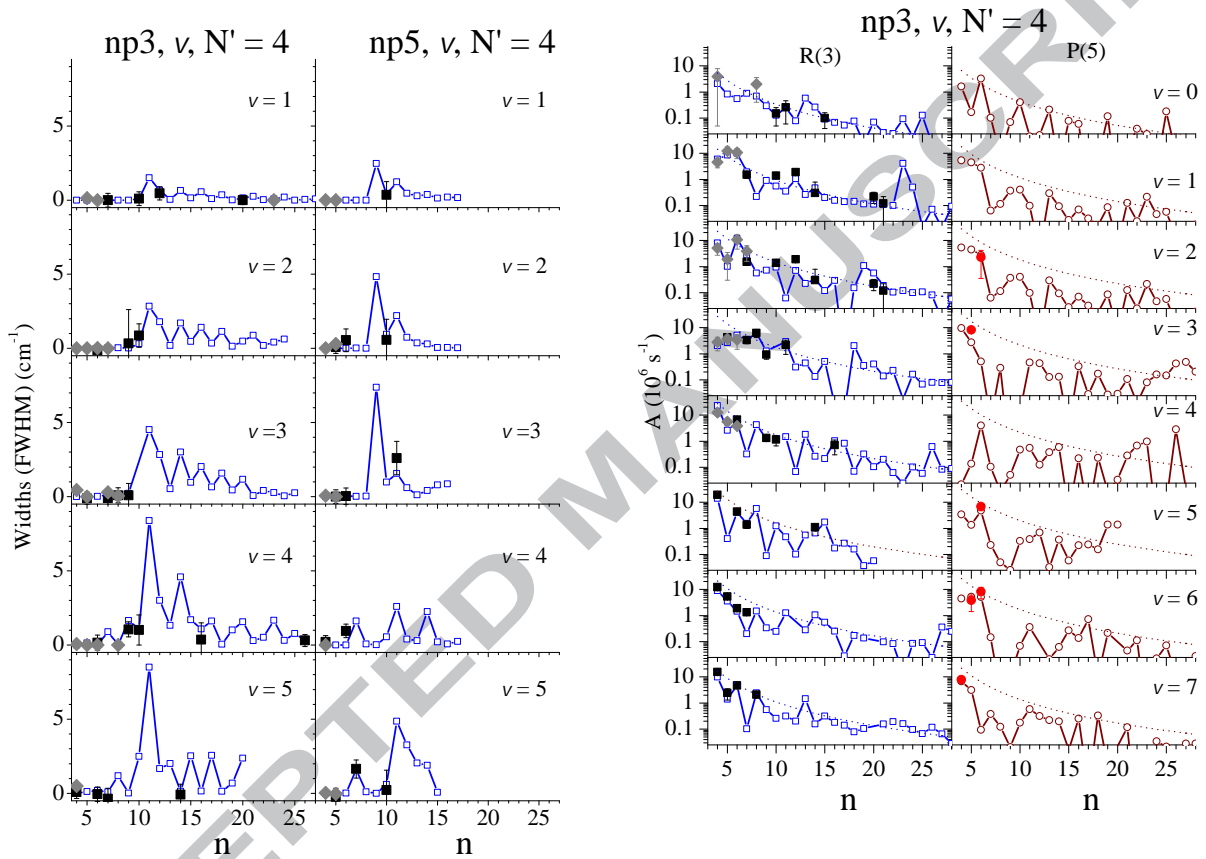


Figure 21: (Color online) Calculated and measured widths of transitions to $np3$ and $np5, v = 1$ to 5 levels (all $N' = 4$). Open blue connected squares: calculated MQDT values; grey diamonds: FT experimental values; black squares: NIM experimental values.

Figure 22: (Color online) Einstein coefficients A for the R(3) lines (left panel) and for the P(5) lines (right panel) for transitions to $np3, v = 0$ to 7 levels. Full black squares: measured R(3) NIM values; full grey diamonds: measured R(3) FT values; open blue squares: calculated R(3) values; full red circles: measured P(5) NIM values; open dark red circles: calculated P(5) values. Dotted lines: adiabatic values.

to blending with the $16p1, v = 0$, R(1), $9p\pi, v = 3$, Q(4) and $6p\pi, v = 7$, P(3) lines, respectively. For the complex resonances, $6p\pi, v = 4$ embedded in the $np3, v = 2$ Rydberg series and $7p3, v = 6$ embedded in the $np5, v = 4$ Rydberg series, the measured values are compared with the calculated ones summed over the resonance. Nevertheless, a few discrepancies remain: the $4p\sigma, v = 7$ and 10 and $5p\sigma, v = 6$, R(3) lines, and the $4p\sigma, v = 8$ and 10, P(5) lines are such cases for which the uncertainties of the calculated values are higher than 15%. These transitions involve upper states corresponding to high vibrational excitation, where the approximation of the isolated np configuration starts to break down. Similar cases were found for lower N'' values (see above).

Overall, the variations of A are seen to follow a pattern corresponding to a $1/n^3$ dependence (*cf.* the dotted lines shown in Figs. 22 and 23, corresponding to the adiabatic approximation). However, pronounced deviations from the regular pattern are found, which may be attributed to strong local perturbations. These perturbations reflect the occurrence of widespread non-adiabatic interactions. Further, the MQDT calculations and/or experimental A values of the P(5) lines are seen to be systematically lower than the adiabatic predictions for the $np3$ levels, and higher for the $np5$ levels. As has been discussed in the above, this is due to the gradual evolution of the upper levels from Hund's case (b) towards Hund's case (d). This evolution is accounted for by the multichannel theory (MQDT), but is disregarded in the adiabatic approximation.

7.4. Decay dynamics for $N' = 4$

The dynamics observed for the $N' = 4$ levels is similar to what is observed for the lower N' levels (see above). For the np levels with $n \geq 6$, ionization, if energetically possible, is the largely prevailing de-excitation channel. Dissociation and fluorescence may compete for lower n values. This is illustrated in Fig. 24.

8. Results for $N' = 5$ levels

The results for $N' = 5$ excited levels are collected in Table 6.

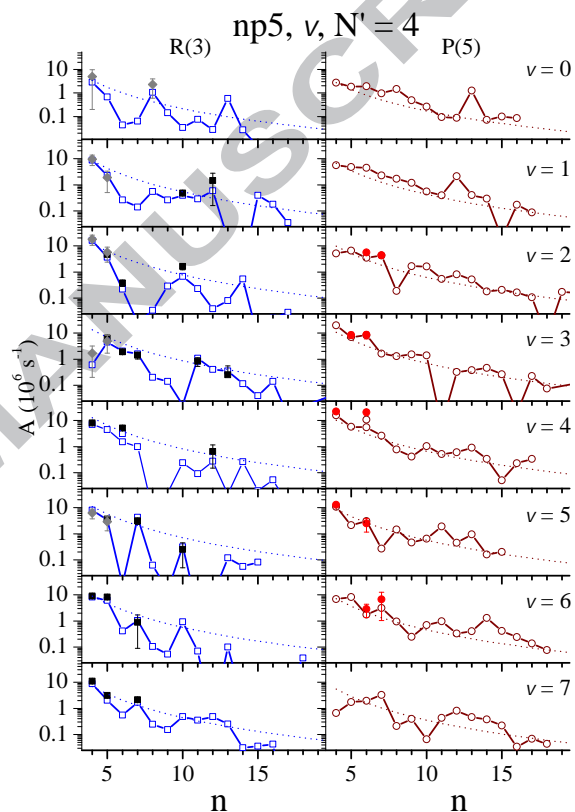


Figure 23: (Color online) Same as Fig. 22 for R(3) and P(5) transitions to $np5, v = 0$ to 7 levels.

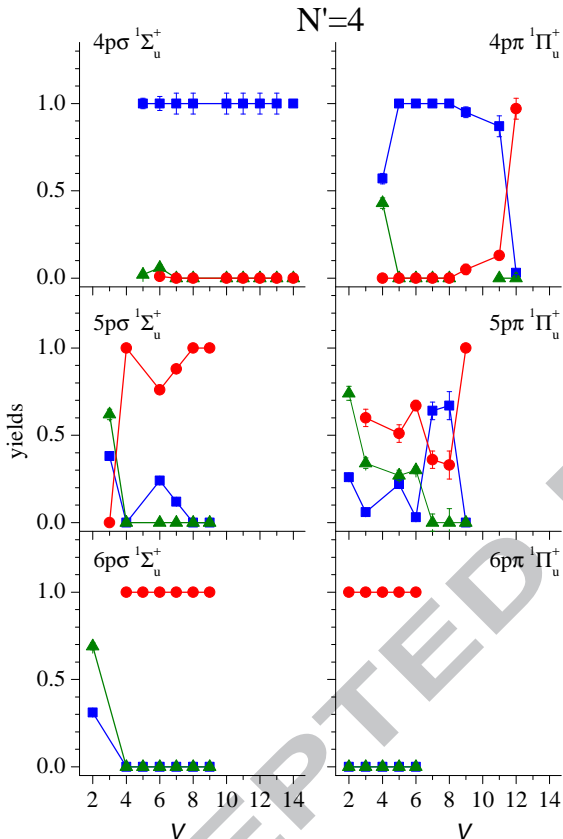


Figure 24: (Color online) Measured yield values for the $N' = 4$ $4p\sigma$, $5p\sigma$, $6p\sigma$, and $4p\pi$, $5p\pi$, $6p\pi$, levels of D_2 , plotted as functions of the excited-state vibrational quantum number v . Dissociation: (blue) squares; fluorescence: (green) triangles; and ionization: (red) circles.

8.1. Level energies of $N' = 5$

The relative population of the $N'' = 4$ level is only 1% at 150 K and 10^{-3} at 100K. The only R(4) lines observed in the FT spectrum lie at low energy below $126\,000\text{ cm}^{-1}$. 23 R(4) lines were observed, of which 15 had been reported previously in [35]. Even though the accuracy of the energy measurement is rather low for these very weak lines, an improvement of accuracy is achieved. No disagreements with previous identifications were found within the error bars. 80 R(4) lines could be assigned in the NIM spectra, among them 11 observed in the FT spectrum, and 3 more previously reported in [35]. A single disagreement is found for the assignments based on MQDT calculation: the $4p\pi, v = 8$, R(4) line, previously located at $128\,860.7\text{ cm}^{-1}$, is calculated at $128\,849.01\text{ cm}^{-1}$ and observed at $128\,851 \pm 1\text{ cm}^{-1}$; the previous value corresponds to the position of the $4p\sigma, v = 10$, R(1) line. Altogether from the NIM spectra, 65 new level energies were measured.

The deviations between experimental and theoretical values (displayed as obs.-calc. in Table 6) yields an average of $0.43 \pm 0.06\text{ cm}^{-1}$ with a spread of 1.6 cm^{-1} . Some levels with low n and high v values show marked discrepancies however: for the $4p\sigma, v = 13$ (obs.-calc. = $7.8 \pm 1.0\text{ cm}^{-1}$), and $4p\pi, v = 13$ (obs.-calc. = $-24.0 \pm 1.0\text{ cm}^{-1}$).

8.2. Widths for $N' = 5$

The transitions observed in the FT spectrum are too faint to allow for a reliable determination of widths. All experimental values of level widths are derived from the NIM measurements. Fig. 25 compares the experimental values with the calculated ones for the $N' = 5$ levels, showing a good overall agreement.

8.3. Intensities for $N' = 5$

The NIM spectra provide intensities for 79 R(4) lines, and the FT-spectra for 11 R(4) lines were estimated. These measured A values extend over two orders of magnitude. The experimental values are compared to calculations which were performed for 200 pairs of R(4) and P(6) lines in the range $117\,000 - 137\,000\text{ cm}^{-1}$. The results are displayed

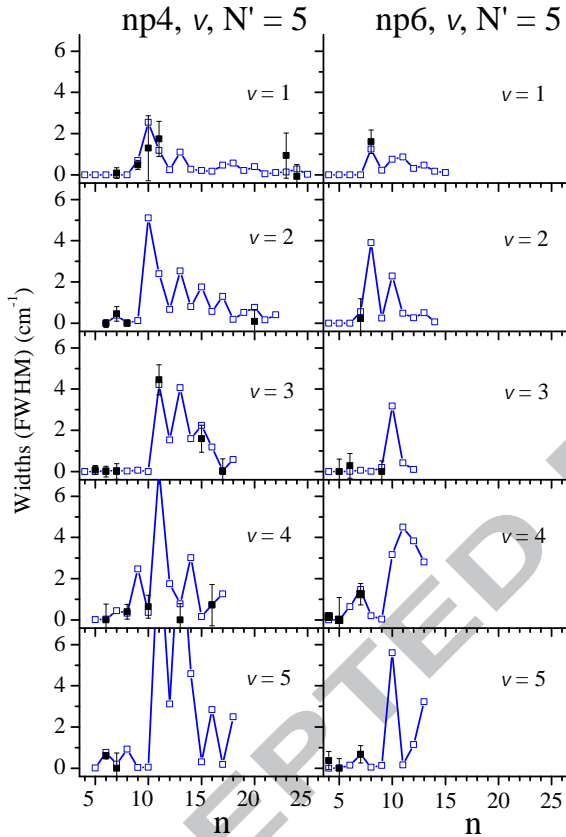


Figure 25: (Color online) Widths of the $np4$ and $np6$, $v = 1 - 5$ levels in D_2 (all $N' = 5$). Open (blue) connected squares: calculated MQDT values; black squares: NIM experimental values.

in Fig. 26. Overall, the measured values and calculated values are found to be in good agreement. Again, similar as for $N' = 4$ a ratio between measured and calculated values is found at $\rho_A = 1.15$ with a spread of 0.5, where the width of the distribution reflects mainly the uncertainties of the measurements. Apart from this trend some pronounced discrepancies between experiment and theory are found. One of these concerns a value $\rho_A < 1$: the $R(4) 5p\pi$, $v = 8$ line which is blended with 3 other lines and measurement corresponds to the dissociation channel only, *i.e.* on a partial cross section.

In addition cases with $\rho_A > 1$ are found. These are: the $6p\sigma$, $v = 2$, $11p4$, $v = 0$, and $4p\sigma$, $v = 7$ and 8 , $R(4)$ lines. In the first case the upper level is part of a complex resonance. By assuming the A_{calc} values over all sublevels of the complex resonance we obtain a value that agrees to within the experimental uncertainty (15%) with the observed value. In the second case the observed transition appears isolated in the spectrum and is observed in the dissociation spectrum. Couplings may possibly be invoked here, but the reason for the discrepancy between experiment and theory remains unclear at this point. Finally, the $4p\sigma$, $v = 7$ and 8 , $N' = 5$ are not well reproduced by MQDT, no doubt for reason of breaking down of the single electron configuration $1snp$.

8.4. Decay dynamics for $N' = 5$

Again, the dynamics observed for the $N' = 5$ levels follows the pattern found for lower N' . For the $n \geq 6$, ionization is the preferred de-excitation channel if energetically allowed, while dissociation and fluorescence may compete for lower n values. Results for the decay dynamics of $N' = 5$ levels are illustrated in Fig. 27.

A few levels located above the ionization threshold have been observed to fluoresce. This can happen only when dissociation and ionization themselves are very slow decay processes with decay times of the order of 1 ns or 0.1 ns. A 6% fluorescence yield has been observed for the $4p\sigma$, $v = 6$, $N' = 5$ upper level. From the various measured yield values for this level and the corresponding fluorescence lifetime measured on H_2 [89] the dissociation width may be estimated at 10^{-2} cm^{-1} and the ionization width at 10^{-4} cm^{-1} .

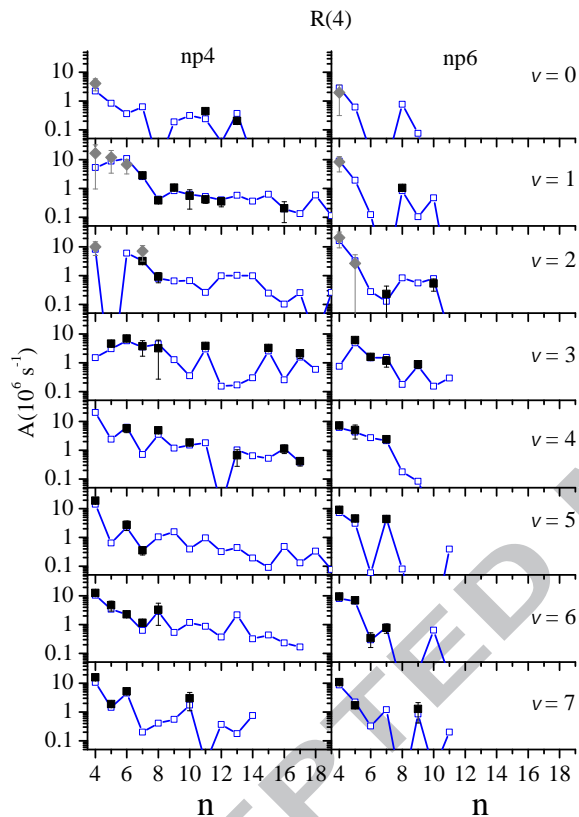


Figure 26: (Color online) Einstein coefficients A for R(4) transitions to $np4$ and $np6$, $v = 0$ to 7 levels for $N' = 5$. Full (black) squares: measured NIM values; full (grey) diamonds: measured FT values; open (blue) squares: calculated MQDT values.

The MQDT calculated value of the ionization width is $2 \times 10^{-4} \text{ cm}^{-1}$ and the dissociation width may be estimated to be $4 \times 10^{-2} \text{ cm}^{-1}$ by use of a perturbative approach similar to that in [28]. The orders of magnitude are thus consistent.

9. Results for $N' = 6$ levels

Results for $N' = 6$ are listed in Table 7.

9.1. Level energies for $N' = 6$

The $N' = 6$ levels are observed only via R(5) transitions. In the FT spectra no R(5) lines were detected whereas 23 R(5) lines were observed on the NIM spectra, none of them having been previously reported. The deviations between obs.-calc. values for $N' = 6$ lie between -2.7 and $+2.4 \text{ cm}^{-1}$.

9.2. Widths for $N' = 6$

The R(5) lines are very faint even on the NIM spectra because the relative population of $N'' = 5$ at room temperature is only 1.4%. Therefore only transitions with low n ($n \leq 8$) and intrinsically high A are observed. The observed widths agree with the calculated values in all cases within the error bars.

9.3. Intensities for $N' = 6$

On the NIM spectra, 23 R(5) lines were identified but only 16 of them allowed intensity measurements because the 8 others were isolated only in the fluorescence or dissociation channels. Due to the small value of the relative population of the $N'' = 5$ level, these lines appear only weakly in the spectrum. The measured A values are spread over one order of magnitude only. All observations correspond to low Rydberg states with $n \leq 8$ with a single exception: the $23p5$, $v = 1$, R(5) line located at 125645 cm^{-1} . Its upper level is strongly mixed with the $8p5$, $v = 2$, the $6p5$, $v = 3$ and $4p\sigma$, $v = 7$ levels; this strong mixing induces an abnormally large A value for this R(5) transition.

The experimentally determined Einstein A coefficients have been compared with calculations, which were performed for nearly 200 R(5) lines in the $117000 - 137000 \text{ cm}^{-1}$ energy range. The ratios

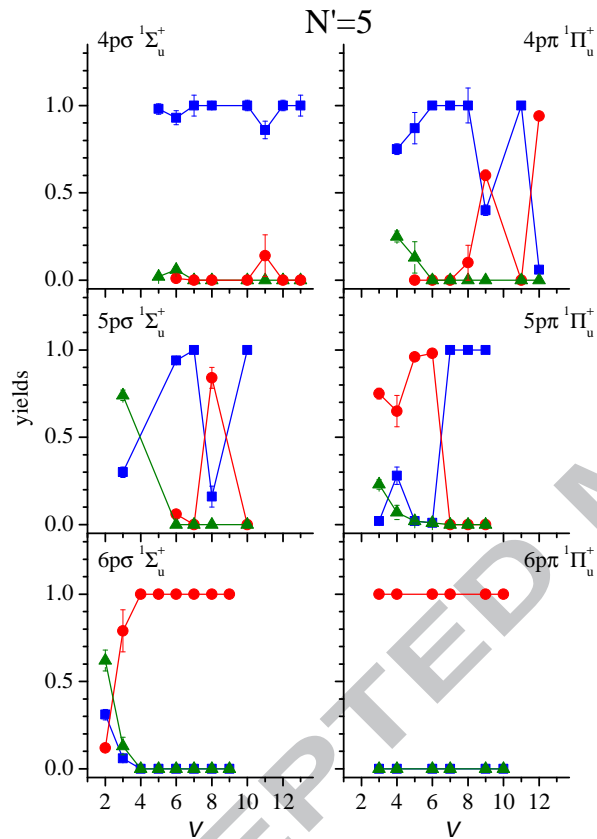


Figure 27: (Color online) Measured yield values for the $4p\sigma$, $5p\sigma$, $6p\sigma$, and $4p\pi$, $5p\pi$, $6p\pi$, levels of D_2 (all $N' = 5$), plotted as function of the excited-state vibrational quantum number v . Dissociation: (blue) squares; fluorescence: (green) triangles; and ionization: (red) circles.

ρ_A are reasonably close to unity with two large exceptions: the $6p\sigma, v = 2$ and $5, R(5)$ lines with $\rho_A = 1.7 \pm 0.2$ and 2.2 ± 0.4 , respectively. For these lines no blending was observed that might easily explain the discrepancy.

10. Discussion and Conclusion

This study presents the experimental observation of rovibrational states of Rydberg character in the D_2 molecule in absorption from the ground state in the energy range above the second dissociation limit $D(n = 2) + D(n = 1)$. Two different experimental techniques and setups are used, both connected to synchrotron radiation facilities. One is the Fourier-transform spectrometer in the vacuum ultraviolet wavelength range, a unique instrument attached to the DESIRS beamline at the SOLEIL synchrotron, providing high resolution absorption spectra. The other is the BESSY-II 10m normal incidence monochromator, providing excitation spectra yielding information on dissociation, ionization and fluorescence alongside with direct absorption providing absolute cross sections. The paper focuses on the physical properties of $np\sigma^1\Sigma_u^+$ and $np\pi^1\Pi_u^+$ series (for $n \geq 4$) and for excited rotational states with $N' = 1 - 6$, where previously states of $N' = 0$ [27, 33], and $np\pi^1\Pi_u^-$ character [34, 26], as well as the $3p\pi D^1\Pi_u$ state [31] had been investigated. Also the $2p\pi C^1\Pi_u$, $2p\sigma B^1\Sigma_u^+$ states, and the $3p\sigma B^1\Sigma_u^+$ state below the second dissociation limit in D_2 [32] had been studied with the FT-VUV-SOLEIL setup, in the range where dissociation effectively does not occur. The present work considerably extends the knowledge of the $^1\Sigma_u^+$ and $^1\Pi_u^+$ excited states of the D_2 molecule beyond what was the early work of Monfils [36] and Takezawa and Tanaka [35]. Specifically the observations have been extended to higher vibrational quantum numbers up close to the $D(1s) + D(n = 4)$ dissociation limit. Further, the use of the VUV Fourier-Transform spectrometer at the SOLEIL synchrotron facility has enabled the accuracy to be improved considerably, namely to a few 0.01 cm^{-1} and the measurements of the natural widths of the excited levels, down to $1/3$ of the Doppler width of 0.15 cm^{-1}). The use of the BESSY II 10-m normal

incidence monochromator enabled the measurements of the line intensities, on an absolute scale, not only for the most intense lines but also for lines with A values as small as a few 10^4 s^{-1} . It enables the study of the dynamics of the levels with evidence of decay processes slower than 1 ns.

Of the entire data set recorded, covering nearly 2000 lines, a significant fraction was previously assigned to $np\pi^1\Pi_u^-, N'$ [34, 26] and $np\sigma^1\Sigma_u^+, N' = 0$ [27, 33]. In this study more than a thousand lines were assigned to $np\sigma^1\Sigma_u^+$ and $np\pi^1\Pi_u^+$ series (for $n \geq 4$) and transition frequencies, natural linewidths, line intensities, and competing decay channels quantitatively addressed, and results tabulated. While the $np\sigma^1\Sigma_u^+, N' = 0$ levels do not exhibit $\Pi \sim \Sigma$ interactions for the reason that Π states do not support $N' = 0$ levels, the $np\pi^1\Pi_u^-, N'$ states neither exhibit $\Pi \sim \Sigma$ interactions, in this case for reasons of electronic symmetry. The presently observed $np\sigma^1\Sigma_u^+$ and $np\pi^1\Pi_u^+$ states do exhibit the full range of possible interactions including those of $\Pi \sim \Sigma$ nature. The combination of these studies marks the complete analysis of the VUV absorption spectrum of the D_2 molecule.

The MQDT approach has served as a theoretical tool for the analysis of the complex D_2 absorption spectra. A great advantage of this MQDT-framework is that it describes both the level structure of the excited states as well as their dynamics in a comprehensive formalism.

The overall agreement between observed and calculated excited level positions is very good. For transitions to the lowest levels $N' = 1 - 3$ the averaged deviations are as low as 0.1 cm^{-1} , with a spread of the distribution function 0.25 cm^{-1} for $N' = 1$, 0.42 cm^{-1} for $N' = 2$, and 0.58 cm^{-1} for $N' = 3$. This establishes an indication for the accuracy of the fully *ab initio* MQDT calculations for these highly excited autoionizing states in D_2 : at the level of a few 0.1 cm^{-1} . For transitions to higher angular momentum states the deviations are larger, with spread of the distribution function of deviations amounting to 1.6 cm^{-1} for $N' = 5$ and 2.5 cm^{-1} for $N' = 6$. The higher N' values are probed mainly in the NIM-spectra, hence at lower accuracy, for the most part explaining the deviations. It might be possible also that the MQDT

theory is slightly less accurate. The inaccuracy of the frame transformation applied in QDT increases with the splitting of the ion thresholds as well as with the multipole moments of the ion core. The former scales with the operator $2BN^+$, so that the approach might become less accurate for higher N' values [68]. However, in the case of the MQDT-analysis of the CaF molecule discrepancies were not observed to increase with N' up to 14 [90], although the detailed analysis based on the formulae given in [68] indicates that the deviations should be as serious as in D_2 .

Larger deviations up to 10 cm^{-1} occur for a number of lines and are attributed to specific shortcomings of the theory. As stated in the theoretical section above, electronic core-excited channels are not explicitly included in the multichannel calculations, but only indirectly inasmuch as they contribute to the core-ground state channels (this is the case because the Born-Oppenheimer potential curves from which the quantum defects are extracted do include configuration interaction (CI) contributions that stem from core-excited electronic states). In addition, $\ell > 1$ partial waves have been disregarded. Despite these in principle rather severe restrictions - and indeed somewhat surprisingly - only 27 spectral lines remain unassigned at this stage. These are listed in Table 8. Based on past experience with H_2 [70], we conjecture that these represent mainly transitions to nf Rydberg levels, but this remains to be verified. The fact that these lines appear all in fluorescence, demonstrating the resistance of the excited states to rapid dissociation and ionization, may be regarded as evidence for this hypothesis. Some of the lines (7 in total) are however also observed in the dissociation channel, but here dissociation must be slow, since the lines do also appear in fluorescence. These unassigned lines may in the future be applied as long-lived stepping stones in multi-step laser excitation, as e.g. in [91, 92, 93, 94] and in searches for states of Σ^- symmetry in the hydrogen molecule [95, 96, 97]. Another shortcoming of the present theoretical analysis lies in the implicit exclusion of dissociation processes. Future re-analysis shall yield theoretical values for the various quantum yields listed in the present experimental Tables.

The spectroscopic results can be compared with re-

sults of previous studies, as reported by Monfils [36] and Takezawa and Tanaka [35], and tabulated by Freund et al. [13]. It is obvious that the older work, relying on classical absorption techniques and lacking the theoretical support was less complete and less accurate. The deviations found in Ref. [35] mostly fall consistently within the experimental accuracy of $\pm 0.6 \text{ cm}^{-1}$ claimed in their study. For several additional lines, mostly leading to Rydberg levels with $n > 7$, the discrepancies remain below $\pm 1.6 \text{ cm}^{-1}$, still within fair agreement considering a possible pressure shift, an effect already mentioned previously [3, 26]. A few discrepancies were found that are likely to be misprints: $4p\sigma, v = 4$, $P(2)$, $8p\sigma, v = 0$, $P(3)$, $9p\pi, v = 0$, $R(2)$, and $6p\pi, v = 0$, $R(2)$ lines. For each N' level some specific misassignments were found, in total 53, which are listed in Table 9. Many of them concern the Rydberg levels for which the coupling case (b) is no longer valid; the transition from case (b) to (d) as illustrated in Fig. 3 had not been considered in the earlier studies. The levels are not pure BO-levels, but due to non-adiabatic couplings form mixtures of levels. When labeling the states according to their main configuration the $5p\sigma, v + 1, N'$ and $6p\sigma, v, N'$ levels, had to be interchanged (for $N' = 1 - 3$):

$$\begin{aligned} 5p\sigma, v = 2 &\leftrightarrow 6p\sigma, v = 1 \\ 5p\sigma, v = 3 &\leftrightarrow 6p\sigma, v = 2 \\ 5p\sigma, v = 4 &\leftrightarrow 6p\sigma, v = 3 \end{aligned}$$

In Ref. [35], the non-adiabatic couplings were limited to pairs of levels while a full multichannel study is necessary. Several reassignments are linked to these multichannel couplings: for instance, the line previously assigned to the $9p\sigma, v = 0$, $R(0)$ line is the $6p\pi, v = 1$, $R(0)$ line; the line previously assigned to the $5p\sigma, v = 2$, $R(2)$ at $123\,122.6 \text{ cm}^{-1}$ is the $8p\pi, v = 0$, $R(2)$ line. Many reassignments are due to the blending of rotational lines of various vibronic levels: the reported $10p1, v = 1$, $R(1)$ line is in fact the $3p\pi, v = 9$, $P(2)$ line, and many other examples.

The use of the BESSY-NIM instrument enabled the measurements of the intensities of nearly 1000 lines, on an absolute cross section scale, in the $124\,000 - 137\,000 \text{ cm}^{-1}$ spectral range; it permit-

ted also the calibration of the absorption FT spectra on an absolute scale, extending the line intensity measurement to the $117\,000 - 124\,000 \text{ cm}^{-1}$ spectral range. The experimental data show that strong variations occur (up to two orders of magnitude) with respect to a smooth adiabatic decrease. These effects, due to local non-adiabatic perturbations, are well reproduced in the MQDT-calculations. The transition, as n increases, from coupling case (b) to coupling case (d) is clearly observed. The various histograms of $\rho_A = A_{\text{meas}}/A_{\text{calc}}$ can be fitted by Gaussian functions centered at 1.2 ± 0.2 with a width (FWHM) around 0.5. The uncertainty of the A_{calc} values can be estimated at 10 to 20%, depending on the importance of the influence of the dissociation continuum. The values of the ratios ρ_A are compatible with unity within the error bars for a very large majority of the cases, demonstrating agreement with theory. All the disagreements are discussed and attributed to the limits of the MQDT treatment with a single configuration.

Natural line widths were determined from the observed spectra via deconvolution of the Doppler width and apparatus function. The natural widths observed ($> 0.15 \text{ cm}^{-1}$) for the levels under study ($n \geq 4$) are only due to ionization. Even for the $4p\sigma$ levels the broadening due to dissociation could not be experimentally proven, except for a single level $N' = 4, 4p\sigma, v = 5$. Hence, the experimental widths can be compared with calculated autoionization widths. Good agreement was found for all levels except for those forming complex resonances for which the observed width equals the envelope of the resonances. The largest widths for H_2 had been found for $n = 8$ [21, 22], whereas the largest widths in D_2 occur at $n = 10$. This may be attributed to the relative location of the ionic level v^+, N^+ with respect to the excited states in the neutral, falling in between $8pN^+$ and $9pN^+$, ($v' = v^+ - 1$) levels for H_2 and in between the $10pN^+$ and $11pN^+$ levels for D_2 , written in Hund's coupling case (d). This phenomenon is entirely due to the location of the ionization potential and governed by the propensity rule for strong vibrational autoionization (cf. Table 1).

The BESSY-NIM experiment with the simultaneous measurements of the absorption spectrum with

the dissociation, ionization and fluorescence excitation spectra allowed the study of the competing decay behavior of the $np\pi^1\Pi_u^+$ and $np\sigma^1\Sigma_u^+$ levels with $4 \leq n \leq 6$. The general trend is primarily dissociation at $n = 4$, going through a transition regime at $n = 5$ to $n = 6$, where ionization becomes fully dominant. Due to our absolute absorption and partial decay cross section measurements, we were able to characterize these slow processes in detail despite the fact that the corresponding natural widths of the excited states studied here are orders of magnitude smaller than their experimental spectral broadening, limited by the Doppler width. So, while the fast dynamical processes are sampled in a direct manner via a linewidth measurement, the slow decay processes are indirectly quantified from comparison of absolute line intensities in absorption and emission.

From estimated fluorescence lifetimes, it was possible to estimate dissociation widths as small as 10^{-5} cm^{-1} , for example for the $10p0, v = 0, N' = 1$ level, far below the limits of the FT line width measurements. The $4p\sigma$ levels of H_2 present a dissociation width of around 2 cm^{-1} [14], but all the $4p\sigma$ levels in D_2 , except the aforementioned $N' = 4, 4p\sigma, v = 5$ level, exhibit widths smaller than 0.15 cm^{-1} , and were even found to fluoresce in which case the corresponding dissociation width may be estimated at about 10^{-2} cm^{-1} . Such results on widths strongly deviate from values corresponding to mass-dependent scaling laws.

Our analysis of the newly recorded absorption spectrum of D_2 considerably extends the knowledge on the spectroscopy and dynamics of highly excited singlet *ungerade* states of diatomic deuterium. The detailed information is laid down in the extensive Tables accompanying the present text. Beyond their intrinsic value, these data may also become useful for the analysis of novel experimental developments. In H_2 for instance, it has recently become possible to perform precision measurements of highly excited vibrational states in the ground state ($v'' = 11$ and 12) at an accuracy of 0.002 cm^{-1} [98, 99]. These levels are populated via the photodissociation of H_2S , while their detection requires a 3-photon scheme leading to photoionization of the hydrogen molecule into the singlet *ungerade* channels. The last step involves ex-

citation from the $F^1\Sigma_g^+, v = 0$ level, which replaces the $X^1\Sigma_g^+, v = 0$ level of ordinary absorption [100]. The planning and success of such experiments, as well as their analysis, hinge on the quantitative understanding of the channel structures governing the ionization step.

In conclusion, a wealth of spectral data in the vacuum ultraviolet spectrum of the D_2 molecule is presented, listing accurate wavelength positions for a thousand spectral lines, with line intensities, line widths and information on competing decay processes. The experimental data are compared with results from fully *ab initio* MQDT calculations finding excellent agreement on the various properties of the spectra, making this study a benchmark in molecular spectroscopy of highly excited states in diatomic molecules.

Acknowledgements

The authors thank N. de Oliveira and D. Joyeux for their help in the data acquisition at SOLEIL and L. Nahon for his constant support. We are also indebted to the general staff of Synchrotron SOLEIL for their support on the DESIRS beamline. We acknowledge the Helmholtz-Zentrum Berlin - Electron storage ring BESSY II - for providing synchrotron radiation at the beamline U125/2-10m-NIM. In particular we would like to thank G. Reichardt and A. Balzer for their assistance with the experiments at Berlin. The research leading to these results has received funding from the European Community's Seventh Framework Programme (FP7/2007-2013) under grant agreement No. 226716. CJ thanks the Miescher Foundation (Basel, Switzerland) for partial support. WU acknowledges the European Research Council for an ERC-Advanced grant under the European Union's Horizon 2020 research and innovation programme (grant agreement No 670168).

References

- [1] T. Lyman, The spectrum of hydrogen in the region of extremely short wavelengths, *Astroph. J.* **23** (1906) 181–210.

- [2] S. Werner, Hydrogen bands in the ultra-violet Lyman region, Proc. R. Soc. London Ser. A 113 (1926) 107–119.
- [3] G. Herzberg, Ch. Jungen, Rydberg series and ionization potential of the H₂ molecule, J. Mol. Spectr. 41 (1972) 425–486.
- [4] P. M. Dehmer, W. A. Chupka, Very high resolution study of photoabsorption, photoionization, and predissociation in H₂, J. Chem. Phys. 65 (1976) 2243–2273.
- [5] W. A. Chupka, Photoionization of molecular Rydberg states: H₂, C¹Π_u and its doubly excited states, J. Chem. Phys. 87 (1987) 1488–1498.
- [6] P. Borrell, P. M. Guyon, M. Glass-Maujean, H₂ and D₂ photon impact predissociation, J. Chem. Phys. 66 (1977) 818–827.
- [7] P. M. Guyon, J. Breton, M. Glass-Maujean, Predissociation of the ¹Π_u states of H₂: Measurement of the various dissociation yields, Chem. Phys. Lett. 68 (1979) 314–319.
- [8] J. Breton, P. M. Guyon, M. Glass-Maujean, Radiative emission from singlet superexcited levels of H₂, Phys. Rev. A 21 (1980) 1909–1913.
- [9] H. Bredohl, G. Herzberg, The Lyman and Werner bands of deuterium, Can. J. Phys. 51 (1973) 867–887.
- [10] I. Dabrowski, G. Herzberg, The absorption spectrum of D₂ from 1100 to 840 Å, Can. J. Phys. 52 (1974) 1110–1136.
- [11] P. C. Hinnen, W. Hogervorst, S. Stolte, W. Ubachs, Sub-Doppler laser spectroscopy of H₂ and D₂ in the range 92–98 nm, Can. J. Phys. 72 (1994) 1032–1042.
- [12] M. Roudjane, T. I. Ivanov, M. O. Vieitez, C. A. de Lange, W.-U. L. Tchang-Brillet, W. Ubachs, Extreme ultraviolet laser calibration of D₂ Lyman and Werner transitions, Mol. Phys. 106 (2008) 1193–1197.
- [13] R. S. Freund, J. A. Schiavone, H. M. Crosswhite, The electronic spectrum and energy levels of the deuterium molecule, J. Phys. Chem. Ref. Data 14 (1985) 235–383.
- [14] M. Glass-Maujean, S. Klumpp, L. Werner, A. Ehresmann, H. Schmoranzer, Study of the B''B¹Σ_u⁺ state of H₂: Transition probabilities from the ground state, dissociative widths, and Fano parameters, J. Chem. Phys. 126 (2007) 144303.
- [15] M. Glass-Maujean, S. Klumpp, L. Werner, A. Ehresmann, H. Schmoranzer, Transition probabilities from the ground state of the npπ¹Π_u⁻ states of H₂, Mol. Phys. 105 (2007) 1535–1542.
- [16] M. Glass-Maujean, S. Klumpp, L. Werner, A. Ehresmann, H. Schmoranzer, The study of the D¹Π state of H₂: Transition probabilities from the ground state, predissociation yields, and natural linewidths, J. Chem. Phys. 128 (2008) 094312.
- [17] M. Glass-Maujean, S. Klumpp, L. Werner, A. Ehresmann, H. Schmoranzer, The study of the fifth ¹Σ_u⁺ state 5pσ of H₂: Transition probabilities from the ground state, natural line widths and predissociation yields, J. Mol. Spectr. 249 (2008) 51–59.
- [18] M. Glass-Maujean, Ch. Jungen, G. Reichardt, A. Balzer, H. Schmoranzer, A. Ehresmann, I. Haar, P. Reiss, Competing decay-channel fluorescence, dissociation, and ionization in superexcited levels of H₂, Phys. Rev. A 82 (2010) 062511.
- [19] M. Glass-Maujean, Ch. Jungen, H. Schmoranzer, A. Knie, I. Haar, R. Hentges, W. Kielich, K. Jänkälä, A. Ehresmann, H₂ superexcited states: Experimental and theoretical characterization of their competing decay-channel fluorescence, dissociation, and ionization, Phys. Rev. Lett. 104 (2010) 183002.
- [20] M. Glass-Maujean, Ch. Jungen, H. Schmoranzer, I. Haar, A. Knie, P. Reiss,

- A. Ehresmann, The transition probabilities from the ground state to the excited $J = 0$ ${}^1\Sigma_u^+$ levels of H_2 ; Measurements and ab initio quantum defect study, *J. Chem. Phys.* 135 (2011) 144302.
- [21] M. Glass-Maujean, H. Schmoranzer, I. Haar, A. Knie, P. Reiss, A. Ehresmann, The $J = 1$ para levels of the $v = 0$ to 6 np singlet Rydberg series of molecular hydrogen revisited, *J. Chem. Phys.* 136 (2012) 134301.
- [22] M. Glass-Maujean, H. Schmoranzer, I. Haar, A. Knie, P. Reiss, A. Ehresmann, The $J = 2$ ortho levels of the $v = 0$ to 6 np singlet Rydberg series of molecular hydrogen revisited, *J. Chem. Phys.* 137 (2012) 084303.
- [23] M. Glass-Maujean, Ch. Jungen, A. Spielfiedel, H. Schmoranzer, I. Tulin, A. Knie, P. Reiss, A. Ehresmann, Experimental and theoretical studies of excited states of H_2 observed in the absorption spectrum: I. The $5p\pi$ D'' ${}^1\Pi_u$ state, *J. Mol. Spectr.* 293–294 (2013) 1–10.
- [24] M. Glass-Maujean, Ch. Jungen, H. Schmoranzer, I. Tulin, A. Knie, P. Reiss, A. Ehresmann, Experimental and theoretical studies of excited states of H_2 observed in the absorption spectrum: II. The $6p\pi$ and $7p\pi$ ${}^1\Pi_u$ states, *J. Mol. Spectr.* 293–294 (2013) 11–18.
- [25] M. Glass-Maujean, Ch. Jungen, H. Schmoranzer, I. Tulin, A. Knie, P. Reiss, A. Ehresmann, Experimental and theoretical studies of excited states of H_2 observed in the absorption spectrum: III. The $5p\sigma$, $6p\sigma$ and $7p\sigma$ states, *J. Mol. Spectr.* 293–294 (2013) 19–26.
- [26] M. Glass-Maujean, A.-M. Vasserot, Ch. Jungen, H. Schmoranzer, A. Knie, S. Kübler, A. Ehresmann, Experimental and theoretical study of the $(np\pi)$ ${}^1\Pi_u^-$ ($n \leq 4$) excited states of D_2 : Absolute absorption cross sections and branching ratios for ionization, dissociation and fluorescence, *J. of Mol. Spectr.* 315 (2015) 155–171.
- [27] M. Glass-Maujean, A.-M. Vasserot, Ch. Jungen, H. Schmoranzer, A. Knie, S. Kübler, A. Ehresmann, Experimental and theoretical study of the $(np\sigma)$ ${}^1\Sigma_u^+$ ($n \leq 4$) $N' = 0$ excited states of D_2 : Absolute absorption cross sections and branching ratios for ionization, dissociation and fluorescence, *J. Mol. Spectr.* 320 (2016) 25–32.
- [28] G. D. Dickenson, T. I. Ivanov, M. Roudjane, N. de Oliveira, D. Joyeux, L. Nahon, W. U. L. Tchang-Brillet, M. Glass-Maujean, I. Haar, A. Ehresmann, W. Ubachs, Synchrotron vacuum ultraviolet radiation studies of the $D^1\Pi_u$ state of H_2 , *J. Chem. Phys.* 133 (2010) 144317.
- [29] T. I. Ivanov, M. Roudjane, M. O. Vieitez, C. A. de Lange, W.-Ü. L. Tchang-Brillet, W. Ubachs, HD as a probe for detecting mass variation on a cosmological time scale, *Phys. Rev. Lett.* 100 (2008) 093007.
- [30] G. D. Dickenson, W. Ubachs, The $D^1\Pi_u$ state of HD and the mass scaling relation of its predissociation widths, *J. Phys. B* 45 (2012) 145101.
- [31] G. D. Dickenson, T. I. Ivanov, W. Ubachs, M. Roudjane, N. de Oliveira, D. Joyeux, L. Nahon, W. U. L. Tchang-Brillet, M. Glass-Maujean, H. Schmoranzer, A. Knie, S. Kübler, A. Ehresmann, VUV spectroscopic study of the $D^1\Pi_u$ state of molecular deuterium, *Mol. Phys.* 109 (2011) 2693–2708.
- [32] A. de Lange, G. D. Dickenson, E. J. Salumbides, W. Ubachs, N. de Oliveira, D. Joyeux, L. Nahon, VUV Fourier-transform absorption study of the Lyman and Werner bands in D_2 , *J. Chem. Phys.* 136 (2012) 234310.
- [33] M. Glass-Maujean, Ch. Jungen, G. Dickenson, N. de Oliveira, W. Ubachs, The excited $J = 0$ ${}^1\Sigma_u^+$ levels of D_2 : Measurements and ab initio quantum defect study, *J. Mol. Spectr.* 320 (2016) 33–38.
- [34] M. Glass-Maujean, Ch. Jungen, G. Dickenson, W. Ubachs, N. de Oliveira, D. Joyeux, L. Nahon, VUV Fourier-Transform absorption study of the

- ($np\pi$) ${}^1\Pi_u^-, v, N - X^1\Sigma_g^+, v'' = 0, N$ transitions in D_2 , *J. Mol. Spectr.* 315 (2015) 147–154.
- [35] S. Takezawa, Y. Tanaka, The absorption spectrum of D_2 in the vacuum-uv region, Rydberg bands, $np\sigma^1\Sigma_u^+ - X^1\Sigma^+$ and $np\pi^1\Pi_u - X^1\Sigma_g^+$ with $n=4-6$ and the ionization energy, *J. Mol. Spectr.* 54 (1975) 379–401.
- [36] A. Monfils, The absorption spectra of the molecules H_2 , HD, and D_2 : Part VI. Rotational analysis of the B' , B'' , D , D' , and D'' states, *J. Mol. Spectr.* 15 (1965) 265–307.
- [37] Private communication with Ch. Jungen (1970).
- [38] H. Abgrall, E. Roueff, F. Launay, J. Y. Roncin, J. L. Subtil, The Lyman and Werner band systems of molecular hydrogen, *J. Mol. Spectr.* 157 (1993) 512–523.
- [39] H. Abgrall, E. Roueff, F. Launay, J.-Y. Roncin, The $B^1\Sigma_u^+ \rightarrow X^1\Sigma_g^+$ and $D^1\Pi_u^+ \rightarrow X^1\Sigma_g^+$ band systems of molecular hydrogen, *Can. J. Phys.* 72 (1994) 856–865.
- [40] H. Abgrall, E. Roueff, F. Launay, J. Y. Roncin, J. L. Subtil, Table of the Lyman Band System of Molecular Hydrogen, *Astron. Astroph. Suppl.* 101 (1993) 273–322.
- [41] H. Abgrall, E. Roueff, F. Launay, J. Y. Roncin, J. L. Subtil, Table of the Werner Band System of Molecular Hydrogen, *Astron. Astroph. Suppl.* 101 (1993) 323–362.
- [42] H. Abgrall, E. Roueff, X. M. Liu, D. E. Shemansky, G. K. James, High-resolution far ultraviolet emission spectra of electron-excited molecular deuterium, *J. Phys. B* 32 (1999) 3813–3838.
- [43] M. Roudjane, F. Launay, W. Ü. L. Tchang-Brillet, High resolution vacuum ultraviolet emission spectrum of D_2 from 78 to 103 nm: The $D^1\Pi_u - X^1\Sigma_g^+$ and $D^1\Pi_u^- - X^1\Sigma_g^+$ band systems, *J. Chem. Phys.* 125 (2006) 214305.
- [44] M. Roudjane, W. Ü. L. Tchang-Brillet, F. Launay, High resolution vacuum ultraviolet emission spectrum of D_2 : The $B^1\Sigma_u^+ - X^1\Sigma_g^+$ band system, *J. Chem. Phys.* 127 (2007) 054307.
- [45] M. Glass-Maujean, Ch. Jungen, M. Roudjane, W. U. L. Tchang-Brillet, Theory of vibronic interactions in D_2 and H_2 : A comparison between multichannel-quantum-defect and coupled-equation approaches, *J. Chem. Phys.* 134 (2011) 204305.
- [46] Ch. Jungen, O. Atabek, Rovibronic interactions in the photoabsorption spectrum of molecular hydrogen and deuterium: An application of multichannel quantum defect methods, *J. Chem. Phys.* 66 (1977) 5584–5609.
- [47] Ch. Jungen, Unified treatment of dissociation and ionization processes in molecular hydrogen, *Phys. Rev. Lett.* 53 (1984) 2394–2397.
- [48] C. H. Greene, Ch. Jungen, Molecular applications of quantum defect theory, *Advances in Atomic and Molecular Physics* 21 (1985) 51–121.
- [49] M. Sommavilla, F. Merkt, J. Z. Mezei, Ch. Jungen, Absorption, autoionization, and predissociation in molecular hydrogen: High-resolution spectroscopy and multichannel quantum defect theory, *J. Chem. Phys.* 144 (2016) 084303.
- [50] G. Staszewska, L. Wolniewicz, Adiabatic energies of excited ${}^1\Sigma_u$ states of the hydrogen molecules, *J. Mol. Spectr.* 212 (2002) 208–212.
- [51] L. Wolniewicz, G. Staszewska, Excited ${}^1\Pi_u$ states and the ${}^1\Pi_u - X^1\Sigma_g^+$ transition moments of the hydrogen molecules, *J. Mol. Spectr.* 220 (2003) 45–51.
- [52] L. Wolniewicz, G. Staszewska, ${}^1\Sigma_u^+ - X^1\Sigma_g^+$ transition moments for the hydrogen molecules, *J. Mol. Spectr.* 217 (2003) 181–185.
- [53] N. de Oliveira, M. Roudjane, D. Joyeux, D. Phalippou, J.-C. Rodier, L. Nahon, High-resolution broad-bandwidth Fourier-transform absorption spectroscopy in the VUV range down to 40 nm, *Nature Photon.* 5 (2011) 149–253.

- [54] N. de Oliveira, D. Joyeux, M. Roudjane, J.-F. Gil, B. Pilette, L. Archer, K. Ito, L. Nahon, The high-resolution absorption spectroscopy branch on the VUV beamline DESIRS at SOLEIL, *J. Synch. Rad.* 23 (2016) 887–900.
- [55] G. Reichardt, J. Bahrdt, J.-S. Schmidt, W. Gudat, A. Ehresmann, R. Müller-Albrecht, H. Molter, H. Schmoranzner, M. Martins, N. Schwentner, S. Sasaki, A 10 m-normal incidence monochromator at the quasi-periodic undulator U125-2 at BESSY II, *Nucl. Instrum. Methods Phys. Res. Sect. A* 467–468 (2001) 462–465.
- [56] M. Glass-Maujean, H. Frohlich, J. A. Beswick, Experimental evidence of an interference between photodissociation continua, *Phys. Rev. Lett.* 61 (1988) 157–160.
- [57] K. E. McCulloh, J. A. Walker, Photodissociative formation of ion pairs from molecular hydrogen and the electron affinity of the hydrogen atom, *Chem. Phys. Lett.* 25 (1974) 439–442.
- [58] W. A. Chupka, P. M. Dehmer, W. T. Jivry, High resolution photoionization study of ion-pair formation in H_2 , HD, and D_2 , *J. Chem. Phys.* 63 (1975) 3929–3944.
- [59] E. Reinhold, W. Ubachs, Heavy Rydberg states, *Mol. Phys.* 103 (2005) 1329–1352.
- [60] M. O. Vieitez, T. I. Ivanov, E. Reinhold, C. A. de Lange, W. Ubachs, Spectroscopic observation and characterization of H^+H^- heavy Rydberg states, *J. Phys. Chem. A* 113 (2009) 13237–13245.
- [61] J. Z. Mezei, I. F. Schneider, M. Glass-Maujean, Ch. Jungen, Resonances in photoabsorption: Predissociation line shapes in the $3p\pi D^1\Pi_u^+ - X^1\Sigma_g^+$ system in H_2 , *J. Chem. Phys.* 141 (2014) 064305.
- [62] J. Komasa, K. Piszczatowski, G. Lach, M. Przybytek, B. Jeziorski, K. Pachucki, Quantum electrodynamic effects in rovibrational spectra of molecular hydrogen, *J. Chem. Theory Comput.* 7 (2011) 3105–3115.
- [63] J.M. Brown, J.T. Hougen, K.-P. Huber, J.W.C. Johns, I. Kopp, H. Lefebvre-Brion, A.J. Merer, D.A. Ramsay, J. Rostas, and R.N. Zare, *J. Mol. Spectr.* 55 (1975), 500–503.
- [64] J. K. Watson, Reflection symmetries of linear-molecular rovibronic levels, *J. Mol. Spectr.* 145 (1991) 130–141.
- [65] U. Fano, Quantum defect theory of l uncoupling in H_2 as an example of channel-interaction treatment, *Phys. Rev. A* 2 (1970) 353–365.
- [66] M. J. Seaton, Quantum defect theory, *Rep. Progr. Phys.* 46 (1983) 167–257.
- [67] Ch. Jungen, D. Dill, Calculation of rotational-vibrational preionization in H_2 by multichannel quantum defect theory, *J. Chem. Phys.* 73 (1980) 3338–3345.
- [68] Ch. Jungen, Handbook of High Resolution Spectroscopy, Editors F. Merkt and M. Quack, Chapter: Elements of Quantum Defect Theory, Wiley, Chichester and New York, 2011.
- [69] M. Glass-Maujean, Ch. Jungen, Nonadiabatic ab initio multichannel quantum defect theory applied to absolute experimental absorption intensities in H_2 , *J. Phys. Chem. A* 113 (2009) 13124–13132.
- [70] Ch. Jungen, M. Glass-Maujean, Direct optical access to the triplet manifold of states in H_2 , *Phys. Rev. A* 93 (2016) 032514.
- [71] S. C. Ross, Ch. Jungen, Multichannel quantum-defect theory of $n = 2$ and 3 gerade states in H_2 : Rovibronic energy levels, *Phys. Rev. A* 50 (1994) 4618–4629.
- [72] A. Osterwalder, A. Wüest, F. Merkt, Ch. Jungen, High-resolution millimeter wave spectroscopy and multichannel quantum defect theory of the hyperfine structure in high Rydberg states of molecular hydrogen H_2 , *J. Chem. Phys.* 121 (2004) 11810–11838.

- [73] C. Haase, M. Beyer, Ch. Jungen, F. Merkt, The fundamental rotational interval of para- H_2^+ by MQDT-assisted Rydberg spectroscopy of H_2 , *J. Chem. Phys.* 142 (2015) 064310.
- [74] T. A. Paul, H. A. Cruse, H. J. Wörner, F. Merkt, Structure and dynamics of the high gerade Rydberg states of D_2 in the vicinity of the adiabatic ionization threshold, *Mol. Phys.* 105 (2007) 871–883.
- [75] H. A. Cruse, Ch. Jungen, F. Merkt, Hyperfine structure of the ground state of para- D_2^+ by high-resolution Rydberg-state spectroscopy and multichannel quantum defect theory, *Phys. Rev. A* 77 (2008) 042502.
- [76] Ch. Jungen, S. C. Ross, Unified quantum-defect-theory treatment of molecular ionization and dissociation, *Phys. Rev. A* 55 (1997) R2503–R2506.
- [77] S. Martin, J. Chevalyere, M. C. Bordas, S. Valignat, M. Broyer, B. Cabaud, A. Hoareau, Highly excited Rydberg states of Na_2 : Decoupling between electronic and nuclear motion, *J. Chem. Phys.* 79 (1983) 4132–4141.
- [78] S. Fredin, D. Gauyacq, M. Horani, Ch. Jungen, G. Lefevre, F. Masnou-Seeuws, *s* and *d* Rydberg series of NO probed by double resonance multiphoton ionization, *Mol. Phys.* 60 (1987) 825–866.
- [79] P. Julienne, Predissociation of the H_2 $D^1\Pi_u$ state, *Chem. Phys. Lett.* 8 (1971) 27–28.
- [80] F. Fiquet-Fayard, O. Gallais, Predissociation of H_2 and D_2 ($D^1\Pi_u$): comparison of calculated and experimental line-widths, *Chem. Phys. Lett.* 16 (1972) 18–19.
- [81] W. Kołos, Ab initio potential energy curves and vibrational levels for the B'' and B' states of the hydrogen molecule, *J. Mol. Spectr.* 62 (1976) 429–441.
- [82] E. Reinhold, W. Hogervorst, W. Ubachs, L. Wolniewicz, Experimental and theoretical investigation of the $H''\bar{B}^1\Sigma_g^+$ state in H_2 , D_2 , and HD, and the $B''\bar{B}^1\Sigma_u^+$ state in HD, *Phys. Rev. A* 60 (1999) 1258–1270.
- [83] A. de Lange, W. Hogervorst, W. Ubachs, Double-well states of ungerade symmetry in H_2 : First observation and comparison with ab initio calculations, *Phys. Rev. Lett.* 86 (2001) 2988–2991.
- [84] R. C. Ekey, A. Marks, E. F. McCormack, Double resonance spectroscopy of the $B''\bar{B}^1\Sigma_u^+$ state of H_2 , *Phys. Rev. A* 73 (2006) 023412.
- [85] M. Glass-Maujean, J. Breton, P. Guyon, Photoabsorption probabilities for the $3p\pi$ $D^1\Pi_u$ vibrational bands of H_2 , *Chem. Phys. Lett.* 112 (1984) 25–28.
- [86] J. Croman, E. F. McCormack, Energies and lifetimes of the predissociative $v = 12$ and 13 levels of the $D^1\Pi_u^+$ state in H_2 , *J. Phys. B* 41 (2008) 035103.
- [87] M. Glass-Maujean, H. Schmoranzer, Ch. Jungen, I. Haar, A. Knie, P. Reiss, A. Ehresmann, *Ab initio* nonadiabatic study of the $3p\pi$ $D^1\Pi_u^+$ state of H_2 and D_2 , *Phys. Rev. A* 86 (2012) 052507.
- [88] M. Glass-Maujean, J. Breton, P. M. Guyon, Accidental predissociation of the $4p\pi^1\Pi_u^+$ state of H_2 , *Phys. Rev. Lett.* 40 (1978) 181–184.
- [89] M. Glass-Maujean, J. Breton, B. Thieblemont, K. Ito, Lifetimes of radiative excited levels of H_2 , *J. Phys. (Paris)* 45 (1984) 1107–1111.
- [90] R. W. Field, C. M. Gittins, N. A. Harris, Ch. Jungen, Quantum defect theory of dipole and vibronic mixing in Rydberg states of CaF, *J. Chem. Phys.* 122 (2005) 184314.
- [91] J. C. J. Koelemeij, A. de Lange, W. Ubachs, Search for outer-well states above the ionization potential in H_2 , *Chem. Phys.* 287 (2003) 349–354.
- [92] M. Beyer, F. Merkt, Observation and calculation of the quasibound rovibrational levels of the electronic ground state of H_2^+ , *Phys. Rev. Lett.* 116 (2016) 093001.

- [93] M. Beyer, F. Merkt, Structure and dynamics of H_2^+ near the dissociation threshold: A combined experimental and computational investigation, *J. Mol. Spectr.* 330 (2016) 147-157.
- [94] A. M. Chartrand, R. C. Ekey, E. F. McCormack, Observations of high vibrational levels of the $4f\sigma^1\Sigma_u^+$ state of H_2 , *J. Chem. Phys.* 145 (2016) 024306.
- [95] F. Martín, Non-autoionizing doubly excited states of H_2 : the Σ^- symmetry, *J. Phys. B* 32 (1999) L181–L187.
- [96] J. Komasa, The Σ^- states of the molecular hydrogen, *Phys. Chem. Chem. Phys.* 10 (2008) 3383–3389.
- [97] F. Argoubi, S. Bezzaouia, H. Oueslati, M. Telmini, Ch. Jungen, Highly excited Σ^- states of molecular hydrogen, *Phys. Rev. A* 83 (2011) 052504.
- [98] M. L. Niu, E. J. Salumbides, W. Ubachs, Communication: Test of quantum chemistry in vibrationally hot hydrogen molecules, *J. Chem. Phys.* 143 (2015) 081102.
- [99] T. M. Trivikram, M. L. Niu, P. Wcisło, W. Ubachs, E. J. Salumbides, Precision measurements and test of molecular theory in highly excited vibrational states of H_2 ($v = 11$), *Appl. Phys. B* 122 (2016) 294.
- [100] Ch. Jungen, S. T. Pratt, S. C. Ross, Multichannel quantum defect theory and double-resonance spectroscopy of autoionizing levels of molecular hydrogen, *J. Phys. Chem.* 99 (1995) 1700–1710.

Table 1: Propensity rules, approximate quantum number and mass dependences in predissociation, autoionization and fluorescence processes

	predissociation		autoionization		fluorescence
	vibrational	rotational	vibrational	rotational	
Rydberg series, n	$-^a$	-	n^{-3}	n^{-3}	n^{-3}
vibrational sequence, v^+	-	-	$v^+ + 1$	-	$1^b, \text{FC}^c$
rotational sequence, N' or N^+	-	$N'(N'+1)^d$	1^e	1	-
propensity rule, v^+, N^+	-	-	$\Delta v^+ = -1$	$\Delta v^+ = 0$	-
	-	-	$\Delta N^+ = 0^f$	$ \Delta N^+ \leq 2\ell$	$ N^+ - N'' \leq \ell''^f$
selection rule, N'	$\Delta N' = 0$	$\Delta N' = 0$	$\Delta N' = 0$	$\Delta N' = 0$	$N' - N'' = 0, \pm 1$
reduced mass, M	$M^{-3/2}$	M^{-2}	$M^{-1/2}$	1	1

Unless specified otherwise the dependences correspond to the natural width.

^a no simple rule.

^b no dependence (natural width).

^c Franck-Condon factor (intensity of individual transition).

^d if upper state in case (b).

^e no dependence.

^f if upper state in case (d).

Table 2: Photoabsorption transitions of D₂ involving $N' = 1$ upper levels

state	$\frac{E}{hc}$ (cm ⁻¹)		$\frac{\Gamma}{hc}$ (cm ⁻¹)		$A(R0)$ (10 ⁶ s ⁻¹)		$A(P2)$ (10 ⁶ s ⁻¹)		γ_d (%)	γ_f (%)	γ_i (%)
	obs ^{a,b}	o-c ^a	calc	obs	calc	obs	calc	obs	obs	obs	obs
4pσ, v = 0	117224.15±0.02	-0.58		0.00±0.10	1.58	2.1±0.7 ^c	2.58	7.3±2.6 ^c			
4pπ, v = 0	118189.85±0.02	-0.06		0.00±0.10	3.66	3.4±1.0 ^c	1.95				
4pσ, v = 1	118714.40±0.03	-0.58		0.00±0.11	3.90	5.9±1.8 ^c	6.99	11±3 ^c			
4pπ, v = 1	119775.45±0.02	-0.08		0.00±0.10	9.75	8.0±2.4 ^c	4.61	4.1±1.4 ^c			
5pσ, v = 0	120050.14±0.05	-0.34		0.00±0.12	0.49	0.45±0.16 ^c	0.57				
4pσ, v = 2	120138.45±0.01	-0.74		0.00±0.10	6.22	7.1±2.1 ^c	12.34	18±5 ^c			
5pπ, v = 0	120528.23±0.05	-0.03		0.02±0.11	1.60	1.2±0.4 ^c	1.18	1.0±0.7 ^c			
4pπ, v = 2	121295.45±0.02	-0.06		0.00±0.10	15.19	13±4 ^c	6.03	6.7±2.1 ^c			
4pσ, v = 3	121479.67±0.03	-0.35		0.00±0.10	3.06	3.9±1.2 ^c	8.89	12±4 ^c			
6pσ, v = 0	121513.06±0.04	-0.17		0.00±0.11	1.02	1.3±0.4 ^c	3.14	3.4±1.2 ^c			
5pσ, v = 1	121627.60±0.03	-0.67		0.00±0.10	5.59	5.6±1.7 ^c	7.74	11±3 ^c			
6pπ, v = 0	121812.75±0.10	-0.09		0.04±0.23	0.73	0.6±0.3 ^c	1.20	1.0±0.3 ^c			
5pπ, v = 1	122109.30±0.02	-0.12		0.00±0.10	4.28	4.4±1.4 ^c	3.01	3.2±1.1 ^c			
7pσ, v = 0	122425.62±0.07	-0.22		0.00±0.14	0.79	0.66±0.22 ^c	0.70				
7pπ, v = 0	122594.13±0.11	-0.08		0.08±0.22	0.43	0.40±0.18 ^c	0.60				
4pπ, v = 3	122738.93±0.03	-0.19		0.18±0.11	21.71	19±6 ^c	0.04				
4pσ, v = 4	122779.92±0.05	-0.21		0.12±0.16	0.28		19.32	25±8 ^c			
8pσ, v = 0	122979.43±0.05	-0.03		0.00±0.16	0.78	0.7±0.2 ^c	0.77	0.6±0.4 ^c			
5pσ, v = 2	123008.33±0.07	-0.08		0.15±0.18	0.37	0.6±0.2 ^c	1.65	2.3±0.9 ^c			
8pπ, v = 0	123104.94±0.05	-0.08		0.04±0.16	0.95	1.2±0.4 ^c	0.01				
6pσ, v = 1	123161.71±0.03	-0.75		0.00±0.10	6.31	6.1±1.8 ^c	8.94	11±3 ^c			
9pσ, v = 0	123370.20±0.06	-0.16		0.00±0.17	1.22	1.2±0.4 ^c	0.00				
6pπ, v = 1	123391.73±0.04	-0.08		0.00±0.15	1.58	1.5±0.5 ^c	2.92	3.6±1.3 ^c			
9pπ, v = 0	123461.50±0.07	-0.05		0.06	0.06		0.69	0.7±0.4 ^c			
5pπ, v = 2	123625.69±0.03	-0.10		0.00±0.15	6.06	4.4±0.8	3.98	4.6±1.5 ^c	21±5	77±5	
10p0, v = 0	123639.13±0.04	0.00		0.00±0.16	0.25	0.24±0.08 ^c	0.04		23±7	77±7	
10p2, v = 0	123717.20±0.10	0.00		0.0±0.6	0.01		0.30	0.4±0.1	23±9	77±9	
11p0, v = 0	123835.43±0.07	0.07		0.00±0.19	0.23	0.31±0.06	0.00		38±12	62±12	
11p2, v = 0	123906.96				0.03		0.14				
4pσ, v = 5	123970.51±0.05	-0.63		0.00±0.15	8.54	8.9±1.1	9.10	12.2±1.6	89±4	11±4	
12p0, v = 0	123980.60±1.00	-0.40		0.0±0.6	0.11	0.19±0.06	0.54	0.8±0.2	59±16	41±16	
7pσ, v = 1	123990.50±0.04	-0.18		0.00±0.15	1.66	1.4±0.4 ^c	0.78		26±8	74±8	
12p2, v = 0	124055.5±1.0	0.2		0.30±0.10	0.07		0.34	0.5±0.2	38±21	62±21	
13p0, v = 0	124099.30±1.00	-0.10		0.6±0.5	0.21	0.15±0.03	0.02				
4pπ, v = 4	124152.95±0.03	0.00		0.00±0.15	13.45	9.8±1.3	10.32	14.5±2.0	27±4	73±4	
13p2, v = 0	124165.27±0.05	-0.20		0.00±0.20	0.31	0.23±0.09 ^c	0.00				
7pπ, v = 1	124170.97±0.05	-0.06		0.00±0.17	0.69	1.0±0.2	1.44	1.9±0.9 ^c	38±9	62±9	
14p0, v = 0	124192.17				0.00		0.02				
15p0, v = 0	124251.08				0.07		0.05				
14p2, v = 0	124270.49				0.02		0.10				
16p0, v = 0	124315.09				0.00		0.03				
15p2, v = 0	124338.82				0.00		0.10				
17p0, v = 0	124366.28				0.00		0.02				
16p2, v = 0	124395.70				0.00		0.05				
18p0, v = 0	124409.60				0.06		0.01				
5pσ, v = 3	124410.89±0.03	-0.02		0.00±0.15	1.78	2.9±0.4	3.36	5.5±0.7	37±6	63±6	
19p0, v = 0	124438.7±1.0	-0.2			0.04	0.05±0.02	0.01		100±30		
17p2, v = 0	124450.38				0.01		0.08				
20p0, v = 0	124470.8±1.0	0.0			0.04	0.07±0.02	0.00		70±30	30±30	
18p2, v = 0	124488.56				0.00		0.05				
21p0, v = 0	124498.33				0.08		0.00				
22p0, v = 0	124517.27				0.03		0.01				
19p2, v = 0	124526.0±1.0	0.1		0.0±0.5	0.00		0.06	0.07±0.01	100		
23p0, v = 0	124538.3±1.0	0.0			0.03	0.05±0.01	0.00				
8pσ, v = 1	124545.2±1.0	-0.8		0.0±0.4	0.00		0.22	bl			
20p2, v = 0	124558.37				0.01		0.00				
25p0, v = 0	124569.86				0.02		0.00				
23p2, v = 0	124625.20				0.03		0.00				
31p0, v = 0	124631.33				0.01		0.00				
32p0, v = 0	124637.71				0.01		0.03				
24p2, v = 0	124641.02±0.04	-0.02			0.47	0.8±0.4	0.20				
6pσ, v = 2	124643.89±0.03	-0.57		0.00±0.20	7.89	7.6±1.1	5.10	5.5±1.6 ^c	32±6	68±6	
34p0, v = 0	124650.6±1.0	0.2			0.03	0.023±0.017	0.00				
43p0, v = 0	124685.96±0.17	0.04			0.00		0.67	1.8±1.0 ^c			
8pπ, v = 1	124686.97±0.09	-0.02		0.00±0.19	0.05	0.07±0.03	3.08	5.3±0.6	35±5	65±5	
44p0, v = 0	124688.7±1.0	-0.1			0.02		0.32	0.2±0.2			
45p0, v = 0	124691.4±1.0	0.3			0.02		0.16	0.32±0.17			
6pπ, v = 2	124902.60±0.04	-0.04	0.04	0.00±0.15	4.33	6.2±0.8	3.62	3.8±0.7	0±1	10±4	90±9
9pσ, v = 1	124944.0±1.0	-0.5	2.25	2.2±0.8	0.76	0.7±0.2	0.77	bl			100

Table 2: Photoabsorption transitions of D₂ involving $N' = 1$ upper levels (cont'd)

state	$\frac{E}{hc}$ (cm ⁻¹)		$\frac{\Gamma}{hc}$ (cm ⁻¹)		$A(R0)$ (10 ⁶ s ⁻¹)		$A(P2)$ (10 ⁶ s ⁻¹)		γ_d (%)	γ_f (%)	γ_i (%)
	obs ^{a,b}	o-c ^a	calc	obs	calc	obs	calc	obs	obs	obs	obs
9pπ, v = 1	125035.19				0.18	bl	1.17	bl			
5pπ, v = 3	125078.93±0.04	-0.19	0.00	0.13±0.15	6.74	6.3±1.2	3.98	4.3±1.7 ^c	10±4	61±12	29±6
4pσ, v = 6	125106.11±0.06	-0.53	0.00	0.08±0.15	5.94	8.1±1.1	8.95	16±3	87±11	13±11	0
10p0, v = 1	125212.40±0.14	-0.37	1.35	1.67±0.26	0.77	1.0±0.1	0.06				100
10p2, v = 1	125288.6±1.0	-0.8	0.81	1.5±0.6	0.09	0.15±0.04	0.72	1.1±0.2			100
11p0, v = 1	125409.34±0.11	-0.10	0.73	0.65±0.02	0.15	0.31±0.15	0.00				100
11p2, v = 1	125467.17±0.05	-0.10	0.26	0.14±0.16	0.98	1.2±0.3	0.00				100
4pπ, v = 5	125486.43±0.06	-0.04	0.00	0.18±0.16	11.88	9.0±1.5	7.06	5.7±2.6 ^c	49±7	40±5	11±2
7pσ, v = 2	125496.79±0.07	-0.16	0.59	0.68±0.20	0.89	0.7±0.3 ^c	2.42	2.8±1.6			100
12p0, v = 1	125560.79±0.06	-0.06	0.44	0.43±0.18	0.87	0.9±0.3	0.01				100
12p2, v = 1	125627.3±1.0	-0.1	0.44	0.50±0.32	0.08	bl	0.62	0.8±0.6			100
13p0, v = 1	125674.65±0.04	-0.03	0.13	0.06±0.15	1.29	1.8±0.3	0.57	1.6±1.6 ^c			100
7pπ, v = 2	125683.18±0.04	0.03	0.03	0.02±0.15	0.85	bl	1.64	2.4±0.4			100
13p2, v = 1	125739.16				0.08		0.50	bl			
5pσ, v = 4	125752.07±0.04	-0.07	0.00	0.00±0.15	2.04	2.4±0.5	3.33	4.2±0.7	33±6	12±4	55±8
14p0, v = 1	125768.50±0.05	-0.07	0.04	0.02±0.16	0.22	0.16±0.10	0.09				100
15p0, v = 1	125826.0±1.0	0.6	0.66	0.1±0.6	0.14	bl	0.16				100
14p2, v = 1	125845.3±1.0	-0.3	0.10	2.0±1.9	0.10	0.18±0.17	0.21				100
16p0, v = 1	125891.4±1.0	0.5	0.34		0.20	0.2±0.4	0.01				100
15p2, v = 1	125912.50				0.01		0.25				
17p0, v = 1	125942.72±0.08	-0.06	0.14	0.05±0.18	0.19	0.34±0.16	0.00				100
16p2, v = 1	125969.3±1.0	0.4	0.44	0.0±0.4	0.01		0.21	0.17±0.04			100
18p0, v = 1	125986.08				0.14	bl	0.04				
8pσ, v = 2	126010.92±0.06	-0.15	0.16	0.04±0.17	0.48	0.6±0.3 ^c	0.94	1.5±0.5			100
19p0, v = 1	126017.94±0.08	-0.21	0.12	0.09±0.18	0.25	0.3±0.2 ^c	0.97	1.3±0.3			100
17p2, v = 1	126025.72±0.07	0.00	0.10	0.00±0.16	0.25	0.2±0.2 ^c	0.00				
20p0, v = 1	126047.57				0.03		0.04				
18p2, v = 1	126062.44±0.06	-0.08	0.23	0.17±0.17	0.12	0.2±0.2 ^c	0.00				
21p0, v = 1	126074.85				0.07	bl	0.04				
22p0, v = 1	126091.57±0.06	-0.20	0.14	0.40±0.16	0.74	0.8±0.2	0.59	0.6±0.6			100
19p2, v = 1	126098.76±0.04	-0.17	0.01	0.00±0.15	2.40	2.8±0.4	0.86	1.5±0.7			100
6pσ, v = 3	126104.31±0.05	-0.25	0.11	0.09±0.15	3.19	4.1±0.5	2.82	2.2±1.4 ^c			100
23p0, v = 1	126115.19±0.04	-0.01	0.07	0.00±0.15	0.31	0.4±0.2 ^c	0.02				100
20p2, v = 1	126128.10±0.05	-0.09	0.22	0.16±0.16	0.27	0.22±0.18	0.23	0.14±0.14			100
24p0, v = 1	126133.85				0.02		0.08				
25p0, v = 1	126146.54±0.09	0.04	0.07	0.01±0.17	0.13	0.1±0.2 ^c	0.00				100
21p2, v = 1	126155.0±1.0	0.0	0.15		0.04	bl	0.08	0.06±0.06			
26p0, v = 1	126161.04				0.06	bl	0.02				
4pσ, v = 7	126165.82±0.04	-0.54	0.00	0.00±0.15	6.42	8.1±1.3	9.24	10.4±1.4	85±23	15±23	0
27p0, v = 1	126171.35±0.06	-0.02	0.07	0.01±0.17	0.11	0.2±0.2 ^c	0.00				
22p2, v = 1	126177.67				0.03		0.05				
28p0, v = 1	126183.12				0.05		0.07				
29p0, v = 2	126190.98±0.07	-0.05	0.05	0.05±0.20	0.17	0.25±0.08	0.50	bl			100
8pπ, v = 1	126194.72±0.20	0.30	0.00	0.4±0.6	0.11	0.10±0.05	2.33	3.6±0.5			100
23p2, v = 1	126197.66				0.00		1.03	bl			
30p0, v = 1	126201.31				0.02		0.00				
31p0, v = 1	126208.25				0.03		0.03				
6pπ, v = 3	126352.50±0.04	0.03	0.01	0.07±0.15	4.82	3.3±1.3 ^d	4.32	5.0±1.1 ^d	4±2	22±11	74±11
45p2, v = 1	126352.79				0.37		0.23				
9pσ, v = 2	126450.01±0.34	-0.24	5.43	5.8±3.5	1.51	1.1±0.2	0.76	0.8±0.3			100
5pπ, v = 4	126469.55±0.04	-1.37	0.00	0.00±0.15	5.95	5.0±0.9	3.57	bl	21±6	78±6	
5pπ, v = 4	126472.29±0.04	1.37	0.00	0.00±0.27	5.95	1.9±0.6	3.57	1.3±0.7	11±9	26±7	63±13
9pπ, v = 2	126543.5±1.0	-0.8	1.25	1.5±0.4	0.27	0.31±0.06	1.38	1.4±0.2			100
10p0, v = 2	126720.28±0.19	-0.07	3.06	3.2±0.7	1.01	1.4±0.3	0.07				100
4pπ, v = 6	126760.64±0.05	-0.09	0.00	0.00±0.15	10.05	8.8±1.3	5.27	5.5±1.0	72±11	19±4	9±1
10p2, v = 2	126796.2±1.0	-0.1	1.21	1.0±0.5	0.26	0.42±0.07	0.82	1.3±0.7			100
7pσ, v = 3	126900.85±0.06	-0.19	0.24	0.12±0.16	0.34	0.5±0.2 ^c	1.20	1.2±0.6			100
11p0, v = 2	126930.82±0.05	0.01	1.17	1.30±0.16	2.67	2.7±0.4	0.58	bl			100
11p2, v = 2	126993.0±1.0	0.1	1.66	3.4±1.4	0.09	bl	1.82	2.6±0.5			100
5pσ, v = 5	127020.48±0.04	-0.08	0.00	0.00±0.16	0.84	1.4±0.2	1.97	3.3±1.2	50±5	0	50±5
12p0, v = 2	127071.68±0.13	-0.17	0.92	1.31±0.19	1.17	1.1±0.3	0.01				100
7pπ, v = 3	127130.15±0.07	0.06	0.10	0.04±0.16	2.04	2.1±0.8 ^c	1.47	1.9±0.5			100
12p2, v = 2	127135.4±1.0	0.0	1.53	0.9±0.6	0.04	bl	1.91	2.3±0.5			100
4pσ, v = 8	127150.15±0.04	-0.64	0.00	0.04±0.15	4.18	6.0±0.9	6.98	10.6±1.8	94±6	6±6	0
13p0, v = 2	127188.12±0.06	-0.05	0.38	0.39±0.16	0.46	0.52±0.10	0.02				100
13p2, v = 2	127246.92				0.06		0.54	bl			
14p0, v = 2	127280.34±0.05	-0.05	0.09	0.01±0.15	0.38	0.5±0.2 ^c	0.12	0.12±0.16			100
14p2, v = 2	127334.11				0.21	bl	0.30				
15p0, v = 2	127356.48±0.09	-0.05	0.10	0.12±0.20	0.17	0.2±0.2 ^c	0.27	0.3±0.1			100
6pσ, v = 4	127392.92±0.04	-0.52	0.06	0.00±0.15	3.16	3.2±0.7	4.87	5.9±0.9			100

Table 2: Photoabsorption transitions of D₂ involving $N' = 1$ upper levels (cont'd)

state	$\frac{E}{hc}$ (cm ⁻¹)		$\frac{\Gamma}{hc}$ (cm ⁻¹)		$A(R0)$ (10 ⁶ s ⁻¹)		$A(P2)$ (10 ⁶ s ⁻¹)		γ_d (%)	γ_f (%)	γ_i (%)
	obs ^{a,b}	o-c ^a	calc	obs	calc	obs	calc	obs	obs	obs	obs
16p0, v = 2	127401.89				0.00		0.17				
15p2, v = 2	127421.88				0.20		0.13				
17p0, v = 2	127455.1±1.0	0.8	0.34		0.13	0.2±0.2	0.04				
16p2, v = 2	127476.94				0.17		0.01				100
18p0, v = 2	127497.79±0.05	-0.08	0.07	0.00±0.16	0.15	0.2±0.2 ^c	0.15				
8pσ, v = 3	127516.43±0.04	-0.25	0.11	0.05±0.15	2.16	2.0±0.3	1.32	1.2±0.9			100
19p0, v = 2	127531.49±0.04	-0.09	0.37	0.18±0.15	2.97	2.8±0.4	1.34	1.3±1.0			100
17p2, v = 2	127537.42±0.06	-0.03	0.24	0.16±0.16	0.44	0.5±0.3 ^c	1.27	1.0±0.5			100
20p0, v = 2	127559.69±0.05	-0.08	0.34	0.14±0.16	0.57	0.9±0.4 ^c	0.06				
18p2, v = 2	127573.39				0.14	bl	0.47				
21p0, v = 2	127586.71±0.08	-0.05	0.08	0.14±0.22	0.23	0.25±0.06	0.02				100
22p0, v = 2	127604.29±0.10	-0.02	0.55	0.42±0.21	0.27	0.2±0.2 ^c	0.09				
19p2, v = 2	127611.79				0.02		0.18				
23p0, v = 2	127636.87±0.08	0.05	0.34	0.34±0.22	0.26	0.38±0.09	0.15				100
8pπ, v = 3	127641.48±0.05	0.03	0.12	0.17±0.17	0.63	0.65±0.14	3.18	bl			100
6pπ, v = 4	127738.66±0.06	0.01	0.00	0.00±0.16	6.34	6.6±0.8	4.84	6.6±2.2	13±2	22±6	65±9
5pπ, v = 5	127799.26±0.04	-4.37	0.00	0.00±0.15	4.16	2.8±0.6	2.05	1.6±0.3	18±4	42±8	39±8
5pπ, v = 5	127805.55±0.04	1.92	0.00	0.00±0.15	4.16	1.4±0.4	2.05	0.9±0.4	24±8	41±12	35±21
62p2, v = 2	127887.56				0.06		0.01				
63p2, v = 2	127888.44				0.08		0.02				
64p2, v = 2	127889.26				0.10		0.03				
65p2, v = 2	127890.05				0.11		0.04				
9pσ, v = 3	127891.9±1.0	1.2			0.12	1.1±0.2 ^d	0.05	0.26±0.10 ^d			100
66p2, v = 2	127891.50				0.11		0.06				
67p2, v = 2	127892.19				0.10		0.06				
68p2, v = 2	127892.85				0.08		0.05				
69p2, v = 2	127893.50				0.07		0.05				
4pπ, v = 7	127973.72±0.05	-0.07	0.00	0.09±0.15	8.57	7.7±1.0	2.38	2.0±0.6	93±2	7±2	0±2
9pπ, v = 3	127990.01±0.19	-0.47	2.04	1.16±0.64	0.42	0.3±0.3 ^c	1.52	1.4±0.3			100
4pσ, v = 9	128049.71±0.04	-0.49	0.00	0.03±0.15	0.55	1.3±0.2	4.69	7.2±0.9	94±12	6±12	0
10p0, v = 3	128160.4±1.0	-1.2	4.43	3.60±0.14	0.68	0.7±0.2	0.01				100
5pσ, v = 6	128232.18±0.04	-0.19	0.33	0.30±0.15	3.47	3.5±0.6	1.81	3.1±0.4			100
10p2, v = 3	128239.36±0.09	-0.17	0.77	0.91±0.20	0.39	0.6±0.1	5.14	6.4±0.8			100
7pσ, v = 4	128285.61±0.08	0.13	0.88	0.68±0.16	0.45	0.5±0.3 ^c	1.40	bl			100
11p0, v = 3	128371.74±0.12	0.15	3.02	3.03±0.39	1.76	1.6±0.2	0.10				100
11p2, v = 3	128436.3±1.0	0.0	2.83	3.4±0.8	0.00		1.48	1.3±0.3			100
7pπ, v = 4	128513.53±0.06	0.00	0.57	0.66±0.16	3.74	3.0±0.6	0.96	1.4±0.4			100
12p0, v = 3	128523.65				0.04		0.50	bl			
12p2, v = 3	128579.31				0.00		0.92	bl			
13p0, v = 3	128636.62±0.07	-0.03	0.64	0.63±0.17	0.58	0.6±0.3 ^c	0.04				
13p2, v = 3	128691.14				0.02		0.46	bl			
6pσ, v = 5	128699.68±0.05	-0.68	0.05	0.00±0.16	2.83	3.7±0.7	5.33	5.2±1.1			100
14p0, v = 3	128729.12±0.06	-0.04	0.17	0.20±0.16	0.47	0.7±0.2	0.12				100
14p2, v = 3	128778.69				0.04		0.13				
15p0, v = 3	128804.61±0.05	-0.09	0.08	0.07±0.16	0.35	0.4±0.2 ^c	0.19				100
15p2, v = 3	128846.48				0.01		0.01				
16p0, v = 3	128866.81±0.06	-0.15	0.24	0.25±0.16	0.61	0.7±0.3 ^c	0.03				100
4pσ, v = 10	128888.52±0.04	-0.44	0.01	0.09±0.15	1.06	1.7±0.6 ^c	1.47	2.1±0.5	100		100
8pσ, v = 4	128893.17±0.15	0.09	0.01	0.00±0.22	2.94	2.4±1.0 ^c	3.34	1.9±2.1 ^c	20±10		80±10
17p0, v = 3	128906.03±0.06	-0.02	0.56	0.71±0.17	2.06	2.1±0.3	0.43	bl			100
16p2, v = 3	128928.59±0.09	0.05	1.34	1.04±0.28	0.60	0.8±0.3	1.15	1.6±0.4			100
18p0, v = 3	128946.76±0.05	-0.02	0.20	0.08±0.16	0.44	0.4±0.1	0.02				100
17p2, v = 3	128972.45±0.17	-0.04	1.44	2.00±0.07	0.44	0.4±0.3 ^c	0.28				100
19p0, v = 3	128984.23±0.09	-0.09	0.06	0.00±0.19	0.13	0.12±0.20 ^c	0.21				
20p0, v = 3	129007.27±0.07	0.02	0.69	0.66±0.17	0.66	0.9±0.3	0.03				100
18p2, v = 3	129019.29				0.10		0.03				
8pπ, v = 4	129025.39±0.04	0.32	0.10	0.05±0.15	2.56	2.8±0.4	4.64	5.2±1.3			100
21p0, v = 3	129036.13				0.01		0.15				
5pπ, v = 6	129050.96±0.03	-1.34	0.15	0.00±0.15	6.99	4.7±0.6 ^d	2.69	4.2±1.2 ^d	2±1		98±1
19p2, v = 3	129051.18±0.05	-0.06	0.84	0.72±0.15	1.33		2.39				
5pπ, v = 6	129055.00±0.04	2.70	0.15	0.00±0.15	6.99	8.3±1.5	2.69	1.7±1.8 ^c			
22p0, v = 3	129060.00				0.03		0.03				
23p0, v = 3	129075.66				0.11	bl	0.05				
20p2, v = 3	129084.23				0.00		0.22				
6pπ, v = 5	129088.58±0.05	0.02	0.03	0.07±0.16	0.26	0.4±0.2 ^c	0.01				
24p0, v = 3	129095.4±1.0	1.0	0.07	0.0±0.8	0.10	0.11±0.05	0.00				100
25p0, v = 3	129106.23				0.04		0.13				
21p2, v = 3	129112.00				0.01		0.12				
26p0, v = 3	129121.92				0.07		0.00				
22p2, v = 3	129130.55				0.02		0.12				

Table 2: Photoabsorption transitions of D₂ involving $N' = 1$ upper levels (cont'd)

state	$\frac{E}{hc}$ (cm ⁻¹)		$\frac{\Gamma}{hc}$ (cm ⁻¹)		$A(R0)$ (10 ⁶ s ⁻¹)		$A(P2)$ (10 ⁶ s ⁻¹)		γ_d (%)	γ_f (%)	γ_i (%)
	obs ^{a,b}	o-c ^a	calc	obs	calc	obs	calc	obs	obs	obs	obs
27p0, v = 3	129135.54				0.03		0.06				
4pπ, v = 8	129137.86±0.05	-0.09	0.00	0.09±0.16	3.86	3.5±1.2 ^c	2.53	3.5±0.6	15±3	84±9	8±4
9pσ, v = 4	129246.05				0.00		0.00				
5pσ, v = 7	129370.61±0.04	-0.31	0.17	0.15±0.15	2.31	2.7±0.5	1.98	2.9±0.7	1.0±0.3		99.0±0.3
9pπ, v = 4	129376.52±0.09	0.70	1.93	1.97±0.22	0.02		3.65	4.1±1.5			100
10p0, v = 4	129528.69				0.13	bl	0.01				
7pσ, v = 5	129586.30±0.07	0.21	2.08	2.04±0.19	2.16	2.0±0.3	0.36	0.45±0.12			100
10p2, v = 4	129637.9±1.0	1.0	4.77	4.4±1.0	0.00		2.11	2.2±0.5			100
4pσ, v = 11	129671.64±0.04	0.29	0.00	0.14±0.15	1.08	2.4±0.3	1.99	4.6±0.6	100		
11p0, v = 4	129755.16±0.29	0.07	4.30	4.5±1.5	1.42	1.3±0.4	0.04				100
11p2, v = 4	129818.71				0.07		1.14	bl			
7pπ, v = 5	129842.18±0.04	0.00	0.06	0.08±0.15	3.11	3.3±0.5	0.74	0.9±0.2			100
12p0, v = 4	129906.52±0.25	0.47	2.81	2.2±1.1	0.47	0.58±0.11	0.02				100
6pσ, v = 6	129945.43±0.04	-0.84	0.02	0.04±0.15	2.39	2.9±0.5	4.69	6.1±1.9			100
12p2, v = 4	129962.41				0.08		1.84	bl			
13p0, v = 4	130023.26±0.09	-0.08	1.08	1.20±0.25	0.64	0.67±0.09	0.02				100
13p2, v = 4	130072.75				0.00		0.40				
14p0, v = 4	130116.16±0.06	-0.09	0.28	0.25±0.17	0.45	0.59±0.15	0.13				100
14p2, v = 4	130157.54				0.07		0.00				
15p0, v = 4	130191.19±0.05	-0.05	0.09	0.07±0.15	0.72	0.8±0.3 ^c	0.27				100
8pσ, v = 5	130205.18±0.05	-0.18	0.16	0.16±0.16	1.92	2.2±0.7 ^c	1.27	1.6±0.2			100
4pπ, v = 9	130226.94±0.05	-0.21	0.01	0.00±0.15	8.37	8.1±1.4	3.86	5.1±0.9	40±6	11±4	49±7
16p0, v = 4	130240.08±0.14	0.20	2.08	2.37±0.35	1.11	0.9±0.1	0.56	0.4±0.2			100
15p2, v = 4	130256.7±1.0	0.1	0.90	0.00±0.13	0.01		0.75	1.0±0.8			100
5pπ, v = 7	130280.09±0.04	0.19	0.01	0.00±0.15	2.95	2.8±0.9 ^c	1.55	bl			
17p0, v = 4	130290.35±0.09	0.03	1.27	0.95±0.27	0.38	0.46±0.10	0.06				100
16p2, v = 4	130311.6±1.0	0.8	1.58	1.59±0.07	0.05		0.46	0.9±0.4			100
18p0, v = 4	130333.30±0.06	-0.03	0.33	0.31±0.16	0.61	bl	0.17				100
6pπ, v = 6	130343.60±0.04	-0.10	0.02	0.02±0.15	1.18	1.1±0.2	1.95	2.2±0.5			100
17p2, v = 4	130354.46				0.03		0.05				
8pπ, v = 5	130359.0±0.8	-0.24	1.10	2.7±2.3	0.00		0.77	0.71±0.09			100
19p0, v = 4	130371.15±0.07	-0.16	0.04	0.05±0.17	0.09	0.13±0.05	0.04				100
4pσ, v = 12	130385.40±0.06	0.05	0.00	0.04±0.16	0.22	0.35±0.08	0.34		100		
20p0, v = 4	130393.8±1.0	-0.3	1.23	0.5±1.4	0.12	0.2±0.4	0.12				100
18p2, v = 4	130404.89				0.02		0.23				
21p0, v = 4	130422.80±0.15	-0.01	0.42	0.5±0.3	0.15	0.13±0.09	0.00				100
19p2, v = 4	130436.02				0.01		0.19				
22p0, v = 4	130446.76±0.13	-0.24	0.03	0.00±0.25	0.10	bl	0.04				
5pσ, v = 8	130457.93±0.04	-0.55	0.00	0.00±0.15	2.00	3.9±0.6	6.30	10.3±1.5	79±13	21±13	
23p0, v = 4	130461.91±0.24	0.04	0.89	1.3±0.8	0.16	0.1±0.3	0.16				100
20p2, v = 4	130469.63				0.01		0.16				
24p0, v = 4	130481.51±0.17	-0.03	0.19	0.64±0.34	0.11	0.11±0.02	0.00				100
21p2, v = 4	130491.54				0.02		0.10				
25p0, v = 4	130498.38±0.09	-0.10	0.04	0.3±0.2	0.06		0.06				
26p0, v = 4	130508.84±0.16	-0.06	0.33	0.25±0.33	0.07	0.1±0.2 ^c	0.00				
22p2, v = 4	130515.63				0.00		0.08				
27p0, v = 4	130522.54±0.08	0.04	0.02	0.06±0.18	0.06	0.11±0.17 ^c	0.03				
28p0, v = 4	130530.78±0.08	-0.07	0.31	0.00±0.19	0.04	0.04±0.17 ^c	0.00				
23p2, v = 4	130535.96				0.01		0.05				
29p0, v = 4	130541.98±0.16	-0.22	0.02	0.31±0.34	0.05	0.05±0.18 ^c	0.02				
30p0, v = 4	130548.84				0.02		0.00				
24p2, v = 4	130552.97				0.02		0.02				
31p0, v = 4	130558.45				0.05		0.02				
32p0, v = 4	130563.80				0.00		0.01				
25p2, v = 4	130567.01±0.08	-0.14	0.14	0.05±0.28	0.06	0.07±0.19 ^c	0.00				
33p0, v = 4	130571.88±0.09	-0.07	0.01	0.41±0.28	0.06		0.01				
34p0, v = 4	130576.27				0.01		0.07				
26p2, v = 4	130578.28±0.06	-0.16	0.01	0.00±0.17	0.19	0.19±0.06	0.05				100
35p0, v = 4	130582.96±0.07	-0.01	0.02	0.00±0.18	0.13	0.09±0.06	0.01				100
9pσ, v = 5	130586.48±0.05	-0.12	0.11	0.21±0.16	0.19	0.43±0.07 ^d	0.32	0.64±0.10 ^d			100
36p0, v = 4	130586.61				0.19		0.31				
37p0, v = 4	130591.89±0.08	-0.07	0.09	0.00±0.19	0.12	0.07±0.05	0.02				100
38p0, v = 4	130595.64±0.15	-0.04	0.28	0.87±0.36	0.17	0.18±0.06	0.13				100
39p0, v = 4	130599.96				0.05		0.00				
40p0, v = 4	130603.6±1.0	0.3	0.12	0.0±0.4	0.08	0.06±0.02	0.01				100
41p0, v = 4	130606.4±1.0	0.4	0.33	1.3±0.9	0.08	0.12±0.04	0.11				100
28p2, v = 4	130607.33				0.00		0.06				
45p2, v = 4	130692.78				0.01		0.00				
46p2, v = 4	130695.11				0.02		0.01				
47p2, v = 4	130697.18				0.12		0.15				

Table 2: Photoabsorption transitions of D₂ involving $N' = 1$ upper levels (cont'd)

state	$\frac{E}{hc}$ (cm ⁻¹)		$\frac{\Gamma}{hc}$ (cm ⁻¹)		$A(R0)$ (10 ⁶ s ⁻¹)		$A(P2)$ (10 ⁶ s ⁻¹)		γ_d (%)	γ_f (%)	γ_i (%)
	obs ^{a,b}	o-c ^a	calc	obs	calc	obs	calc	obs	obs	obs	obs
9p π , v = 5	130697.82±0.08	-0.30	0.14	0.08±0.18	0.64	1.2±0.2 ^d	0.90	bl			100
48p ₂ , v = 4	130699.53				0.04		0.06				
49p ₂ , v = 4	130701.41				0.01		0.01				
50p ₂ , v = 4	130703.22				0.00		0.01				
7p σ , v = 6	130792.95				0.07		0.37				100
10p ₀ , v = 5	130885.4±1.0	-0.7	9.26	8.8±0.5	1.48	1.2±0.3	0.32				100
10p ₂ , v = 5	130956.1±1.0	0.2	4.78	4.2±0.8	0.18	bl	1.18	1.3±0.3			100
4p σ , v = 13	131064.25±0.05	4.08	0.00	0.12±0.15	0.82	1.4±0.3	1.08	1.8±0.2	88±17	12±17	
11p ₀ , v = 5	131076.80				0.72	tb	0.02				100
7p π , v = 6	131099.10±0.04	-0.15	0.12	0.23±0.15	4.54	4.7±0.7	0.02			13±8	87±8
11p ₂ , v = 5	131137.2±1.0	0.4	0.80	0.0±0.8	0.18	bl	0.81	0.66±0.22			100
6p σ , v = 7	131147.5±1.0	-0.3	5.76	5.2±0.6	0.18	bl	5.51	5.6±0.7			100
12p ₀ , v = 5	131231.03±0.25	-0.25	3.91	2.6±1.1	0.74	1.1±0.4	0.03				100
4p π , v = 10	131274.45±0.04	0.05	0.00	0.08±0.15	4.22	4.6±0.8	2.30	3.8±1.2	14±4	24±12	62±12
12p ₂ , v = 5	131283.37				0.01		0.63	tb			
13p ₀ , v = 5	131348.97±0.28	-0.01	1.12	1.7±0.9	0.48	0.39±0.10	0.04				100
13p ₂ , v = 5	131390.32				0.05		0.16				
5p π , v = 8	131420.92±0.04	-0.20	0.07	0.21±0.15	2.44	3.2±1.0 ^c	0.02				
14p ₀ , v = 5	131441.97				0.01		0.10				
14p ₂ , v = 5	131447.75±0.07	0.00	0.40	0.33±0.16	2.24	2.5±0.4	0.17				100
5p σ , v = 9	131472.75±0.10	-0.07	0.30	0.09±0.22	0.18	0.2±0.2 ^c	3.90	5.5±1.1			100
8p σ , v = 6	131501.17±0.21	1.09	4.16	4.0±0.6	1.36	1.5±0.5	2.35	2.8±0.5			100
15p ₀ , v = 5	131518.30±0.06	-0.10	0.10	0.00±0.16	0.22	0.2±0.2 ^c	0.28	bl			
6p π , v = 7	131553.71±0.06	-0.25	0.19	0.23±0.16	1.57	1.7±0.3	1.32	1.1±1.0			100
16p ₀ , v = 5	131562.03				0.18		0.81	tb			
15p ₂ , v = 5	131581.38				0.03		0.35	bl			
8p π , v = 6	131613.58±0.13	0.03	1.23	1.6±0.4	0.72	0.6±0.2	0.08				100
17p ₀ , v = 5	131622.2±1.0	-0.3	0.56	0.0±1.7	0.07		0.91	1.2±1.3			100
16p ₂ , v = 5	131635.13				0.00		0.59	bl			
18p ₀ , v = 5	131662.1±1.0	1.3	0.71		0.20	bl	0.00				
17p ₂ , v = 5	131680.71				0.02		0.34				
4p σ , v = 14	131687.44±0.05	1.75	0.03	0.01±0.15	0.93	1.3±0.2	1.89	2.5±0.3	46±11		54±11
19p ₀ , v = 5	131698.2±1.0	0.2	0.08	0.0±0.3	0.14	0.3±0.2	0.04				100
20p ₀ , v = 5	131718.60				0.09		0.12				
18p ₂ , v = 5	131730.56				0.05		0.14				
21p ₀ , v = 5	131748.99				0.12		0.00				
19p ₂ , v = 5	131760.10				0.00		0.14				
22p ₀ , v = 5	131773.81				0.10		0.02				
23p ₀ , v = 5	131786.02				0.01		0.04				
20p ₂ , v = 5	131795.30				0.07		0.06				
24p ₀ , v = 5	131807.43				0.03		0.01				
21p ₂ , v = 5	131813.92				0.07		0.00				
25p ₀ , v = 5	131825.13±0.07	-0.06	0.03		0.09	0.1±0.2 ^c	0.02				
9p σ , v = 6	131828.00±0.10	-0.36	0.02	0.00±0.20	0.14	0.2±0.3 ^c	0.16				
26p ₀ , v = 5	131837.66±0.09	0.04	0.23	0.09±0.19	0.21	0.2±0.3	0.03				100
22p ₂ , v = 5	131844.25				0.08		0.27				
27p ₀ , v = 5	131849.47				0.09		0.00				
28p ₀ , v = 5	131858.5±1.0	-0.1	0.62		0.14	0.26±0.09	0.05				100
9p π , v = 6	131948.88±0.06	-0.67	0.09	0.31±0.17	0.71	0.9±0.2	0.05				100
7p σ , v = 7	131982.5±1.0	-1.6	0.09		0.03		0.99	0.9±0.4			100
10p ₀ , v = 6	132136.11				0.59	tb	0.07				100
10p ₂ , v = 6	132214.51±0.12	-0.46	1.54	1.6±0.2	1.01	1.3±0.4	0.16				100
6p σ , v = 8	132248.22±0.24	0.11	2.99	2.7±0.9	1.09	bl	2.17	2.6±0.9			100
4p π , v = 11	132257.99±0.04	-0.43	0.01	0.01±0.15	3.31	2.7±0.6	1.17	1.5±0.4	56±12	22±12	22±10
7p π , v = 7	132323.00±0.08	0.18	1.31	1.6±0.2	1.75	1.3±0.3	0.87	1.2±0.8			100
11p ₀ , v = 6	132345.02				0.16		0.51	tb			
11p ₂ , v = 6	132404.7±1.0	-0.6	6.88		0.19		0.41	tb			100
5p σ , v = 10	132412.84±0.09	0.53	1.01	1.0±0.2	1.90	2.4±0.4	4.45	4.3±0.8			100
12p ₀ , v = 6	132495.6±1.0	0.6	5.54	4.2±1.5	0.47	0.5±0.2	0.00				100
5p π , v = 9	132537.38±0.07	0.16	0.24	0.40±0.16	1.96	1.8±0.5	2.12	2.0±0.4			100
12p ₂ , v = 6	132544.24				0.00		0.04				
13p ₀ , v = 6	132611.62				0.04		0.27				
8p σ , v = 7	132634.97±0.05	-0.63	0.14	0.10±0.15	1.15	1.3±0.2	0.21				100
13p ₂ , v = 6	132681.32±0.36	0.87	4.83	6.9±2.7	0.94	bl	1.23	1.3±0.4			100
6p π , v = 8	132705.49±0.05	-0.45	0.14	0.04±0.15	1.46	1.4±0.2	1.23	1.8±2.1	14±6		86±6
14p ₀ , v = 6	132712.36				0.04		0.19				
14p ₂ , v = 6	132756.59				0.29	tb	0.70	tb			
15p ₀ , v = 6	132785.82±0.08	-0.08	0.13	0.22±0.18	0.24	0.23±0.08	0.13				
8p π , v = 7	132822.72±0.36	1.00	4.15	4.5±1.0	0.67	1.1±0.4	0.01				100
16p ₀ , v = 6	132831.9±1.0	0.3	1.56	2.1±1.1	0.09		1.08	1.3±0.5			100

Table 2: Photoabsorption transitions of D₂ involving $N' = 1$ upper levels (cont'd)

state	$\frac{E}{hc}$ (cm ⁻¹)		$\frac{\Gamma}{hc}$ (cm ⁻¹)		$A(R0)$ (10 ⁶ s ⁻¹)		$A(P2)$ (10 ⁶ s ⁻¹)		γ_d (%)	γ_f (%)	γ_i (%)
	obs ^{a,b}	o-c ^a	calc	obs	calc	obs	calc	obs	obs	obs	obs
15p2, v = 6	132848.12				0.07		0.18				
17p0, v = 6	132881.94				0.17	tb	0.11				
16p2, v = 6	132900.30				0.05		0.16				
18p0, v = 6	132928.22±0.49	0.63	1.56	4.0±3.0	0.50	0.5±0.1	0.00				100
17p2, v = 6	132944.34				0.00		0.19				
19p0, v = 6	132965.57				0.12		0.03				
9pσ, v = 7	132978.68				0.00		0.02				
7pσ, v = 8	132994.23				0.17		0.03				
18p2, v = 6	132998.84				0.01		0.16				
20p0, v = 6	133016.97				0.13		0.02				
19p2, v = 6	133027.29				0.00		0.14				
22p0, v = 6	133041.45				0.10		0.01				
20p2, v = 6	133052.46				0.00		0.04				
23p0, v = 6	133062.83				0.08		0.04				
24p0, v = 6	133073.17				0.01		0.02				
21p2, v = 6	133079.36±0.07	-0.25	0.04	0.00±0.20	0.23	0.14±0.05	0.00				
25p0, v = 6	133088.84±0.26	0.06	0.79	1.4±0.4	0.22	0.29±0.08	0.24				
26p0, v = 6	133092.88±0.08	-0.08	0.13	0.00±0.17	0.11	bl	0.01				
9pπ, v = 7	133175.10±0.06	-0.45	0.08	0.02±0.16	0.25	bl	0.47				
4pπ, v = 12	133183.48±0.04	-5.82	0.00	0.00±0.15	1.65	1.8±0.3	1.31	1.4±0.4	69±13	12±16	19±6
5pσ, v = 11	133244.24				0.01		0.13				
6pσ, v = 9	133395.21±0.15	1.39	3.68	3.1±0.4	4.24	3.6±0.5	2.08	2.0±0.3			100
10p2, v = 7	133431.17				0.04		1.77	tb			
7pπ, v = 8	133478.61±0.05	-0.18	0.22	0.10±0.15	0.66	0.5±0.1	1.75	2.3±0.4			100
11p0, v = 7	133545.62				0.51		0.27				
5pπ, v = 10	133576.93±0.04	0.29	0.03	0.00±0.15	1.43	1.3±0.4	1.11	1.9±0.4	24±7		76±7
11p2, v = 7	133610.09				0.09		0.43	tb			
12p0, v = 7	133695.43				0.11		0.02				
12p2, v = 7	133738.07±0.07	-1.43	0.93	0.84±0.17	0.61	0.5±0.1	0.01				100
8pσ, v = 8	133788.3±1.0	1.0	2.08	2.5±2.4	0.79	0.6±0.4	0.53	0.8±0.2			100
6pπ, v = 9	133801.93±0.06	-1.05	0.09	0.19±0.16	0.80	1.2±0.2	1.20	1.6±0.4			100
13p0, v = 7	133830.06				0.49	tb	0.12				100
13p2, v = 7	133875.60				0.13		0.82	tb			
14p0, v = 7	133919.75±0.31	-0.20	1.41	1.9±0.5	0.39	bl	0.02				
14p2, v = 7	133958.92				0.23		0.22				
8pπ, v = 8	133976.17±0.06	-0.69	0.37	0.38±0.16	0.55	0.4±0.1	0.58	bl			100
15p0, v = 7	133995.74				0.10		0.05				
5pσ, v = 12	134004.12				0.06		0.34				
4pπ, v = 13	134053.57±0.04	-3.53	0.08	0.00±0.15	1.17	1.2±0.4	0.52	0.42±0.07	69±13	12±16	19±6
9pπ, v = 8	134322.1±1.0	-2.30	0.26	0.9±0.6	0.81	0.9±0.2	0.13				
6pσ, v = 10	134399.17±0.08	-1.96	0.63	0.76±0.17	1.07	bl	2.34	1.8±0.3	58±12		42±12
5pπ, v = 11	134555.24±0.07	0.23	0.58	0.55±0.17	1.61	1.8±0.3	1.70	1.3±0.3	4±1		96±1
8pσ, v = 9	134819.7±1.0	-0.9	0.89	0.6±0.5	0.24	bl	0.34				
6pπ, v = 10	134837.32±0.07	-2.77	0.79	0.72±0.17	1.38	1.4±0.3	0.46		22±6		78±6
4pπ, v = 14	134870.6±1.0	0.3	0.79	6.8±0.6	0.66	0.48±0.06	0.43	0.4±0.4	100		
4pπ, v = 15	135623.7±0.6	0.5	0.07	6.5±2.9	0.51	0.31±0.04	0.30		100		
4pπ, v = 16	136311.69±0.36	0.38	0.00	4.4±1.8	0.90	0.8±0.1	0.43		100		
4pπ, v = 17	136944.8±0.7	-2.1	0.00	5.0±1.6	0.40	0.9±0.1	0.23		100		

E/hc , upper state level energy. Γ/hc , calculated ionization width and observed total level width (FWHM). $A(R0)$, $A(P2)$ emission probability to the ground state for $R(0)$ and $P(2)$ transitions, respectively. $\gamma_d, \gamma_f, \gamma_i$, quantum yields for dissociation, fluorescence and ionization, respectively. The $P(2)$

transition energies are obtained from the upper state energy by subtracting the ground-state rotational energy 179.01 cm⁻¹ ($N'' = 2$).

^a When no observed-calculated value is given, the energy corresponds to the calculated value.

^b Transition energies with uncertainties = 1 cm⁻¹ are based on the NIM spectra.

^c Value based on the FT spectrum.

^d Complex resonance. The A value given corresponds to the sum over all components.

tb, too broad to be detected. bl, blended line.

Table 3: Photoabsorption transitions of D₂ involving $N' = 2$ upper levels

state	$\frac{E}{hc}$ (cm ⁻¹)		$\frac{\Gamma}{hc}$ (cm ⁻¹)		$A(R1)$ (10 ⁶ s ⁻¹)		$A(P3)$ (10 ⁶ s ⁻¹)		γ_d (%)	γ_f (%)	γ_i (%)
	obs ^{a,b}	o-c ^a	calc	obs	calc	obs	calc	obs	obs	obs	obs
4pσ, v = 0	117278.05±0.04	-0.66		0.00±0.15	2.00	2.6±0.8 ^c	2.14				
4pπ, v = 0	118250.66±0.04	-0.07		0.01±0.16	3.22	3.0±0.8 ^c	2.37				
4pσ, v = 1	118767.10±0.03	-0.65		0.00±0.15	4.81	5.8±1.3 ^c	6.02	9±7 ^c			
4pπ, v = 1	119831.75±0.03	-0.85		0.00±0.15	8.94	6.6±1.4 ^c	5.41	8±7 ^c			
5pσ, v = 0	120102.22±0.12	-0.43		0.00±0.22	0.66	0.8±0.4 ^c	0.39				
4pσ, v = 2	120190.30±0.05	-0.60		0.21±0.15	7.41	9.7±2.0 ^c	11.03	21±9 ^c			
5pπ, v = 0	120591.90±0.07	0.01		0.00±0.18	1.20	1.0±0.6 ^c	1.57				
4pπ, v = 2	121347.81±0.05	0.11		0.00±0.15	14.24	13.4±2.7 ^c	6.75	6±4 ^c			
4pσ, v = 3	121531.75±0.05	-0.42		0.00±0.15	2.99	4.2±1.0 ^c	8.62	13±7 ^c			
6pσ, v = 0	121564.14±0.09	-0.20		0.02±0.18	0.95	1.5±0.5 ^c	3.05	6±6 ^c			
5pσ, v = 1	121675.50±0.05	-0.69		0.00±0.15	7.23	8.1±1.7 ^c	6.10	13±8 ^c			
6pπ, v = 0	121881.19				0.28		1.54				
5pπ, v = 1	122169.23±0.05	-0.31		0.13±0.15	3.21	3.6±0.9 ^c	3.72				
7pσ, v = 0	122469.96±0.09	-0.23		0.00±0.19	0.84	1.0±0.4 ^c	0.25				
7pπ, v = 0	122665.89				0.21		0.79				
4pπ, v = 3	122774.90±0.05	-0.13		0.00±0.15	21.90	20±4 ^c	0.00				
4pσ, v = 4	122843.82±0.07	-0.23		0.00±0.16	0.40		19.52	27±7 ^c			
8p1, v = 0	123023.36±0.08	-0.12		0.00±0.17	0.80	0.8±0.4 ^c	0.26				
5pσ, v = 2	123055.73±0.08	-0.08		0.00±0.18	0.64	1.0±0.5 ^c	1.96				
8p3, v = 0	123176.30±0.06	-0.10		0.00±0.15	2.55	3.0±0.8 ^c	0.23				
6pσ, v = 1	123212.46±0.05	-0.67		0.00±0.15	6.68	6.4±1.4 ^c	6.48	11±7 ^c			
9p1, v = 0	123406.50±0.07	-0.19		0.00±0.16	0.92	0.8±0.4 ^c	0.01				
6pπ, v = 1	123456.10±0.13	0.05		0.04±0.26	1.00	0.9±0.4 ^c	3.64				
9p3, v = 0	123540.83				0.00		0.63				
10p1, v = 0	123674.24±0.10	0.12		0.00±0.20	0.53	0.6±0.4 ^c	0.03				
5pπ, v = 2	123682.65±0.06	-0.02		0.04±0.15	4.73	5.8±0.8	5.09	8±6 ^c	25±10	75±10	
10p3, v = 0	123796.44				0.00	tl	0.30				
11p1, v = 0	123871.19±0.09	-0.16		0.00±0.16	0.23	tl	0.04				
11p3, v = 0	123980.77				0.00	tl	0.05				
4pσ, v = 5	124010.55±0.06	-0.46		0.00±0.15	10.60	11.6±1.4	5.67	10.0±1.0	93±2	7±2	
12p1, v = 0	124024.18±0.05	-0.03		0.00±0.15	0.43	0.55±0.17	0.02	tl	40±15	60±15	
7pσ, v = 1	124034.49±0.09	-0.22		0.00±0.19	1.82	1.4±0.6 ^c	0.87	1.1±0.2	41±12	59±12	
13p1, v = 0	124116.3±1.0	-0.4			0.31	0.50±0.08	0.01	tl	24±6	76±6	
12p3, v = 0	124153.16				0.01	tl	0.06	tl			
4pπ, v = 4	124208.27±0.05	0.06		0.00±0.15	10.17	10.6±1.9	13.26	16.4±2.3	36±4	64±4	
14p1, v = 0	124212.8±1.0	0.4			0.20	tl	0.00	tl			
7pπ, v = 1	124237.3±1.0	0.3			0.65	0.7±0.2	1.63	1.8±0.4	51±19	49±19	
13p3, v = 0	124260.02				0.00	tl	0.19	tl			
15p1, v = 0	124289.44				0.01	tl	0.00	tl			
16p1, v = 0	124339.37				0.09	tl	0.03	tl			
14p3, v = 0	124358.58				0.01	tl	0.10	tl			
17p1, v = 0	124393.5±1.0	-0.6			0.07	0.14±0.12	0.00	tl	100		
15p3, v = 0	124423.83				0.04	tl	0.13	tl			
18p1, v = 0	124439.08				0.02	tl	0.09	tl			
5pσ, v = 3	124461.09±0.06	-0.07		0.16±0.17	2.20	3.8±0.6	2.99	tl	34±8	66±8	
19p1, v = 0	124468.85				0.05	tl	0.00	tl			
16p3, v = 0	124486.69				0.00	tl	0.08	tl			
20p1, v = 0	124501.55				0.04	tl	0.01	tl			
21p1, v = 0	124524.07				0.03	tl	0.01	tl			
17p3, v = 0	124536.81				0.00	tl	0.07	tl			
22p1, v = 0	124548.92				0.03	tl	0.01	tl			
23p1, v = 0	124566.05				0.02	tl	0.00	tl			
18p3, v = 0	124576.88				0.00	tl	0.09	tl			
24p1, v = 0	124585.52				0.03	tl	0.02	tl			
8p1, v = 1	124590.80				0.03	tl	0.20	tl			
25p1, v = 0	124598.07				0.03	tl	0.01	tl			
26p1, v = 0	124610.58				0.01	tl	0.00	tl			
19p3, v = 0	124615.93				0.01	tl	0.01	tl			
27p1, v = 0	124624.47				0.03	tl	0.00	tl			
28p1, v = 0	124634.30				0.01	tl	0.00	tl			
29p1, v = 0	124642.16				0.00	tl	0.00	tl			
20p3, v = 0	124646.22				0.01	tl	0.01	tl			
30p1, v = 0	124653.02				0.02	tl	0.00	tl			
31p1, v = 0	124660.29				0.01	tl	0.00	tl			
32p1, v = 0	124666.62				0.00	tl	0.00	tl			
21p3, v = 0	124670.37				0.02	tl	0.00	tl			
33p1, v = 0	124674.48				0.02	tl	0.00	tl			
34p1, v = 0	124679.84				0.01	tl	0.00	tl			
6pσ, v = 2	124684.90±0.06	-0.68		0.25±0.15	9.79	7.4±0.9	3.69	11±7 ^c	51±7	49±8	
36p1, v = 0	124689.4±1.0	-0.1			0.14	0.10±0.02	0.04	tl	100		

Table 3: Photoabsorption transitions of D₂ involving $N' = 2$ upper levels (cont'd)

state	$\frac{E}{hc}$ (cm ⁻¹)		$\frac{\Gamma}{hc}$ (cm ⁻¹)		$A(R1)$ (10 ⁶ s ⁻¹)		$A(P3)$ (10 ⁶ s ⁻¹)		γ_d (%)	γ_f (%)	γ_i (%)
	obs ^{a,b}	o-c ^a	calc	obs	calc	obs	calc	obs	obs	obs	obs
26p3, v = 0	124760.00				0.02		0.40				
8p3, v = 1	124760.22±0.11	0.28		0.00±0.21	0.15	0.32±0.10 ^d	1.98	3.7±0.5			100
87p1, v = 0	124760.40				0.04		0.37				
88p1, v = 0	124760.71				0.01		0.10				
6pπ, v = 2	124960.98±0.07	0.07			3.52	3.0±0.9 ^c	4.21	5.1±0.8			100
9pσ, v = 1	124984.1±1.0	0.5			0.31	0.44±0.09	1.27	bl			100
9pπ, v = 1	125109.0±1.0	-0.5			0.02	tl	1.54	1.6±0.2			100
5pπ, v = 3	125132.69±0.06	-0.05	0.00	0.00±0.16	5.94	5.5±1.0	4.89		11±3	38±9	51±9
4pσ, v = 6	125146.32±0.05	-0.46	0.00	0.00±0.15	7.44	9.4±1.5	7.37	13.4±2.6	90±7	9±3	1±3
10p1, v = 1	125248.27±0.17	0.14	0.89	0.5±0.3	0.85	0.93±0.13	0.00	tl			100
10p3, v = 1	125363.5±1.0	-0.2			0.00	tl	0.68	0.7±0.4			100
11p1, v = 1	125445.69±0.15	-0.42	0.33	0.25±0.29	0.52	0.38±0.12 ^c	0.19	bl			
7pσ, v = 2	125519.78±0.08	-0.22	0.09	0.04±0.16	1.90	1.7±0.5	0.31	0.36±0.11			100
4pπ, v = 5	125537.10±0.21	0.09	0.00	0.00±0.15	9.88	10.1±1.2	8.96	11.7±1.9	75±10	18±3	7±7
11p3, v = 1	125561.53±0.20	-0.18	1.23	0.77±0.40	1.21	1.4±0.4 ^c	1.13	1.8±0.6			100
12p1, v = 1	125599.16±0.09	0.03	0.05	0.07±0.16	0.32	1.0±0.5 ^c	0.29	bl			
13p1, v = 1	125688.87±0.21	-0.10	0.95	1.3±0.5	0.61	0.87±0.17	0.06	tl			100
12p3, v = 1	125725.01				0.59	bl	0.00	tl			
7pπ, v = 2	125742.98±0.06	-0.07	0.01	0.00±0.15	0.88	bl	3.18	bl		7±3	93±3
14p1, v = 1	125787.73±0.21	0.05	0.44	0.4±0.4	0.34	0.40±0.12	0.07	tl			100
5pσ, v = 4	125800.95±0.07	-0.13	0.00	0.00±0.15	2.50	3.8±0.6	2.66	3.2±1.5	34±6	12±3	54±9
13p3, v = 1	125830.35				0.00	tl	0.44	bl			
15p1, v = 1	125864.42±0.11	-0.11	0.12	0.00±0.19	0.40	0.5±0.5	0.02	tl			100
16p1, v = 1	125912.1±1.0	0.2			0.17	bl	0.10	tl			
14p3, v = 1	125931.38±0.20	0.03	0.07	0.20±0.34	0.13	0.3±0.3	0.09	tl			100
17p1, v = 1	125968.84				0.29	bl	0.00	tl			
15p3, v = 1	125994.8±1.0	0.1			0.00	tl	0.25	tl			
18p1, v = 1	126013.88				0.14	tl	0.04	tl			
19p1, v = 1	126043.3±1.0	0.5			0.14	tl	0.08	tl			
16p3, v = 1	126056.9±1.0	0.3			0.04	tl	0.71	0.9±1.1			100
8pσ, v = 2	126064.73±0.08	-0.33	0.06	0.06±0.16	0.89	1.3±0.5 ^c	0.98	1.0±0.3			100
20p1, v = 1	126076.76				0.05	tl	0.05	tl			
21p1, v = 1	126098.43				0.01	tl	0.01	tl			
17p3, v = 1	126108.73±0.13	-0.07	0.09	0.29±0.21	0.28	0.4±0.4 ^c	0.01	tl			
22p1, v = 1	126124.15±0.10	0.06	0.05	0.00±0.17	0.01	tl	0.06	tl			
6pσ, v = 3	126134.94±0.07	-0.43	0.01	0.00±0.16	5.81	6.2±0.8	1.56	2.1±0.4	11±3	89±3	
23p1, v = 1	126142.52±0.09	-0.11	0.15	0.14±0.16	2.21	2.7±0.3	0.45	0.32±0.25			100
18p3, v = 1	126151.4±1.0	0.5			0.54	bl	0.48	tl			
24p1, v = 1	126160.70				0.10	tl	0.01	tl			
25p1, v = 1	126174.12±0.10	-0.07	0.11	0.14±0.17	0.16	0.3±0.3 ^c	0.01	tl			
19p3, v = 1	126183.48				0.07	tl	0.10	tl			
26p1, v = 1	126189.72				0.03	tl	0.04	tl			
27p1, v = 1	126199.97				0.07	tl	0.00	tl			
4pσ, v = 7	126204.75±0.07	-0.45	0.00	0.02±0.15	7.80	9.8±1.4	7.68	12±2	98±17	2±2	0±17
28p1, v = 1	126209.35				0.10	tl	0.02	tl			
8pπ, v = 2	126265.0±1.0	0.3			0.01	tl	2.65	3.4±1.0			100
6pπ, v = 3	126409.41±0.07	0.08	0.00	0.00±0.15	3.65	4.3±1.1	6.27	8.3±1.8		15±6	85±6
9pσ, v = 2	126488.3±1.0	0.9			1.43 ^d	1.3±0.3 ^d	0.09 ^d	tl			100
5pπ, v = 4	126521.26±0.07	-0.11	0.00	0.00±0.15	5.14	5.1±0.9	4.50	7.7±2.9	5±1	19±4	76±5
9pπ, v = 2	126613.6±1.0	0.2			0.01	tl	1.86	1.9±0.5			100
10p1, v = 2	126756.76±0.46	0.08	2.05	2.6±0.8	1.20	1.4±0.3	0.01	tl			100
4pπ, v = 6	126807.57±0.08	0.11	0.00	0.00±0.16	9.29	8.6±1.3	5.94	8.7±1.9	81±8	19±8	
10p3, v = 2	126863.9±1.0	0.0			0.05	tl	0.72	0.8±0.2			100
11p1, v = 2	126951.07±0.10	-0.08	0.16	0.02±0.18	0.07	tl	1.07	0.9±0.4			100
7pσ, v = 3	126963.86±0.09	-0.02	0.70	0.62±0.16	3.45	3.6±0.9 ^c	0.46	0.8±0.4			100
11p3, v = 2	127061.1±1.0	-0.6			0.85	bl	1.45	1.9±0.5			100
5pσ, v = 5	127066.70±0.08	-0.17	0.06	0.03±0.16	0.79	1.1±0.3	1.59	1.8±0.8	10±4		90±4
12p1, v = 2	127108.93±0.12	-0.09	0.13	0.34±0.19	0.66	0.8±0.5 ^c	0.37	tl			
13p1, v = 2	127183.3±1.0	-0.5			0.31	bl or tl	4.60	5.9±1.4			100
4pσ, v = 8	127189.33±0.06	-0.44	0.15	0.00±0.16	6.49	11.6±1.6	4.35	4.6±1.9	20±4		80±4
7pπ, v = 3	127199.48				0.06	tl	0.64	tl			
12p3, v = 2	127233.6±1.0	0.7			0.11	0.22±0.07	0.37	tl			100
14p1, v = 2	127296.76±0.13	-0.21	1.15	tl	0.42	0.6±0.4	0.02	tl			100
13p3, v = 2	127336.21				0.01	tl	0.56	tl			
15p1, v = 2	127374.83±0.13	0.01	0.34	0.09±0.21	0.61	0.6±0.2	0.02	tl			100
14p3, v = 2	127418.40				0.14	tl	0.27	tl			
16p1, v = 2	127440.00±0.17	-0.29	0.04	tl	0.27	0.4±0.4 ^c	1.26	tl			
6pσ, v = 4	127441.75±0.07	-0.50	0.01	0.02±0.15	3.12	5.2±1.4 ^c	3.53	bl			
17p1, v = 2	127478.53±0.11	0.14	0.66	tl	0.07	tl	0.01	tl			

Table 3: Photoabsorption transitions of D₂ involving $N' = 2$ upper levels (cont'd)

state	$\frac{E}{hc}$ (cm ⁻¹)		$\frac{\Gamma}{hc}$ (cm ⁻¹)		$A(R1)$ (10 ⁶ s ⁻¹)		$A(P3)$ (10 ⁶ s ⁻¹)		γ_d (%)	γ_f (%)	γ_i (%)
	obs ^{a,b}	o-c ^a	calc	obs	calc	obs	calc	obs	obs	obs	obs
15p3, v = 2	127500.95±0.14	0.14	0.61	tl	0.20	tl	0.10	tl			
18p1, v = 2	127524.21±0.13	0.02	0.14	0.16±0.22	0.20	tl	0.01	tl			
19p1, v = 2	127547.75±0.09	-0.23	0.36	0.47±0.17	1.26	1.3±0.2	0.23	tl			100
8pσ, v = 3	127561.24±0.08	-0.14	0.09	0.06±0.15	3.45	4.6±1.1 ^c	0.37	tl			
16p3, v = 2	127570.40±0.08	-0.13	0.36	0.35±0.15	2.26	2.4±0.7	1.43	bl			100
20p1, v = 2	127587.50±0.11	-0.01	0.23	0.26±0.19	0.50	0.7±0.4 ^c	0.00	tl			
21p1, v = 2	127608.10±0.21	-0.18	0.72	0.80±0.40	0.48	0.7±0.2	0.20	tl			100
17p3, v = 2	127617.79				0.00	tl	0.22	tl			
22p1, v = 2	127634.83±0.16	0.05	0.20	tl	0.24	bl or tl	0.00	tl			
23p1, v = 2	127650.09±0.22	-0.17	0.57	tl	0.22	0.2±0.2	0.10	tl			100
18p3, v = 2	127658.32				0.01	tl	0.15	tl			
24p1, v = 2	127671.19±0.13	-0.06	0.12	0.18±0.22	0.16	tl	0.03	tl			
25p1, v = 2	127683.71±0.20	0.01	0.35	tl	0.16	tl	0.00	tl			
19p3, v = 2	127691.00				0.00	tl	0.02	tl			
26p1, v = 2	127700.23±0.40	0.46	0.03	tl	0.14	tl	0.43	tl			
8p3, v = 3	127704.42±0.12	0.01	0.01	0.00±0.20	0.07	tl	2.67	bl			
27p1, v = 2	127711.52				0.04	tl	0.42	tl			
28p1, v = 2	127719.09				0.02	tl	0.54	tl			
20p3, v = 2	127723.69				0.02	tl	0.11	tl			
29p1, v = 2	127731.68				0.07	tl	0.00	tl			
30p1, v = 2	127739.47				0.06	tl	0.04	tl			
21p3, v = 2	127745.08				0.01	tl	0.19	tl			
31p1, v = 2	127749.08				0.03	tl	0.05	tl			
32p1, v = 2	127755.03				0.07	tl	0.78	tl			
33p1, v = 2	127760.95				0.05	tl	0.01	tl			
23p3, v = 2	127790.49				0.15	tl	0.23	tl			
6pπ, v = 4	127792.44±0.07	0.11	0.00	0.00±0.15	4.80	4.9±0.8	6.76	9.5±1.7	13±8	7±5	80±9
5pπ, v = 5	127850.66±0.07	-0.22	0.00	0.00±0.15	3.74	4.2±0.9	2.38	3.1±0.9	20±7	59±15	21±6
38p3, v = 2	127920.91				0.07	tl	0.01	tl			
39p3, v = 2	127924.60				0.17	tl	0.00	tl			
40p3, v = 2	127927.15±0.22	-0.59			0.46	0.4±0.4 ^c	0.02	tl			100
9pσ, v = 3	127930.35±0.09	0.14			0.27	0.3±0.8	0.09	tl			100
41p3, v = 2	127932.63±0.12	-0.11			0.28	0.5±0.7	0.09	tl			100
42p3, v = 2	127935.55±0.15	0.02	0.16	0.3±0.3	0.38	0.3±0.3	0.01	tl			100
4pπ, v = 7	128011.42±0.07	-0.01	0.00	0.06±0.15	8.45	9.8±1.5	1.99	2.4±0.5	100		
9pπ, v = 3	128054.09				0.07	tl	1.99	bl			
4pσ, v = 9	128092.20±0.10	-0.50	0.00	0.00±0.17	0.24	0.6±0.1	5.47	7.4±1.1	100		
10p1, v = 3	128200.41±0.40	-0.11	3.02	3.30±1.00	1.03	1.14±0.16	0.03	tl			100
5pσ, v = 6	128279.31±0.07	-0.27	0.14	0.17±0.15	3.98	4.7±0.6	3.98	2.9±0.9 ^c			100
10p3, v = 3	128290.6±1.0	-0.9			0.00	tl	1.95	2.6±0.6			100
7pσ, v = 4	128342.63±0.48	-0.14	2.36	2.40±0.90	0.95	0.8±0.6 ^c	1.69	1.8±0.5			100
11p1, v = 3	128404.29±0.16	0.06	1.59	1.78±0.28	1.54	1.9±0.2	0.10	tl			100
11p3, v = 3	128501.90				0.84	tb	1.21	tb			
12p1, v = 3	128555.02±0.09	-0.03	0.26	0.26±0.16	1.50	1.8±0.3	0.83	tl			100
7pπ, v = 4	128569.51±0.07	-0.07	0.04	0.05±0.15	1.57	1.9±0.6 ^c	1.27	1.7±0.6			100
13p1, v = 3	128639.5±1.0	-0.5			0.25	0.3±0.3	0.44	tl			100
12p3, v = 3	128678.07±0.11	-0.19	0.31	0.31±0.19	0.27	0.2±0.2	0.36	tl			100
14p1, v = 3	128742.33				0.11	tl	0.03	tl			
6pσ, v = 5	128747.46±0.07	-0.78	0.19	0.19±0.15	3.84	4.2±0.8	4.72	4.6±1.8			100
13p3, v = 3	128779.5±1.0	0.3			0.05	tl	0.55	1.0±0.3			100
15p1, v = 3	128821.97±0.43	0.22	0.62	0.5±0.7	0.37	0.34±0.16	0.03	tl			100
14p3, v = 3	128860.33				0.02	tl	0.16	tl			
16p1, v = 3	128886.89±0.12	-0.06	0.06	0.08±0.22	0.38	0.8±0.4	0.16	tl			100
17p1, v = 3	128917.92				0.04	tl	0.03	tl			
4pσ, v = 10	128920.93±0.08	-0.49	0.11	0.20±0.15	3.52	4.5±0.8	2.34	3.4±1.1	44±10		56±10
8pσ, v = 4	128934.49±0.08	-0.08	0.28	0.20±0.15	3.67	4.4±1.2	0.35	tl			100
15p3, v = 3	128952.21±0.19	0.52	0.99	1.25±0.22	1.34	2.5±1.3 ^c	1.18	bl			
18p1, v = 3	128971.78±0.11	0.01	0.40	0.43±0.18	0.58	0.6±0.4	0.01	tl			100
19p1, v = 3	128999.1±1.0	0.0			0.59	0.58±0.22	0.23	tl			100
16p3, v = 3	129012.21				0.02	tl	0.28	tl			
20p1, v = 3	129034.29±0.11	-0.20	0.51	0.68±0.23	0.42	0.7±0.4	0.01	tl			100
17p3, v = 3	129052.15				0.19	tl	0.07	tl			
21p1, v = 3	129063.85±0.14	-0.23	0.03	0.23±0.26	0.14	0.16±0.16 ^c	0.20	tl			
22p1, v = 3	129079.40±0.12	-0.16	0.25	tl	0.98	1.3±0.4	1.71	1.7±0.4			100
8p3, v = 4	129086.31±0.11	-0.10	0.10	0.23±0.22	0.37	0.2±0.4 ^c	2.92	5.2±1.5			100
18p3, v = 3	129096.28±0.16	-0.07	0.84	0.7±0.3	0.68	0.6±0.4 ^c	3.21	bl			
5pπ, v = 6	129099.45±0.07	0.11	0.05	0.00±0.15	6.86	6.2±1.0	4.15	3.0±1.1			100
23p1, v = 3	129104.86				0.02	tl	0.01	tl			
24p1, v = 3	129119.16				0.10	tl	0.04	tl			
19p3, v = 3	129130.19				0.04	tl	0.27	tl			

Table 3: Photoabsorption transitions of D₂ involving $N' = 2$ upper levels (cont'd)

state	$\frac{E}{hc}$ (cm ⁻¹)		$\frac{\Gamma}{hc}$ (cm ⁻¹)		$A(R1)$ (10 ⁶ s ⁻¹)		$A(P3)$ (10 ⁶ s ⁻¹)		γ_d (%)	γ_f (%)	γ_i (%)
	obs ^{a,b}	o-c ^a	calc	obs	calc	obs	calc	obs	obs	obs	obs
6p π , v = 5	129135.08				0.11	tl	0.11	tl			
25p1, v = 3	129137.12				0.05	tl	0.07	tl			
26p1, v = 3	129147.86				0.09	tl	0.00	tl			
27p1, v = 3	129157.77				0.06	tl	0.09	tl			
20p3, v = 3	129163.70				0.00	tl	0.16	tl			
28p1, v = 3	129170.94				0.05	tl	0.01	tl			
29p1, v = 3	129179.30				0.07	tl	0.01	tl			
4p π , v = 8	129182.53±0.08	0.03	0.00	0.01±0.15	3.14	4.1±0.8	3.22	3.9±1.0	46±11	54±11	
21p3, v = 3	129186.06				0.02	tl	0.10	tl			
39p1, v = 3	129241.56				0.04	tl	0.17	tl			
44p1, v = 3	129253.78				0.02	tl	0.67	tl			
45p1, v = 3	129256.12				0.02	tl	0.01	tl			
9p1, v = 4	129318.74				0.06	tl	0.01	tl			
5p σ , v = 7	129415.66±0.07	-0.32	0.04	0.04±0.15	2.02	2.7±0.5	3.16	4.0±2.6	8±3	6±5	86±6
9p π , v = 4	129432.38				0.00	tl	0.12	tl			
10p1, v = 4	129574.50±0.34	-0.69	2.03	1.40±0.70	0.34	0.25±0.17	0.08	tl			100
7p σ , v = 5	129620.47±0.23	-0.11	0.80	1.06±0.20	2.11	3.4±0.5	0.13	tl			100
10p3, v = 4	129702.0±1.0	1.1			1.00	1.6±0.9 ^c	3.76	4.6±0.9			100
4p σ , v = 11	129702.07±0.10	-1.05	0.46	0.86±0.17	1.13	1.9±0.9 ^c	0.76	0.74±0.14	19±4		81±4
11p1, v = 4	129788.84±0.40	0.07	2.36	2.9±0.8	1.40	1.5±0.7	0.08	tl			100
11p3, v = 4	129879.41				0.93	tl	0.26	tl			
7p π , v = 5	129887.01±0.11	-0.34	0.74	0.94±0.19	2.48	2.0±0.4	1.30	tl			100
12p1, v = 4	129941.88±0.23	-0.12	0.46	0.38±0.41	0.43	0.5±0.1	0.24	tl			100
6p σ , v = 6	129994.75±0.07	-0.85	0.01	0.00±0.15	2.16	3.2±0.4	4.56	6.7±1.2	2±1	5±3	93±3
13p1, v = 4	130022.89±0.71	1.27	4.67	4.10±1.80	0.59	0.7±0.6 ^c	1.20	tl			
12p3, v = 4	130062.7±1.0	0.1			0.34	0.5±0.1	0.45	0.7±0.6			100
14p1, v = 4	130124.96±0.30	0.09	1.54	1.3±0.5	0.27	0.30±0.11	0.04	tl			100
13p3, v = 4	130160.41				0.24	tl	0.34	tl			
15p1, v = 4	130205.69				0.10	tl	0.08	tl			
14p3, v = 4	130229.46±0.13	-0.40	0.28	0.35±0.21	1.86	2.2±0.4	0.02	tl			100
8p σ , v = 5	130260.25±0.16	0.29	1.90	1.60±0.40	4.21	4.2±1.2 ^c	0.31	tl			100
4p π , v = 9	130266.67±0.07	0.08	0.06	0.00±0.15	5.72	5.7±1.3 ^c	4.88	7.8±2.0	28±8		72±8
16p1, v = 4	130272.40				0.16	tl	0.14	tl			
17p1, v = 4	130311.71±0.47	0.78	2.44	3.0±0.8	1.11	1.1±0.3	0.04	tl			100
5p π , v = 7	130319.47±0.08	-0.29	0.04	0.04±0.16	1.89	2.0±0.5	1.78	2.5±0.5	8±4		92±4
15p3, v = 4	130330.55				0.00	tl	0.47	tl			
18p1, v = 4	130357.5±1.0	0.5			0.41	0.4±0.4 ^c	0.02	tl			
16p3, v = 4	130380.7±1.0	0.1			0.27	tl	0.03	tl			
6p π , v = 6	130393.08±0.09	-0.11	0.08	0.31±0.16	0.73	0.9±0.9 ^c	2.45	tl			
19p1, v = 4	130397.02				0.04	tl	0.04	tl			
8p π , v = 5	130406.3±1.0	0.0			0.10	0.13±0.12	1.24	tl			100
4p σ , v = 12	130419.21±0.11	-0.05	0.03	0.11±0.19	0.49	0.69±0.12	0.70	0.75±0.16	71±6		29±6
20p1, v = 4	130421.50				0.04	tl	0.14	tl			
17p3, v = 4	130435.90				0.00	tl	0.49	tl			
21p1, v = 4	130449.46±0.14	-0.24	0.10	0.00±0.21	0.12	0.2±0.3 ^c	0.02	tl			
22p1, v = 4	130467.63				0.11	tl	0.07	tl			
18p3, v = 4	130478.52				0.00	tl	0.24	tl			
23p1, v = 4	130490.51				0.09	tl	0.03	tl			
5p σ , v = 8	130501.23±0.07	-0.55	0.00	0.03±0.15	1.80	2.3±0.8	5.95	tl	75±13		25±13
24p1, v = 4	130505.0±1.0	0.6			0.26	0.43±0.17	0.32	tl			100
19p3, v = 4	130513.28				0.00	tl	0.23	tl			
25p1, v = 4	130522.57				0.08	tl	0.03	tl			
26p1, v = 4	130533.54				0.08	tl	0.01	tl			
27p1, v = 4	130541.61				0.01	tl	0.09	tl			
28p1, v = 4	130548.34				0.05	tl	0.06	tl			
29p1, v = 4	130556.91				0.07	tl	0.00	tl			
21p3, v = 4	130564.50				0.02	tl	0.03	tl			
30p1, v = 4	130569.84				0.01	tl	0.08	tl			
23p3, v = 4	130609.47				0.07	tl	0.01	tl			
36p1, v = 4	130613.29				0.08	tl	0.01	tl			
37p1, v = 4	130617.29				0.04	tl	0.01	tl			
38p1, v = 4	130620.41				0.06	tl	0.05	tl			
9p σ , v = 5	130621.99±0.11	-0.13	0.01	0.06±0.20	0.30	0.5±0.2	0.03	tl	33±28		67±28
39p1, v = 4	130625.31±0.09	-0.04			0.18	0.3±0.3 ^c	0.01	tl			
40p1, v = 4	130628.61±0.15	-0.10			0.16	0.2±0.2 ^c	0.01	tl			
41p1, v = 4	130631.66±0.08	-0.07	0.18	0.22±0.16	0.26	0.17±0.06	0.07	tl			100
24p3, v = 4	130632.82				0.11	tl	0.17	tl			
42p1, v = 4	130635.04				0.04	tl	0.00	tl			
43p1, v = 4	130637.79				0.06	tl	0.00	tl			
44p1, v = 4	130640.36				0.07	tl	0.00	tl			

Table 3: Photoabsorption transitions of D₂ involving $N' = 2$ upper levels (cont'd)

state	$\frac{E}{hc}$ (cm ⁻¹)		$\frac{\Gamma}{hc}$ (cm ⁻¹)		$A(R1)$ (10 ⁶ s ⁻¹)		$A(P3)$ (10 ⁶ s ⁻¹)		γ_d (%)	γ_f (%)	γ_i (%)
	obs ^{a,b}	o-c ^a	calc	obs	calc	obs	calc	obs	obs	obs	obs
45p1, v = 4	130642.73				0.08	tl	0.02	tl			
46p1, v = 4	130644.77				0.09	tl	0.06	tl			
25p3, v = 4	130646.19				0.03	tl	0.09	tl			
48p1, v = 4	130649.58				0.02	tl	0.00	tl			
37p3, v = 4	130745.38				0.07	tl	0.27	tl			
9p π , v = 5	130747.01±0.18	-0.35	0.16	0.19±0.31	0.17	0.17±0.05 ^c	0.71	tl			
39p3, v = 4	130750.08				0.02	tl	0.10	tl			
7p σ , v = 6	130843.86±0.16	-0.57	0.10	0.00±0.25	0.13	0.09±0.05	0.51	0.6±0.3			100
10p1, v = 5	130816.6±1.0	-0.2			1.77	2.6±0.4	0.03	tl			100
10p3, v = 5	131014.78				0.00	tl	1.24	tb			
4p σ , v = 13	131088.03±0.08	3.00	0.00	0.01±0.16	1.19	1.3±0.2	0.98	1.1±0.2	100		
11p1, v = 5	131112.28				1.38	tb	0.13	tl			
7p π , v = 6	131130.86±0.07	-0.52	0.07	0.12±0.15	4.22	4.8±1.1	0.31	tl			100
11p3, v = 5	131188.1±1.0	-1.0			0.04	tl	0.81	1.2±0.7			100
6p σ , v = 7	131210.3±1.0	1.1			0.41	bl or tl	5.03	6±6			
12p1, v = 5	131267.27±0.21	0.12	0.98	0.9±0.4	0.65	0.8±0.3	0.09	tl			100
4p π , v = 10	131314.08±0.07	-0.01	0.00	0.00±0.15	3.77	3.8±0.5	2.70	2.2±0.4	79±10	21±10	
12p3, v = 5	131338.29				0.12	tb	0.45	tl			
13p1, v = 5	131386.97±0.10	-0.16	0.16	0.01±0.18	0.41	0.6±0.4	0.32	tl			100
14p1, v = 5	131441.00				0.38	tb	0.01	tl			
5p σ , v = 9	131447.86±0.09	0.14	0.31	0.45±0.18	3.92	3.5±0.5	0.12	tl			100
8p σ , v = 6	131476.65±0.09	-0.31	0.12	0.15±0.16	1.69	1.9±0.6 ^c	0.16	tl			100
13p3, v = 5	131500.69±0.22	0.37	1.06	1.30±0.40	1.27	1.7±0.4	0.00	tl			100
5p π , v = 8	131525.7±1.0	-0.40			0.00	tl	3.78	4.5±0.8			100
15p1, v = 5	131536.12±0.17	0.03	1.73	1.10±0.40	1.18	1.2±0.3	0.55	0.5±0.5			100
14p3, v = 5	131570.5±1.0	-0.6			0.69	0.55±0.10	1.04	bl			100
6p π , v = 7	131596.78±0.09	0.03	0.21	0.02±0.17	0.77	0.6±0.3	0.86	bl			100
16p1, v = 5	131599.78±0.22	-0.67	0.16	0.00±0.25	0.25	0.3±0.5 ^c	1.34	2.0±0.4			100
17p1, v = 5	131632.4±1.0	-0.1			0.40	0.48±0.14	0.14	tl			100
15p3, v = 5	131653.60				0.02	tl	0.20	tl			
8p π , v = 6	131667.61±0.13	-0.10	0.07	0.02±0.17	0.27	0.34±0.13	1.57	1.1±0.7			100
18p1, v = 5	131683.95				0.13	tl	0.23	tl			
16p3, v = 5	131704.41				0.02	tl	0.61	tl			
19p1, v = 5	131722.07±0.19	-0.01	0.10	0.1±0.4	0.14	tl	0.05	tl			
20p1, v = 5	131744.48				0.14	tl	0.11	tl			
17p3, v = 5	131758.24				0.01	tl	0.27	tl			
21p1, v = 5	131775.04				0.13	tl	0.01	tl			
18p3, v = 5	131790.3±1.0	-0.7			0.05	tl	0.11	tl			
22p1, v = 5	131801.90				0.04	tl	0.15	tl			
23p1, v = 5	131815.87				0.10	tl	0.00	tl			
19p3, v = 5	131827.45				0.01	tl	0.07	tl			
24p1, v = 5	131836.70				0.05	tl	0.08	tl			
25p1, v = 5	131847.94				0.06	tl	0.01	tl			
20p3, v = 5	131855.94				0.01	tl	0.01	tl			
26p1, v = 5	131863.60±0.08	-0.13	0.06	0.00±0.15	0.14	0.2±0.2	0.01	tl			100
27p1, v = 5	131873.72				0.04	tl	0.04	tl			
9p σ , v = 6	131874.51±0.14	-0.31	0.06	0.00±0.22	0.33	0.6±0.3 ^d	0.11	tl			100
28p1, v = 5	131883.62±0.11	-0.06	0.26	0.12±0.18	0.21	0.45±0.21	0.01	tl			100
29p1, v = 5	131891.57				0.21	tl	0.11	tl			
21p3, v = 5	131895.22				0.00	tl	0.12	tl			
30p1, v = 5	131901.71				0.09	tl	0.00	tl			
51p1, v = 5	131981.88±0.10	0.24	0.01	0.09±0.17	0.02	tl	0.02	tl			
52p1, v = 5	131982.71±0.09	-0.30	0.03	0.08±0.16	0.14	tl	0.03	tl			
7p σ , v = 7	131983.37±0.12	-0.48	0.09	0.02±0.18	0.61	0.69±0.14 ^d	0.06	tl			100
53p1, v = 5	131984.66				0.07	tl	0.00	tl			
32p3, v = 5	132040.33				0.00	tl	0.34	tl			
9p3, v = 6	132043.41				0.00	tl	0.52	tl			
10p1, v = 6	132171.8±1.0	-1.3			0.87	0.7±0.2	0.00	tl			100
6p σ , v = 8	132258.7±1.0	0.5			1.25	bl	0.01	tl			
10p3, v = 6	132288.41±0.09	-1.66	5.97	4.8±0.6	0.82	0.9±0.5	1.97	tb			100
4p π , v = 11	132281.81±0.07	-13.84	0.00	0.12±0.15	3.47	2.1±0.3	1.19	1.4±0.7	100		
4p π , v = 11	132288.40±0.08	-7.25	0.00	0.01±0.15	3.47	1.2±0.2	1.19	tl	100		
7p π , v = 7	132367.78±0.20	0.45	1.71	1.5±0.3	1.52	1.31±0.17	1.30	tl			100
11p1, v = 6	132384.97				0.01	tl	0.22	tl			
5p σ , v = 10	132440.56±0.09	-3.76	0.50	0.36±0.16	2.47	1.3±0.3	2.04	0.2±1.5	14±5		86±5
5p σ , v = 10	132448.39±0.11	4.07		0.36±0.16	2.47	1.2±0.2	2.04	3.5±0.8	0±1		100±1
11p3, v = 6	132459.3±1.0	0.4			0.11	tl	1.37	2.7±2.2			100
12p1, v = 6	132532.76				0.53	bl	0.12	tl			
5p π , v = 9	132584.62±0.11	1.13	0.27	0.43±0.17	1.20	1.3±0.4	2.76	4.3±1.8			100
12p3, v = 6	132593.36				0.03	tl	0.01	tl			

Table 3: Photoabsorption transitions of D₂ involving $N' = 2$ upper levels (cont'd)

state	$\frac{E}{hc}$ (cm ⁻¹)		$\frac{\Gamma}{hc}$ (cm ⁻¹)		$A(R1)$ (10 ⁶ s ⁻¹)		$A(P3)$ (10 ⁶ s ⁻¹)		γ_d (%)	γ_f (%)	γ_i (%)
	obs ^{a,b}	o-c ^a	calc	obs	calc	obs	calc	obs	obs	obs	obs
13p1, v = 6	132652.47±0.10	-0.09	0.19	0.13±0.16	0.51	0.9±0.2	0.13	tl			100
14p1, v = 6	132676.24±0.11	-0.83	0.14	0.24±0.17	0.89	1.1±0.2	0.47	tl			100
8pσ, v = 7	132724.23±0.54	0.97	4.39	4.7±1.3	1.90	1.8±0.4	0.12	tl			100
6pπ, v = 8	132749.08±0.10	-0.32	0.11	0.25±0.16	0.36	0.30±0.19	0.58	tl			100
13p3, v = 6	132753.9±1.0	-0.2			0.03	tl	1.85	bl			100
15p1, v = 6	132799.6±1.0	1.6			0.57	0.6±0.1	0.03	tl			100
14p3, v = 6	132831.14				0.09	tl	0.37	tl			
8pπ, v = 7	132861.85±0.18	-0.18	0.61	1.0±0.4	0.45	0.48±0.09	0.33	tl			100
16p1, v = 6	132872.3±1.0	0.1			0.11	0.08±0.06	0.70	0.5±0.3			100
17p1, v = 6	132898.14				0.06	tl	0.62	tl			
15p3, v = 6	132918.73				0.08	tl	0.19	tl			
18p1, v = 6	132947.50				0.17	tl	0.05	tl			
16p3, v = 6	132966.56				0.00	tl	0.29	tl			
7pσ, v = 8	133042.57				0.13	tl	0.02	tl			
22p1, v = 6	133057.64				0.06	tl	0.12	tl			
18p3, v = 6	133067.70				0.05	tl	0.09	tl			
23p1, v = 6	133081.93				0.08	tl	0.00	tl			
24p1, v = 6	133092.13				0.00	tl	0.07	tl			
19p3, v = 6	133102.62				0.09	tl	0.04	tl			
25p1, v = 6	133112.56				0.02	tl	0.01	tl			
26p1, v = 6	133116.72±0.16	-0.44	0.08	0.38±0.25	0.37	0.46±0.12	0.00	tl			100
9p1, v = 7	133127.46±0.30	0.24	1.37	1.8±0.9	0.40	0.4±0.4	0.06	tl			100
20p3, v = 6	133131.96				0.03	tl	0.12	tl			
27p1, v = 6	133140.20				0.12	tl	0.00	tl			
28p1, v = 6	133148.9±1.0	0.1			0.15	0.17±0.12	0.03	tl			100
21p3, v = 6	133154.67				0.01	tl	0.09	tl			
29p1, v = 6	133160.97				0.04	tl	0.02	tl			
30p1, v = 6	133168.01				0.09	tl	0.00	tl			
24p3, v = 6	133215.60				0.01	tl	0.01	tl			
4pπ, v = 12	133217.24±0.09	0.58	0.01	0.01±0.15	1.63	2.9±0.4 ^d	0.23	tl	25±11		75±11
9pπ, v = 7	133218.09				0.31		0.35				
5pσ, v = 11	133278.14				0.01	tl	0.01	tl			
10p1, v = 7	133367.91				0.01	tl	0.03	tl			
6pσ, v = 9	133420.43±0.13	0.08	2.22	2.44±0.20	4.25	5.2±0.7	0.81	tl			100
10p3, v = 7	133478.1±1.0	-0.4			0.32	tb	0.98	0.9±0.8			100
7pπ, v = 8	133527.9±1.0	-0.1			0.09	tl	3.17	4.3±1.5			100
11p1, v = 7	133584.54				0.63	tb	0.04	tb			
5pπ, v = 10	133617.57±0.09	0.47	0.06	0.10±0.15	1.05	1.2±0.3	1.51	1.7±0.4			100
11p3, v = 7	133655.42				0.00	tl	0.56	tb			
12p1, v = 7	133739.5±1.0	0.5			0.29	0.34±0.10	0.11	tl			100
8pσ, v = 8	133773.2±1.0	-1.1			0.48	0.6±0.2	0.00	tl			100
6pπ, v = 9	133830.89±0.33	0.83	3.96	4.8±0.7	1.83	1.5±0.3	0.00	tl			100
13p1, v = 7	133850.7±1.0	0.2			0.00	tl	1.68	1.3±0.6			100
12p3, v = 7	133861.04				0.14	tl	0.17	tl			
14p1, v = 7	133922.54				0.56	tb	0.33	tb			
13p3, v = 7	133957.60				0.02	tl	0.36	tl			
8pπ, v = 8	134000.5±1.0	1.0			0.69	0.7±0.3	0.04	tl			100
15p1, v = 7	134015.32				0.07	tl	0.35	tl			
14p3, v = 7	134036.00				0.01	tl	0.31	tl			
5pσ, v = 12	134045.34				0.02	tl	0.62	tl			
16p1, v = 7	134071.46				0.17	tl	0.00	tl			
4pπ, v = 13	134088.18±0.09	-2.68	0.00	0.07±0.15	1.16	1.2±0.2	0.89	bl	18±3		82±3
15p3, v = 7	134099.45				0.01	tl	0.31	tl			
17p1, v = 7	134126.11				0.09	tl	0.06	tl			
7pσ, v = 10	134139.82				0.13	tl	0.25	tl			
5pσ, v = 13	134153.7±1.0	-0.7			0.42	0.17±0.03	0.17	tl			
9pπ, v = 8	134361.82±0.13	-0.39	0.15	0.4±0.2	0.74	0.51±0.08	0.02	tl			100
44p1, v = 7	134441.79±0.12	-0.31	0.23	0.18±0.18	0.18		0.19				
45p1, v = 7	134443.39±0.13	-0.52	0.04	0.35±0.20	0.43		0.43				
6pσ, v = 10	134444.99±0.17	-0.34	0.15	0.53±0.28	0.63	0.87±0.16 ^d	1.00	2.3±1.4			100
46p1, v = 7	134446.59				0.04		0.21				
5pπ, v = 11	134593.20±0.11	0.38	0.18	0.35±0.17	0.84	1.1±0.4 ^d	1.25	1.6±0.9	49±12		51±12

Table 3: Photoabsorption transitions of D₂ involving $N' = 2$ upper levels (cont'd)

state	$\frac{E}{hc}$ (cm ⁻¹)		$\frac{\Gamma}{hc}$ (cm ⁻¹)		$A(R1)$ (10 ⁶ s ⁻¹)		$A(P3)$ (10 ⁶ s ⁻¹)		γ_d (%)	γ_f (%)	γ_i (%)
	obs ^{a,b}	o-c ^a	calc	obs	calc	obs	calc	obs	obs	obs	obs
79p3, $v = 7$	134592.98				0.12		0.23				
6p π , $v = 10$	134864.90±0.43	-1.21	0.51	0.6±0.3	1.55	1.7±0.3	0.00	tl	40±8		60±8
12p1, $v = 8$	134879.5±1.0	-1.7			0.42	0.9±0.1	0.81	0.6±0.2			100
8p1, $v = 9$	134899.31				0.16	tl	0.30	tl			
4p π , $v = 14$	134902.69±0.21	0.46	0.17	0.19±0.33	0.53	0.4±0.1	0.46	tl	35±20		65±20
6p σ , $v = 11$	135059.92				0.07	tl	0.21	tl			
8p π , $v = 9$	135114.14±0.10	-0.44	0.13	0.21±0.16	0.09	0.2±0.1	0.09	tl			100

E/hc , upper state level energy. Γ/hc , calculated ionization width and observed total width (FWHM). $A(R1)$, $A(P3)$ emission probability to the ground state for $R(1)$ and $P(3)$ transitions, respectively. $\gamma_d, \gamma_f, \gamma_i$, quantum yields for dissociation, fluorescence and ionization, respectively. The transition energies for the $R(3)$ and $P(5)$ transitions are obtained by subtracting the ground-state rotational energies 59.78 cm⁻¹ ($N'' = 1$) and 357.30 cm⁻¹ ($N'' = 3$), respectively, from the upper state energy.

^a When no observed-calculated value is given, the energy corresponds to the calculated value.

^b Transition energies with uncertainties =1 cm⁻¹ are based on the NIM spectra.

^c Value based on the FT spectrum.

^d Complex resonance. The A value given corresponds to the sum over all components.

tb, too broad to be detected. bl, blended line. tl, too low intensity to be measured.

Table 4: Photoabsorption transitions of D₂ involving N' = 3 upper levels

state	$\frac{E}{hc}$ (cm ⁻¹)		$\frac{\Gamma}{hc}$ (cm ⁻¹)		A(R2) (10 ⁶ s ⁻¹)		A(P4) (10 ⁶ s ⁻¹)		γ_d (%)	γ_f (%)	γ_i (%)
	obs ^{a,b}	o-c ^a	calc	obs	calc	obs	calc	obs	obs	obs	obs
4pσ, v = 0	117358.64±0.04	-0.72		0.01±0.16	2.77	3.5±1.1 ^c	5.78				
4pπ, v = 0	118341.53±0.05	0.06		0.30±0.17	3.01	2.9±0.9 ^c	2.57				
4pσ, v = 1	118845.91±0.02	-0.71		0.05±0.15	4.95	6.9±1.5 ^c	5.12				
4pπ, v = 1	119917.81±0.02	0.05		0.15±0.15	8.69	8.9±1.8 ^c	5.64				
5pσ, v = 0	120180.35±0.10	-0.61		0.01±0.23	0.76	1.1±0.5 ^c	0.26				
4pσ, v = 2	120267.86±0.03	-0.65		0.15±0.15	7.30	11.0±2.2 ^c	9.87	29±17 ^c			
5pπ, v = 0	120686.77±0.06	0.17		0.00±0.18	0.92	1.1±0.4 ^c	1.79				
4pπ, v = 2	121425.44±0.03	0.00		0.20±0.15	15.22	17.0±3.5 ^c	5.85				
4pσ, v = 3	121609.85±0.04	-0.45		0.09±0.18	2.61	4.1±0.9 ^c	9.04	14±8 ^c			
6pσ, v = 0	121640.94±0.06	-0.33		0.00±0.18	0.78	1.3±0.5 ^c	3.16				
5pσ, v = 1	121748.45±0.03	-0.77		0.00±0.15	8.08	10.0±2.0 ^c	5.12				
6pπ, v = 0	121981.52±0.12	0.00		0.00±0.26	0.15	0.2±0.2 ^c	1.90				
5pπ, v = 1	122259.22±0.05	0.08		0.04±0.16	2.77	4.4±1.1 ^c	4.16				
7pσ, v = 0	122539.62±0.06	-0.27		0.00±0.19	1.19	1.2±0.5 ^c	0.19				
7pπ, v = 0	122769.43				0.11		0.93				
4pσ, v = 4	122835.11±0.03	-0.32		0.04±0.15	20.99	29±6 ^c	0.01				
4pπ, v = 3	122932.81±0.10	0.00		0.22±0.23	0.50		19.63	11±6 ^c			
8pσ, v = 0	123092.14±0.06	-0.24		0.00±0.17	0.76	1.1±0.4 ^c	0.06				
5pσ, v = 2	123130.37±0.07	-0.21		0.00±0.18	1.03	1.4±0.5 ^c	2.24				
6pσ, v = 1	123263.91±0.03	-0.54			7.57	9±2 ^c	2.11				
8pπ, v = 0	123301.10±0.03	-0.27		0.00±0.15	2.79	3.2±0.7 ^c	3.20				
9pσ, v = 0	123471.70±0.11	-0.15		0.04±0.25	0.75	1.1±0.5 ^c	0.05				
6pπ, v = 1	123550.68±0.14	-0.16			0.53		4.27				
9pπ, v = 0	123646.73				0.03		0.63				
10p2, v = 0	123741.08±0.14	-0.07		0.02±0.30	0.40	0.4±0.3 ^c	0.06				
5pπ, v = 2	123767.46±0.04	0.06		0.00±0.15	4.17	4.5±0.6	5.90	23±3	77±3		
11p2, v = 0	123893.8±1.0	0.3		0.10±1.00	0.09	0.13±0.04	0.16	13±10	87±10		
10p4, v = 0	123947.5±1.0	0.3		0.9±1.0	0.19	0.33±0.15	0.18	55±34	45±34		
12p2, v = 0	124060.00				0.04		0.00				
4pσ, v = 5	124071.23±0.03	-0.51		0.10±0.15	12.39	13.4±1.7	4.20	85±3	15±3		
7pσ, v = 1	124098.69±0.09	-0.28		0.20±0.19	2.14	3.0±1.3 ^c	0.15				
11p4, v = 0	124123.3±1.0	0.2		0.0±0.7	0.13	0.10±0.04	0.34				
13p2, v = 0	124182.8±1.0	-0.1		0.0±0.5	0.23	0.23±0.05	0.01	52±23	48±23		
12p4, v = 0	124253.0±1.0	-0.6		0.9±1.2	0.16	0.24±0.10	0.10	60±18	40±18		
14p2, v = 0	124282.04				0.12		0.10				
4pπ, v = 4	124290.30±0.04	0.47		0.07±0.15	8.19	7.1±0.8	14.82	18.6±2.8	50±4	50±3	
7pπ, v = 1	124332.0±1.0	-0.5		0.0±0.4	0.41	bl	1.82	1.7±0.4	15±15	85±15	
15p2, v = 0	124342.95				0.10		0.29				
13p4, v = 0	124378.48				0.00		0.20				
16p2, v = 0	124406.31				0.08		0.01				
17p2, v = 0	124449.17±0.04	-0.25		0.0±0.9	0.05	0.06±0.06	0.03				
14p4, v = 0	124471.59				0.00		0.13				
18p2, v = 0	124495.28				0.05		0.02				
19p2, v = 0	124526.1±1.0	-0.2		0.0±0.8	0.01	bl	0.01				
5pσ, v = 3	124536.06±0.05	-0.22		0.12±0.16	2.42	3.4±0.5	2.77	4.6±0.8	27±3	73±3	
15p4, v = 0	124543.94				0.00		0.11				
20p2, v = 0	124560.10				0.04		0.02				
21p2, v = 0	124583.10				0.13		0.66				
16p4, v = 0	124600.38				0.00		0.04				
22p2, v = 0	124609.69				0.03		0.04				
23p2, v = 0	124625.73				0.03		0.00				
24p2, v = 0	124641.16				0.01		0.01				
17p4, v = 0	124650.80				0.03		0.15				
8pσ, v = 1	124658.3±1.0	-0.4		0.2±1.3	0.12	0.13±0.05	0.13	21±17	79±17		
25p2, v = 0	124660.74				0.04		0.05				
26p2, v = 0	124670.3±1.0	-0.7		0.0±0.4	0.03	0.03±0.01	0.01				
27p2, v = 0	124682.18				0.02		0.00				
6pσ, v = 2	124751.58±0.05	-0.71		0.05±0.15	10.39	9.5±2.2 ^c	2.91	4.9±1.0	35±2	65±2	
37p2, v = 0	124752.75±0.08	-0.16		0.00±0.17	1.15	0.9±0.4 ^c	0.28				
8pπ, v = 1	124858.6±1.0	-0.5	3.05		0.29		1.54	1.0±0.2			
25p4, v = 0	124861.5±1.0	-0.4	0.19		0.17	bl	1.31	1.8±0.3			
9pσ, v = 1	125038.45±0.26	-0.12	0.98	0.69±0.34	2.76	2.5±0.5	1.65	1.9±0.6	0	0	100
6pπ, v = 2	125058.8±1.0	-0.9	0.39	1.0±0.6	0.17	0.19±0.04	4.56	4.4±0.6	0	0	100
4pσ, v = 6	125206.23±0.05	-0.58	0.00	0.06±0.16	10.00	11.7±1.6	4.56		84±3	16±3	0
9p4, v = 1	125210.4±1.0	0.3	2.01		0.01		2.86	4.0±0.9	0	0	100
5pπ, v = 3	125212.90±0.05	0.03	0.03	0.19±0.16	3.94	4.2±0.9	6.17	6.2±1.4	5±5	7±5	88±18
10p2, v = 1	125313.8±1.0	0.3	0.46	0.00±0.40	0.78	0.78±0.11	0.09		0	0	100
10p4, v = 1	125458.0±1.0	0.5	1.77		0.10	0.17±0.12	0.42		36±49	0	64±49
11p2, v = 1	125517.94±0.13	-0.02	0.06	0.03±0.26	0.51	0.44±0.07	0.36		0	0	100
7pσ, v = 2	125592.97±0.06	-0.26	0.01	0.00±0.16	1.60	2.3±0.6	0.00		0	0	100

Table 4: Photoabsorption transitions of D₂ involving $N' = 3$ upper levels (cont'd)

state	$\frac{E}{hc}$ (cm ⁻¹)		$\frac{\Gamma}{hc}$ (cm ⁻¹)		$A(R2)$ (10 ⁶ s ⁻¹)		$A(P4)$ (10 ⁶ s ⁻¹)		γ_d (%)	γ_f (%)	γ_i (%)
	obs ^{a,b}	o-c ^a	calc	obs	calc	obs	calc	obs	obs	obs	obs
4p π , v = 5	125612.60±0.04	0.29	0.00	0.00±0.15	9.23	8.3±1.2	9.01		76±3	21±3	3±1
12p2, v = 1	125635.8±1.0	0.3	1.02	1.2±0.5	1.41	bl	0.18		0	0	100
11p4, v = 1	125687.84±0.09	0.08	0.57		0.10		1.28	1.0±0.5	0	0	100
13p2, v = 1	125754.93±0.14	-0.09	0.37	0.52±0.33	0.55	0.8±0.9 ^c	0.00		0	0	100
12p4, v = 1	125817.9±1.0	-1.2	0.74		0.30	0.26±0.05	0.01		0	0	100
7p π , v = 2	125834.6±1.0	0.0	0.18	0.0±0.6	0.18	0.16±0.05	4.47	6.6±1.4	0	0	100
14p2, v = 1	125853.65		0.04		0.21		0.04				
5p σ , v = 4	125874.28±0.04	-0.22	0.00	0.02±0.15	2.94	3.7±0.7	1.99	2.7±0.9	39±8	15±3	46±9
15p2, v = 1	125913.4±1.0	-0.1	0.57		0.20	0.41±0.06	0.06				
13p4, v = 1	125945.64		0.42		0.01		0.40				
16p2, v = 1	125978.83±0.14	-0.09	0.14	0.28±0.29	0.21	0.8±0.8 ^c	0.02				
17p2, v = 1	126020.36		0.52		0.11		0.09				
14p4, v = 1	126039.77		0.14		0.04		0.23				
18p2, v = 1	126067.8±1.0	-0.3	0.13	0.0±1.3	0.15	0.12±0.17	0.01				
19p2, v = 1	126097.37		0.39		0.07		0.10				
15p4, v = 1	126111.97		0.10		0.02		0.29				
20p2, v = 1	126132.82±0.12	0.10	0.07	0.24±0.28	0.27	0.42±0.20	0.02		0	0	100
8p σ , v = 2	126135.04±0.10	-0.53	0.01	0.14±0.15	0.68	0.6±0.1	1.41	bl	0	0	100
21p2, v = 1	126155.67		0.21		0.00		0.02				
16p4, v = 1	126168.91±0.05	-0.17	0.19	0.00±0.18	0.32	bl	0.01				
22p2, v = 1	126181.67		0.02		0.13		0.03				
6p σ , v = 3	126195.88±0.04	-0.40	0.01	0.00±0.15	5.59	5.8±2.7	0.98	2.0±2.1	13±6	26±13	81±19
23p2, v = 1	126199.68±0.07	-0.17	0.09	0.06±0.17	3.21	3.3±0.6	0.31		2±3	0	98±3
24p2, v = 1	126214.00±0.10	-0.14	0.23	0.34±0.22	0.61	0.76±0.12	0.12		0	0	100
17p4, v = 1	126221.94		0.10		0.09		0.20				
25p2, v = 1	126232.04		0.03		0.06		0.02				
26p2, v = 1	126244.21		0.08		0.10		0.00				
27p2, v = 1	126254.84		0.15		0.08		0.01				
18p4, v = 1	126261.59		0.12		0.00		0.02				
4p σ , v = 7	126262.99±0.05	-0.69	0.00	0.15±0.15	8.85	10.4±2.2	7.09	8.4±1.7	94±2	6±2	0
28p2, v = 1	126268.09		0.01		0.02		0.04				
29p2, v = 1	126276.58		0.04		0.05		0.01				
30p2, v = 1	126284.63		0.07		0.05		0.00				
31p2, v = 1	126291.59		0.11		0.04		0.01				
19p4, v = 1	126296.43		0.10		0.00		0.05				
47p2, v = 1	126357.61		0.04		0.00		0.14				
8p π , v = 2	126358.8±1.0	-0.1	0.01		0.07		2.08	4.4±1.3	0	0	100
48p2, v = 1	126359.85		0.02		0.06		0.58				
49p2, v = 1	126361.61		0.04		0.03		0.12				
6p π , v = 3	126493.94±0.05	0.13	0.00	0.05±0.16	2.73	2.9±0.6	7.42	8.1±1.6	7±3	17±5	75±8
42p4, v = 1	126541.09		0.72		0.01		0.01				
43p4, v = 1	126543.94		0.65		0.02		0.04				
44p4, v = 1	126546.56		0.57		0.05		0.00				
45p4, v = 1	126548.92		0.56		0.13		0.07				
46p4, v = 1	126550.42±0.13	-0.39	0.38	0.20±0.23	0.40	0.6±0.7 ^c	0.12		0	0	100
9p σ , v = 2	126552.31±0.06	0.03	0.01	0.18±0.21	0.43	0.4±0.7 ^c	0.06				
47p4, v = 1	126554.08		0.13		0.11		0.00				
48p4, v = 1	126556.02		0.24		0.06		0.10				
5p π , v = 4	126596.66±0.05	-0.01	0.00	0.16±0.16	4.65	4.3±0.8	5.02		36±13	8±2	56±13
9p π , v = 2	126709.1±1.0	0.6	3.51		0.05		2.05	3.4±1.8	0	0	100
10p2, v = 2	126820.68±0.13	-0.21	1.06	0.53±0.28	1.18	0.99±0.17	0.15		0	0	100
4p π , v = 6	126877.34±0.04	0.29	0.00	0.02±0.15	8.76	9.2±1.5	6.40	7.9±2.0	88±7	12±7	0
10p4, v = 2	126952.37		3.61		0.00		0.39				
11p2, v = 2	127022.93±0.10	-0.08	0.28	0.12±0.18	2.33	2.6±0.6	0.03				
7p σ , v = 3	127032.31±0.05	-0.31	0.29	0.29±0.16	1.50	1.6±0.2	1.57	1.4±0.4	0	0	100
5p σ , v = 5	127135.71±0.07	-0.23	0.00	0.08±0.17	1.01	1.3±0.4	1.78	2.7±0.6	100	0	0
12p2, v = 2	127138.4±1.0	-0.3	1.94	1.8±1.8	1.32	1.2±1.2	0.19				
11p4, v = 2	127190.49		0.80		0.01		0.91				
4p σ , v = 8	127245.20±0.04	-0.67	0.00	0.08±0.15	3.78	5.9±1.0	8.41	14.9±1.8	100	0	0
13p2, v = 2	127259.56±0.15	-0.27	0.83	1.05±0.24	2.37	2.7±0.5	0.15				
7p π , v = 3	127274.43±0.08	0.08	0.23	0.13±0.19	0.99	1.13±0.19	1.03	0.9±0.5	0	0	100
12p4, v = 2	127323.86		1.80		0.01		0.92				
14p2, v = 2	127360.97±0.08	0.04	0.16	0.00±0.18	0.50	0.6±0.3	0.16		0	0	100
15p2, v = 2	127419.46		1.26		0.28		0.10				
13p4, v = 2	127448.87		0.50		0.05		0.55				
16p2, v = 2	127487.0±1.0	0.3	0.44	0.1±0.4	0.29	0.51±0.12	0.02		0	0	100
6p σ , v = 4	127512.54±0.04	-0.70	0.04	0.09±0.15	4.37	4.4±0.8	4.43	4.9±1.1	0	0	100
14p4, v = 2	127525.10		1.19		0.03		0.01				
17p2, v = 2	127544.67±0.12	-0.12	0.09	0.07±0.24	0.32	0.4±0.7 ^c	0.16				
18p2, v = 2	127575.79		0.37		0.07		0.02				

Table 4: Photoabsorption transitions of D₂ involving $N' = 3$ upper levels (cont'd)

state	$\frac{E}{hc}$ (cm ⁻¹)		$\frac{\Gamma}{hc}$ (cm ⁻¹)		$A(R2)$ (10 ⁶ s ⁻¹)		$A(P4)$ (10 ⁶ s ⁻¹)		γ_d (%)	γ_f (%)	γ_i (%)
	obs ^{a,b}	o-c ^a	calc	obs	calc	obs	calc	obs	obs	obs	obs
15p4, v = 2	127599.64±0.14	-0.18	0.54	0.28±0.28	0.77	1.02±0.26	0.00				
19p2, v = 2	127616.17±0.05	-0.07	0.04	0.11±0.16	1.95	1.8±0.3	0.00				
8pσ, v = 3	127624.83±0.05	-0.26	0.19	0.19±0.15	4.58	3.5±0.5	1.06	1.1±1.1	0	0	100
20p2, v = 2	127641.42		0.30		0.63		0.00				
21p2, v = 2	127664.0±1.0	0.7	0.69	0.8±0.6	0.54	0.78±0.16	0.12		0	0	100
16p4, v = 2	127674.53		0.22		0.02		0.27				
22p2, v = 2	127689.77		0.12		0.17	bl	0.02				
8pπ, v = 3	127800.4±1.0	0.3	0.31		0.04		1.88	0.8±1.1	0	0	100
48p2, v = 2	127868.60		0.04		0.05		0.01				
49p2, v = 2	127870.46		0.05		0.07		0.02				
50p2, v = 2	127872.23±0.10	0.07	0.04	0.00±0.20	0.56	0.6±1.0 ^c	0.78				
6pπ, v = 4	127872.78±0.04	0.16	0.02	0.00±0.15	3.28	3.7±1.2 ^c	8.07	11.2±1.9	0	7±10	93±10
51p2, v = 2	127873.82		0.08		0.01		0.17				
5pπ, v = 5	127921.30±0.04	-0.10	0.00	0.04±0.15	3.54	4.3±0.9	2.39	1.9±1.0	28±6	55±15	17±8
30p4, v = 2	127982.20		2.03		0.08		0.04				
31p4, v = 2	127989.39±0.08	0.18	1.83	0.94±0.19	0.47	0.37±0.16	0.00		0	0	100
9pσ, v = 3	127992.96±0.05	-0.32	0.09	0.21±0.16	1.02	0.88±0.12	0.07		0	0	100
32p4, v = 2	127998.03±0.08	-0.28	0.35	0.03±0.19	0.20		0.07				
4pπ, v = 7	128066.99±0.04	0.38	0.00	0.19±0.15	8.51	9.6±1.3	1.31	1.3±0.3	100±12	0	0
9pπ, v = 3	128143.20		5.86		0.00		2.15	bl			
4pσ, v = 9	128157.0±1.0	0.2	0.00	0.0±0.4	0.01		5.98	6.9±0.8			
10p2, v = 3	128265.12±0.39	0.44	1.74	2.17±1.05	1.19	1.0±0.3	0.20		0	0	100
5pσ, v = 6	128348.36±0.05	-0.35	0.05	0.08±0.15	3.81	4.4±0.6	4.84	6.6±1.0	0	0	100
10p4, v = 3	128365.81		0.94		0.09		0.62				
7pσ, v = 4	128422.32±0.50	-0.50	3.87	3.97±1.06	2.01	1.7±0.2	1.29	0.9±0.4	0	0	100
11p2, v = 3	128469.23±0.12	0.03	0.22		0.71	1.2±0.9 ^c	0.60				
12p2, v = 3	128579.3±1.0	0.7	4.35	2.6±0.6	1.25	1.46±0.24	0.17		0	0	100
11p4, v = 3	128631.23		0.86		0.05		0.79				
7pπ, v = 4	128644.88±0.05	0.08	0.10	0.15±0.16	2.17	2.0±0.4	1.99		0	0	100
13p2, v = 3	128707.4±1.0	0.3	1.98	2.4±0.6	0.45	0.76±0.12	0.02		0	0	100
12p4, v = 3	128762.26		2.38		0.00		0.72				
14p2, v = 3	128805.9±1.0	0.5	0.37	0.7±0.8	0.30	0.42±0.16	0.24		0	0	100
6pσ, v = 5	128818.82±0.04	-0.81	0.07	0.08±0.15	4.12	4.4±0.8	4.39	3.6±2.0	0	0	100
15p2, v = 3	128860.79		2.65		0.18		0.23				
13p4, v = 3	128890.18±0.14	0.13	0.35	0.06±0.29	0.23		0.44				
16p2, v = 3	128930.99		0.81		0.20		0.01				
14p4, v = 3	128961.73		0.98		0.21		0.20				
4pσ, v = 10	128966.04±0.05	-0.60	0.02	0.17±0.15	3.88	3.6±0.6	1.90	2.3±0.3	100	0	0
8pσ, v = 4	128987.11±0.06	-0.14	0.11	0.14±0.16	1.53	1.7±0.5	0.02		0	0	100
17p2, v = 3	128996.29±0.05	-0.19	0.24	0.17±0.16	3.68	3.1±0.8	0.78		0	0	100
18p2, v = 3	129021.95±0.09	0.09	0.84	0.99±0.22	1.05	1.6±0.7	0.01		0	0	100
15p4, v = 3	129046.71		1.12		0.49	bl	0.37				
19p2, v = 3	129061.86		0.04		0.13	bl	0.12				
20p2, v = 3	129086.25±0.21	0.22	0.66	0.27±0.40	0.37	bl	0.00				
16p4, v = 3	129104.93		1.07		0.18	bl	0.12				
21p2, v = 3	129117.30		0.04		0.06		0.17				
22p2, v = 3	129134.69		0.34		0.26		0.07				
23p2, v = 3	129149.84		0.68		0.21		0.06				
17p4, v = 3	129160.30		0.14		0.00		0.00				
5pπ, v = 6	129168.30±0.04	0.22	0.03	0.07±0.15	7.33	7.4±1.5	10.75	12.1±2.0	22±21	5±3	73±17
8p4, v = 4	129170.30		0.07		0.34		0.46				
24p2, v = 3	129173.40		0.12		0.04		0.45				
25p2, v = 3	129186.48		0.35		0.08		0.15				
26p2, v = 3	129197.30		0.75		0.05		0.30				
18p4, v = 3	129203.78		0.24		0.01		0.23				
6pπ, v = 5	129205.9±1.0	-0.3	0.02		0.01		1.05	bl			
27p2, v = 3	129212.54		0.38		0.07		0.00				
28p2, v = 3	129222.09		0.24		0.08		0.03				
29p2, v = 3	129230.45		0.53		0.06		0.11				
19p4, v = 3	129236.28		0.39		0.00		0.22				
30p2, v = 3	129241.75		0.01		0.12		0.16				
31p2, v = 3	129248.46		0.09		0.13		0.03				
4pπ, v = 8	129248.75±0.06	0.20	0.00	0.10±0.16	2.68	3.2±0.7	3.61	4.5±1.0	78±12	16±12	6±3
32p2, v = 3	129254.96		0.17		0.05		0.01				
33p2, v = 3	129260.73		0.32		0.04		0.05				
9pσ, v = 4	129371.97±0.07	-0.40	0.14	0.00±0.19	1.01	1.43±0.25	0.03		0	0	100
5pσ, v = 7	129482.45±0.04	-0.42	0.00	0.00±0.15	1.84	2.3±0.4	3.56		28±7	7±4	65±13
10p2, v = 4	129644.40±1.00	0.00	2.11	2.30±1.00	0.71	0.9±0.4	0.24		0	0	100
7pσ, v = 5	129682.22±0.08	-0.23	0.27	0.28±0.18	1.91	2.0±0.3	0.11		0	0	100
4pσ, v = 11	129747.36±0.05	-1.19	0.00	0.14±0.15	2.23	2.8±0.5	2.68	3.7±0.6	100	0	0

Table 4: Photoabsorption transitions of D₂ involving $N' = 3$ upper levels (cont'd)

state	$\frac{E}{hc}$ (cm ⁻¹)		$\frac{\Gamma}{hc}$ (cm ⁻¹)		$A(R2)$ (10 ⁶ s ⁻¹)		$A(P4)$ (10 ⁶ s ⁻¹)		γ_d (%)	γ_f (%)	γ_i (%)
	obs ^{a,b}	o-c ^a	calc	obs	calc	obs	calc	obs	obs	obs	obs
10p4, v = 4	129785.0±1.0	0.5	7.37	1.1±1.0	0.72	0.6±0.2	1.26		0	0	100
11p2, v = 4	129851.0±1.0	-0.6	0.44	0.0±0.9	0.91	0.7±0.4	0.51		0	0	100
7pπ, v = 5	129948.25±0.26	0.04	2.24	2.55±0.54	3.62	3.0±0.6	0.12		0	0	100
11p4, v = 4	129960.99		5.65		0.24		0.68				
12p2, v = 4	130010.6±1.0	-0.8	0.63	1.8±0.8	0.27	0.37±0.14	0.64		0	0	100
6pσ, v = 6	130068.30±0.06	-0.82	0.03	0.05±0.16	1.94	2.1±0.3	4.76	4.8±1.0	6±2	0	94±2
13p2, v = 4	130089.3±1.0	-0.1	3.38	4.7±0.8	1.29	1.8±0.4	0.53		0	0	100
12p4, v = 4	130139.61		3.33		0.00		0.97				
14p2, v = 4	130188.35±0.09	0.02	0.78	1.04±0.20	0.49	0.39±0.06	0.08		0	0	100
15p2, v = 4	130237.20		5.27		0.00		0.19				
13p4, v = 4	130270.14±0.04	-0.03	0.12	0.00±0.15	0.73	bl	0.25				
8pσ, v = 5	130300.00±0.05	-0.34	0.02	0.06±0.15	2.21	2.7±0.4	0.16		0	0	100
16p2, v = 4	130317.94±0.08	0.11	1.21	1.08±0.20	3.45	3.0±0.4	0.03		0	0	100
4pπ, v = 9	130324.64±0.04	0.25	0.00	0.04±0.15	5.52	6.2±1.4 ^c	3.89	4.3±0.8	62±10	6±2	32±8
14p4, v = 4	130350.82		2.38		0.72		0.52				
17p2, v = 4	130371.07		0.10		0.26		0.26				
5pπ, v = 7	130377.98±0.05	-0.05	0.01	0.12±0.16	1.92	2.1±0.6	1.64	2.3±0.4	66±20	9±9	25±24
18p2, v = 4	130403.56		1.77		0.44		0.02				
15p4, v = 4	130425.04		1.37		0.05		0.26				
19p2, v = 4	130444.8±1.0	0.2	0.16	1.7±0.6	0.22	0.32±0.12	0.15		0	0	100
6pπ, v = 6	130462.04±0.06	-0.23	0.01	0.00±0.16	0.64	0.62±0.27	1.32	1.5±0.4	30±19	0	70±19
20p2, v = 4	130467.0±1.0	0.1	1.16	0.0±0.9	0.29	0.25±0.17	0.09		0	0	100
4pσ, v = 12	130469.36±0.09	-0.28	0.00	0.64±0.26	0.37	0.76±0.10	1.38	2.1±0.3	100	0	0
16p4, v = 4	130481.14		0.11		0.02		0.39				
8pπ, v = 5	130490.7±1.0	-0.5	0.95		0.02		2.32	bl			
21p2, v = 4	130500.24		0.09		0.10		0.01				
22p2, v = 4	130519.07		0.83		0.13		0.08				
17p4, v = 4	130533.10		1.49		0.02		0.35				
23p2, v = 4	130542.84		0.07		0.06		0.14				
24p2, v = 4	130556.40		0.34		0.09		0.01				
5pσ, v = 8	130566.82±0.04	-0.54	0.05	0.04±0.15	1.33	2.16±0.31	5.50	9.9±1.3	3±2	0	97±13
25p2, v = 4	130569.7±1.0	0.4	0.92	0.2±0.4	0.43	0.38±0.16	1.10		0	0	100
42p2, v = 4	130683.38±0.09	-0.09	0.05	0.13±0.19	0.23	0.28±0.07	0.00		0	0	100
43p2, v = 4	130685.73±0.08	0.10	0.01	0.20±0.18	0.23	0.23±0.12	0.00		0	0	100
44p2, v = 4	130687.8±1.0	-0.3	0.02	0.4±0.8	0.17	0.25±0.13	0.00		0	0	100
45p2, v = 4	130691.0±1.0	0.3	0.05	0.1±0.7	0.11	0.11±0.04	0.00		0	0	100
46p2, v = 4	130693.12±0.06	0.04	0.08	0.11±0.18	0.17	0.13±0.05	0.01		0	0	100
47p2, v = 4	130695.11±0.05	-0.03	0.19	0.02±0.16	0.28	0.4±0.2	0.05		0	0	100
9p2, v = 5	130696.25		0.09		0.15		0.11				
33p4, v = 4	130818.47		1.10		0.04		0.34				
9pπ, v = 5	130821.58		0.07		0.03		0.48				
34p4, v = 4	130826.71		0.67		0.00		0.17				
35p4, v = 4	130831.95		0.94		0.00		0.10				
7pσ, v = 6	130919.5±1.0	-0.7	0.82	0.6±0.6	0.30	0.41±0.07	0.64		0	0	100
10p2, v = 5	130972.8±1.0	0.2	4.39	2.8±0.5	1.72	1.6±0.2	0.03		0	0	100
10p4, v = 5	131094.3±1.0	0.4	15.53		0.18		0.94	0.8±0.5	0	0	100
4pσ, v = 13	131128.53±0.06	5.46	0.03	0.03±0.16	1.34	2.0±0.3	0.77	0.9±0.2	100	0	0
11p2, v = 5	131172.74±0.29	-0.38	1.00	1.7±0.7	2.13	2.3±0.3	0.32		0	0	100
6pσ, v = 7	131185.22±0.05	-0.5	0.07	0.07±0.15	3.40	4.2±0.6	0.13		0	0	100
7pπ, v = 6	131262.24		3.43		0.00		0.79				
12p2, v = 5	131289.5±1.0	0.3	6.10	5.2±0.9	0.84	0.8±0.1	4.19	5.8±2.4	0	0	100
11p4, v = 5	131331.9±1.0	-0.4	0.58		0.25		0.80	0.6±0.3	0	0	100
4pπ, v = 10	131373.13±0.05	0.86	0.04	0.00±0.16	3.63	3.5±0.5	2.80	3.0±0.4	91±5	5±3	4±2
13p2, v = 5	131407.4±1.0	-0.1	5.73		0.43	0.2±0.3	0.08		0	0	100
12p4, v = 5	131455.80		2.68		0.11		0.61				
5pπ, v = 8	131493.53±0.05	0.22	0.00	0.00±0.16	2.73	3.2±0.5	0.02		100±16	0	0
14p2, v = 5	131510.0±1.0	-0.1	1.39		0.13	0.12±0.03	0.07		0	0	100
8pσ, v = 6	131536.83±0.07	-0.59	0.42	0.31±0.23	1.76	1.6±0.2	0.08		0	0	100
15p2, v = 5	131573.8±1.0	0.5	3.42	3.7±0.6	2.00	1.5±0.2	0.02		0	0	100
13p4, v = 5	131594.58		0.14		0.04		0.12				
5pσ, v = 9	131601.87±0.09	-0.01	0.17		0.29	2.6±1.2 ^c	5.05	bl			
16p2, v = 5	131637.2±1.0	0.1	2.86	4.0±1.0	0.93	1.1±0.4	0.03		0	0	100
6pπ, v = 7	131664.78±0.17	-0.02	0.48	0.4±0.6	0.54	0.3±0.9 ^c	0.80				
14p4, v = 5	131668.13		2.25		0.00		1.85				
17p2, v = 5	131693.0±1.0	-0.6	0.37		0.23	0.3±0.4	0.09		0	0	100
18p2, v = 5	131721.53		2.46		0.33		0.06				
4pσ, v = 14	131734.05±0.20	-0.70	0.05		1.20	0.96±0.13	1.40		100	0	0
8p4, v = 6	131740.23		0.01		0.00		1.58				
15p4, v = 5	131748.95		1.22		0.01		2.04				
19p2, v = 5	131768.28		0.61		0.17		0.01				

Table 4: Photoabsorption transitions of D₂ involving $N' = 3$ upper levels (cont'd)

state	$\frac{E}{hc}$ (cm ⁻¹)		$\frac{\Gamma}{hc}$ (cm ⁻¹)		$A(R2)$ (10 ⁶ s ⁻¹)		$A(P4)$ (10 ⁶ s ⁻¹)		γ_d (%)	γ_f (%)	γ_i (%)
	obs ^{a,b}	o-c ^a	calc	obs	calc	obs	calc	obs	obs	obs	obs
20p2, v = 5	131791.57		2.69		0.13		0.32				
16p4, v = 5	131805.84		0.88		0.01		0.37				
21p2, v = 5	131823.20		0.37		0.14		0.01				
22p2, v = 5	131840.72		1.64		0.10		0.11				
17p4, v = 5	131852.78		1.05		0.00		0.25				
23p2, v = 5	131865.58		0.08		0.09		0.04				
24p2, v = 5	131879.21		0.88		0.08		0.01				
18p4, v = 5	131889.68		1.93		0.00		0.14				
25p2, v = 5	131898.99		0.10		0.06		0.09				
26p2, v = 5	131909.47		0.20		0.07		0.01				
27p2, v = 5	131925.04		0.30		0.09		0.05				
28p2, v = 5	131933.0±1.0	-0.1	0.02	0.0±0.7	0.16	0.19±0.08	0.02		0	0	100
29p2, v = 5	131941.19		0.05		0.10		0.07				
9p2, v = 6	131941.5±1.0	-0.3	0.13	0.4±0.5	0.37	0.64±0.11	0.00		0	0	100
30p2, v = 5	131949.8±1.0	0.1	0.27	0.2±0.5	0.19	0.26±0.07	0.00		0	0	100
31p2, v = 5	131957.1±1.0	0.4	0.53	0.2±0.9	0.19	0.22±0.17	0.02		0	0	100
20p4, v = 5	131962.06		0.79		0.12		0.11				
28p4, v = 5	132097.81		4.08		0.00		0.02				
9pπ, v = 6	132114.95		3.36		0.02		0.09				
7pσ, v = 7	132119.56		0.43		0.03		0.55				
6pσ, v = 8	132316.7±1.0	-0.8	1.00	0.7±0.5	1.62	1.6±0.3	0.05		0	0	100
4pπ, v = 11	132350.08±0.08	0.35	0.27	0.17±0.18	2.52	1.9±0.4	1.96	1.4±0.5	16±4	0	84±4
10p2, v = 6	132355.35		15.00		1.73		0.63				
11p2, v = 6	132434.25±0.07	-0.21	0.71	0.7±0.5	0.93	1.3±0.3	0.68		0	0	100
7pπ, v = 7	132446.21		0.57		0.20		0.61				
5pσ, v = 10	132497.97±0.07	-0.04	0.07	0.10±0.17	2.42	3.2±0.4	2.68		0	0	100±8
11p4, v = 6	132532.29		12.38		0.82		1.73				
12p2, v = 6	132594.2±1.0	-0.2	0.34	0.0±0.5	0.34	0.39±0.15	0.51		0	0	100
5pπ, v = 9	132648.21±0.17	-1.82	0.08	0.09±0.33	0.82	0.9±0.3	3.01	5.5±1.5	3±2	0	97±2
13p2, v = 6	132662.92		5.84		0.12		0.00				
12p4, v = 6	132709.78±0.14	0.16	0.77	0.66±0.27	0.70	0.62±0.15	0.07		0	0	100
8pσ, v = 7	132750.91±0.08	-0.26	0.65	0.52±0.20	1.17	1.0±0.2	0.54		0	0	100
14p2, v = 6	132775.75±0.59	-0.04	2.67	3.3±1.2	1.23	1.0±0.2	0.01		0	0	100
6pπ, v = 8	132810.17±0.14	-0.58	0.47	0.37±0.26	0.51	0.66±0.13	1.07		0	0	100
13p4, v = 6	132827.75		15.00		0.31		1.18				
15p2, v = 6	132856.73		0.11		0.14		0.22				
16p2, v = 6	132896.80		5.03		0.50		0.00				
8p4, v = 7	132940.05		0.74		0.10		1.81				
17p2, v = 6	132958.36		0.92		0.15		0.02				
7pσ, v = 8	133110.53		0.31		0.18		0.00				
23p2, v = 6	133129.60		0.43		0.10		0.01				
25p2, v = 6	133162.81		0.06		0.10		0.04				
26p2, v = 6	133171.4±1.0	0.5	0.17		0.19	0.38±0.18	0.00				
9pσ, v = 7	133175.08±0.16	-0.16	0.33	0.44±0.32	0.44	0.62±0.15	0.00		0	0	100
27p2, v = 6	133184.82		1.23		0.33		0.02				
4pπ, v = 12	133264.42±0.07	-8.02	0.00	0.00±0.17	1.30	1.2±0.2	0.57		73±7	0	27±7
10p2, v = 7	133430.67		0.23		0.04		0.12				
58p4, v = 6	133464.89±0.09	-0.08	0.67		0.48		0.07				
59p4, v = 6	133465.64±0.06	-0.29	0.25		1.08		0.19				
6pσ, v = 9	133466.41±0.08	-0.32	0.00	0.26±0.26	1.34	6.3±0.7	0.27		0	0	100
60p4, v = 9	133467.56		0.15		0.71		0.17				
61p4, v = 6	133468.45		0.38		0.31		0.08				
62p4, v = 6	133469.36		0.36		0.15		0.05				
10p4, v = 7	133542.94		23		0.45		0.34				
7pπ, v = 8	133600.7±1.0	-0.5	1.94	2.3±1.3	0.00		3.26	5.2±2.6			
11p2, v = 7	133644.1±1.0	0.7	2.63	2.1±0.6	0.54	0.83±0.15	0.04				
5pπ, v = 10	133667.43±0.06	-8.49	0.06	0.01±0.16	0.84	0.85±0.23	1.76		62±11	0	38±11
11p4, v = 7	133722.95		12		0.06		0.51				
12p2, v = 7	133798.9±1.0	0.3	0.24	0.0±0.5	0.41	0.38±0.09	0.25		0	0	100
8p2, v = 8	133841.60		2.49		0.36		0.00				
6pπ, v = 9	133884.5±1.1	1.0	4.39	4.7±3.4	1.88	1.8±0.4	0.11		0	0	100
13p2, v = 7	133907.27		0.33		0.01		0.66				
12p4, v = 7	133952.37		5.36		0.07		1.13				
14p2, v = 7	133979.2±1.0	-0.2	4.99	3.0±1.2	0.55	0.7±0.3	0.00		0	0	100
15p4, v = 7	134022.98		21.76		0.20		0.26				
15p2, v = 7	134060.54±0.12	-0.46	0.29	0.02±0.23	0.33	0.23±0.18	0.33		0	0	100
8p4, v = 8	134068.17		0.06		0.22		0.38				
16p2, v = 7	134097.54		2.69		0.05		0.01				
5pσ, v = 11	134109.8±1.0	1.9	0.09	0.8±0.7	0.35	0.50±0.11	0.59		28±6	0	72±6
4pπ, v = 13	134134.68±0.06	-6.95	0.01	0.00±0.16	0.94	1.13±0.17	1.12		73±6	0	27±6

Table 4: Photoabsorption transitions of D₂ involving $N' = 3$ upper levels (cont'd)

state	$\frac{E}{hc}$ (cm ⁻¹)		$\frac{\Gamma}{hc}$ (cm ⁻¹)		$A(R2)$ (10 ⁶ s ⁻¹)		$A(P4)$ (10 ⁶ s ⁻¹)		γ_d (%)	γ_f (%)	γ_i (%)
	obs ^{a,b}	o-c ^a	calc	obs	calc	obs	calc	obs	obs	obs	obs
17p2, v = 7	134162.53		2.25		0.16		0.00				
5pσ, v = 12	134201.2±1.0	-0.9	0.02	0.0±0.8	0.28	0.25±0.09	0.25		7±6	0	93±6
18p2, v = 7	134211.71		0.15		0.04		0.18				
19p2, v = 7	134235.24		2.12		0.13		0.03				
16p4, v = 7	134252.04		1.50		0.00		0.22				
20p2, v = 7	134272.9±1.0	-0.2	0.06	0.0±0.5	0.10	0.10±0.02	0.07		0	0	100
21p2, v = 7	134284.60		0.74		0.01		0.02				
9pσ, v = 8	134297.2±1.0	1.0	0.50	0.5±0.9	0.21	0.20±0.07	0.02		0	0	100
22p2, v = 7	134312.04		2.12		0.14		0.03				
17p4, v = 7	134320.99		0.08		0.02		0.06				
23p2, v = 7	134335.39		1.52		0.13		0.00				
24p2, v = 7	134347.97		4.36		0.08		0.04				
18p4, v = 7	134357.83		0.62		0.00		0.06				
25p2, v = 7	134368.62		0.42		0.09		0.01				
26p2, v = 7	134378.60		1.93		0.11		0.01				
19p4, v = 7	134387.03		1.17		0.02		0.04				
27p2, v = 7	134394.9±1.0	-0.6	0.05		0.02	0.05±0.04	0.03		0	0	100
28p2, v = 7	134404.2±1.0	0.9	0.66		0.19	0.14±0.08	0.00		0	0	100
9pπ, v = 8	134408.4±1.0	-0.6	0.76		0.31	0.21±0.08	0.01		0	0	100
29p2, v = 7	134414.7±1.0	-0.4	0.03		0.15	0.12±0.04	0.00		0	0	100
30p2, v = 7	134419.0±1.0	-1.1	0.76		0.29	0.22±0.06	0.04		0	0	100
31p2, v = 7	134423.4±1.0	-0.6	0.11		0.06	0.05±0.03	0.03		0	0	100
24p4, v = 7	134501.11		0.10		0.10		0.04				
51p2, v = 7	134502.61		0.02		0.10		0.03				
52p2, v = 7	134504.09		0.00		0.10		0.03				
53p2, v = 7	134505.55±0.10	0.03	0.01	0.24±0.24	0.10		0.04				
54p2, v = 7	134506.71±0.05	-0.17	0.02	0.04±0.15	0.12		0.05				
55p2, v = 7	134508.15		0.09		0.27		0.21				
6pσ, v = 10	134508.06±0.08	-0.65	0.86	0.79±0.21	0.80	1.2±0.2	1.11	1.7±0.7	0	0	100
5pπ, v = 11	134645.76±0.09	0.17	0.03	0.00±0.19	0.86	0.99±0.16	1.34		57±9	19±10	24±5
11p2, v = 8	134788.9±1.0	-0.5	3.59	2.9±1.3	0.36	0.35±0.08	0.05		0	0	100
6pπ, v = 10	134916.34±0.15	-0.65	1.78	1.73±0.29	2.16	2.2±0.3	0.11		15±3	0	85±3
12p2, v = 8	134946.93		0.26		0.28		0.09				
4pπ, v = 14	134948.3±1.0	0.2	0.11	1.1±1.1	0.44	0.05±0.02	0.56		100	0	0
8pσ, v = 9	134955.42		0.33		0.02		0.76				
13p2, v = 8	135026.94		23.00		0.64		0.30				
4pπ, v = 15	135695.8±1.0	-1.0		9.4±1.1	0.39	0.22±0.04	0.54		100	0	0
4pπ, v = 16	136381.8±1.0	-0.9		8.4±1.9	0.58	0.26±0.07	0.60		100	0	0
4pπ, v = 17	137007.7±1.0	-1.0		5.6±0.8	0.35	0.14±0.02	0.31		100	0	0

E/hc , upper state level energy. Γ/hc , calculated ionization width and observed total width (FWHM). $A(R2)$, $A(P4)$ emission probability to the ground state for $R(2)$ and $P(4)$ transitions, respectively. $\gamma_d, \gamma_f, \gamma_i$, quantum yields for dissociation, fluorescence and ionization, respectively. The transition energies for the $R(3)$ and $P(5)$ transitions are obtained by subtracting the ground-state rotational energies 179.07 cm⁻¹ ($N'' = 2$) and 593.72 cm⁻¹ ($N'' = 4$), respectively, from the upper state energy.

^a When no observed-calculated value is given, the energy corresponds to the calculated value.

^b Transition energies with uncertainties = 1 cm⁻¹ are based on the NIM spectra.

^c Value based on the FT spectrum.

^d Complex resonance. The A value given corresponds to the sum over all components.

bl, blended line.

Table 5: Photoabsorption transitions of D₂ involving $N' = 4$ upper levels

state	$\frac{E}{hc}$ (cm ⁻¹)		$\frac{\Gamma}{hc}$ (cm ⁻¹)		$A(R3)$ (10 ⁶ s ⁻¹)		$A(P5)$ (10 ⁶ s ⁻¹)	
	obs ^{a,b}	o-c ^a	calc	obs	calc	obs	calc	obs
4pσ, v = 0	117465.87 ^c	0.80			2.09	4.0±4.0 ^c	1.62	
4pπ, v = 0	118461.90±0.11	0.15		0.1±0.2	2.84	4.9±4.7 ^c	2.72	
4pσ, v = 1	118950.81 ^c	0.79			5.92	4.6±1.8 ^c	5.38	
4pπ, v = 1	120030.86±0.05	0.29		0.0±0.2	8.70	9±4 ^c	5.61	
5pσ, v = 0	120285.52				0.83		0.17	
4pσ, v = 2	120371.11±0.06	-0.77		0.0±0.2	7.94	5.1±2.4 ^c	10.16	
5pπ, v = 0	120811.75				0.68		1.83	
4pπ, v = 2	121528.31±0.05	0.09		0.0±0.2	15.84	18±7 ^c	5.12	
4pσ, v = 3	121713.99±0.13	-0.52		0.4±0.3	2.05	2.8±1.5 ^c	9.51	
6pσ, v = 0	121744.32				0.56		3.25	
5pσ, v = 1	121847.10±0.06	-0.88		0.1±0.2	8.63	12.1±5.5 ^c	4.48	
6pπ, v = 0	122112.35				0.04		1.92	
5pπ, v = 1	122377.89±0.08	0.17		0.0±0.2	2.26	1.9±1.4 ^c	4.79	
7pσ, v = 0	122636.44				0.89		0.10	
7π5, v = 0	122902.67				0.06		0.96	
4pσ, v = 4	122919.56±0.04	-0.48		0.1±0.2	22.67	13±4 ^c	0.02	
4pπ, v = 3	123046.19±0.09	-0.08		0.1±0.2	0.60	1.7±1.5 ^c	19.65	
8pσ, v = 0	123188.41±0.13	-0.15		0.2±0.3	0.69	2.0±1.6 ^c	0.00	
5pσ, v = 2	123231.87±0.08	-0.07		0.0±0.2	1.01	1.9±1.6 ^c	2.17	
6pσ, v = 1	123363.75±0.04	-0.75		0.0±0.2	10.06	11±5 ^c	2.79	
8pπ, v = 0	123429.49±0.12	0.01		0.0±0.3	1.06	2.3±1.7 ^c	1.46	
9pσ, v = 0	123567.75				0.30		0.07	
6pπ, v = 1	123674.90				0.26		4.47	
9pπ, v = 0	123772.64				0.14		0.49	
10p3, v = 0	123845.7±1.0	0.2		0.0±0.8	0.13	0.15±0.08	0.41	
5pπ, v = 2	123879.71±0.13	0.03		0.3±0.3	3.66	4.7±0.6	6.59	
11p3, v = 0	123999.3±1.0	0.6		0.0±0.4	0.25	0.26±0.20	0.02	
10p5, v = 0	124070.99				0.03		0.27	
4pσ, v = 5	124152.92±0.07	-0.69		0.3±0.3	14.12	19.1±2.6	3.39	
12p3, v = 0	124156.14				0.08		0.02	
7pσ, v = 1	124195.5±1.0	0.1		0.0±0.5	1.93	1.5±0.4	0.06	
13p3, v = 0	124248.51				0.57		0.21	
11p5, v = 0	124283.18				0.08		0.10	
14p3, v = 0	124356.22				0.26		0.00	
4pπ, v = 4	124396.61±0.12	-0.31		0.0±0.2	6.91	8.0±1.0	15.82	22.0±4.0
12p5, v = 0	124405.67				0.03		0.09	
15p3, v = 0	124436.50				0.09	0.10±0.06	0.08	
7pπ, v = 1	124459.37				0.14		2.29	
16p3, v = 0	124488.90				0.07		0.06	
13p5, v = 0	124522.15				0.59		1.26	
17p3, v = 0	124544.06				0.05		0.00	
18p3, v = 0	124580.34				0.08		0.00	
19p3, v = 0	124608.81				0.01		0.12	
14p5, v = 0	124622.66				0.03		0.07	
5pσ, v = 3	124636.65±0.02	0.51		0.0±0.2	2.63	4.3±0.7	2.73	8.0±2.0
15p5, v = 0	124686.28				0.01		0.10	
25p3, v = 0	124748.81				0.13		0.18	
8pσ, v = 1	124755.02				0.22		0.11	
26p3, v = 0	124759.55				0.01		0.00	
18p5, v = 0	124842.09				0.33		0.02	
6pσ, v = 2	124843.63±0.22	-0.71		0.0±0.2	11.74	14.9±1.9	2.56	2.2±1.9
8pπ, v = 1	124986.02				0.55		1.70	
24p5, v = 0	124991.10				0.08		0.46	
46p5, v = 0	125130.04				0.07		0.02	
47p5, v = 0	125132.19				0.07		0.05	
48p5, v = 0	125134.01				0.54		0.28	
9pσ, v = 1	125134.94				0.91		0.37	
49p5, v = 0	125136.41				0.12		0.03	
50p5, v = 0	125138.17				0.03		0.00	
51p5, v = 0	125139.86				0.01		0.00	
120p5, v = 0	125174.49				0.03		0.47	
6pπ, v = 2	125174.2±1.0	-0.3			0.22	0.4±0.1	3.51	5.6±0.8
121p5, v = 0	125174.64				0.08		1.34	
122p5, v = 0	125174.75				0.01		0.20	
4pσ, v = 6	125286.40±0.06	-0.47	0.00	0.3±0.2	8.89	12.3±3.4	4.43	10±2
5pπ, v = 3	125318.81±0.20	-0.06	0.00	0.0±0.2	4.47	6.5±1.3	6.98	8.4±2.2
9pπ, v = 1	125331.88		2.48		0.26		1.20	
10p3, v = 1	125413.1±1.0	0.1	0.11	0.1±0.5	0.55	1.4±0.2	0.40	
11p3, v = 1	125563.07		1.50		0.35		0.10	
10p5, v = 1	125630.8±1.0	-0.3	0.37		0.39	0.5±0.1	0.55	

Table 5: Photoabsorption transitions of D₂ involving $N' = 4$ upper levels (cont'd)

state	$\frac{E}{hc}$ (cm ⁻¹)		$\frac{\Gamma}{hc}$ (cm ⁻¹)		$A(R3)$ (10 ⁶ s ⁻¹)		$A(P5)$ (10 ⁶ s ⁻¹)	
	obs ^{a,b}	o-c ^a	calc	obs	calc	obs	calc	obs
7pσ, v = 2	125691.47±0.20	-0.04	0.03	0.0±0.2	2.79	3.9±2.3 ^c	0.37	
4pπ, v = 5	125710.60±0.10	-1.08	0.00	0.0±0.2	8.00	6.2±2.5 ^c	10.72	13±2
12p3, v = 1	125725.8±1.0	-0.3	0.67	0.5±0.4	1.06	1.9±0.2	0.00	
11p5, v = 1	125810.37		1.23		0.29		0.39	
13p3, v = 1	125850.45		0.05		0.26		0.30	
14p3, v = 1	125923.2±1.0	0.1	0.64		0.48	0.3±0.5	0.09	
7p5, v = 2	125948.8±1.0	0.6	0.01		0.01		4.24	4.3±0.9
12p5, v = 1	125969.4±1.0	0.9	0.46		0.59	1.5±1.3	2.10	
5pσ, v = 4	125974.05±0.20	-0.47	0.13	0.0±0.2	2.58	5.6±2.1 ^c	0.14	
15p3, v = 1	126005.49		0.15		0.20		0.03	
16p3, v = 1	126056.81		0.57		0.16		0.07	
13p5, v = 1	126084.97		0.30		0.01		0.41	
17p3, v = 1	126112.92		0.11		0.14		0.03	
18p3, v = 1	126149.15		0.36		0.15		0.02	
14p5, v = 1	126172.69		0.37		0.00		0.30	
19p3, v = 1	126190.17		0.02		0.11		0.09	
20p3, v = 1	126216.1±1.0	0.3	0.16		0.11	0.22±0.11	0.00	
8pσ, v = 2	126230.7±1.0	-0.3	0.03		0.57	0.73±0.14	1.45	
21p3, v = 1	126238.6±1.0	-0.7	0.26		0.11	0.12±0.07	0.13	
15p5, v = 1	126251.00		0.13		0.39	bl	0.01	
22p3, v = 1	126265.65		0.04		0.10		0.02	
6pσ, v = 3	126281.22±0.12	-0.04	0.02	0.5±0.3	5.14	3.5±2.0	0.50	
23p3, v = 1	126284.37±0.03	0.06	0.09	0.0±0.2	4.04	1.6±0.7 ^c	0.21	
24p3, v = 1	126299.06		0.20		0.50	bl	0.05	
16p5, v = 1	126309.32		0.20		0.18		0.17	
25p3, v = 1	126317.56		0.01		0.02		0.06	
26p3, v = 1	126329.17		0.05		0.07		0.01	
27p3, v = 1	126340.31		0.09		0.01		0.02	
4pσ, v = 7	126340.74±0.16	-0.70	0.00	0.2±0.3	9.85	15.3±2.2	6.61	7.9±2.0
28p3, v = 1	126350.09		0.14		0.09		0.02	
17p5, v = 1	126357.43		0.16		0.04		0.09	
6p5, v = 3	126605.8±1.0	0.5	0.06	0.0±0.6	2.02	1.9±0.4	8.24	8.5±2.5
32p5, v = 1	126634.93		1.44		0.03		0.01	
33p5, v = 1	126640.79		1.47		0.30		0.00	
9pσ, v = 2	126643.5±1.0	0.1	0.01		0.72	0.9±0.9	0.11	
34p5, v = 1	126647.80		0.57		0.08		0.05	
5pπ, v = 4	126696.64±0.27	0.09	0.01	0.0±0.3	4.47	10.5±9.8 ^c	5.64	
9pπ, v = 2	126825.41		4.82		0.29		1.67	
10p3, v = 2	126916.6±1.0	0.4	0.30		0.95	1.1±0.8	0.55	
4pπ, v = 6	126970.74±0.13	1.83	0.00	0.1±0.3	8.23	8.9±1.6	6.84	
11p3, v = 2	127057.45		2.83		0.06		0.11	
7pσ, v = 3	127112.57±0.07	-0.21	0.12	0.3±0.2	3.40	3.3±0.9	0.00	
10p5, v = 2	127142.7±1.0	-0.8	0.95	0.6±1.4	0.67	0.7±0.5	1.62	
5pσ, v = 5	127227.54		0.12		0.40		1.35	
12p3, v = 2	127229.21		1.79		1.77	tb	0.09	
11p5, v = 2	127307.08		2.20		0.23		0.54	
4pσ, v = 8	127322.08±0.09	-0.89	0.00	0.0±0.2	4.75	8.3±2.1	8.45	13.0±2.0
13p3, v = 2	127353.4±1.0	-0.3	0.19		0.70	1.6±1.7	0.36	
7pπ, v = 3	127381.0±1.0	0.2	0.02		1.59	1.4±0.4	1.62	
14p3, v = 2	127428.36		1.71		0.22		0.25	
12p5, v = 2	127467.01		0.73		0.04		0.81	
15p3, v = 2	127509.77		0.45		0.33		0.03	
16p3, v = 2	127558.82		1.42		0.12		0.16	
13p5, v = 2	127584.17		0.36		0.08		0.52	
6pσ, v = 4	127608.28±0.07	-0.84	0.00	0.0±0.2	5.24	5.4±1.1	4.01	
17p3, v = 2	127617.42		0.35		0.30		0.01	
18p3, v = 2	127651.66		1.13		0.00		0.04	
14p5, v = 2	127671.10		0.29		0.54		0.18	
19p3, v = 2	127694.46		0.14		0.16		0.06	
8pσ, v = 3	127704.38±0.08	-0.22	0.02	0.0±0.2	6.04	6.2±1.1	0.29	
20p3, v = 2	127721.54		0.49		1.08	bl	0.02	
21p3, v = 2	127741.57		0.87		0.57	bl	0.25	
15p5, v = 2	127752.92		0.06		0.00		0.21	
22p3, v = 2	127770.54		0.19		0.19		0.01	
23p3, v = 2	127788.07		0.41		0.11		0.04	
24p3, v = 2	127801.42		0.62		0.12		0.09	
16p5, v = 2	127810.34		0.05		0.02		0.17	
17p5, v = 2	127859.54		0.03		0.03		0.11	
8p5, v = 3	127909.44		0.03		0.20		1.29	
6pπ, v = 4	127979.7±1.0	0.4	0.00		1.53	5.2±0.7	5.45	18±7

Table 5: Photoabsorption transitions of D₂ involving $N' = 4$ upper levels (cont'd)

state	$\frac{E}{hc}$ (cm ⁻¹)		$\frac{\Gamma}{hc}$ (cm ⁻¹)		$A(R3)$ (10 ⁶ s ⁻¹)		$A(P5)$ (10 ⁶ s ⁻¹)	
	obs ^{a,b}	o-c ^a	calc	obs	calc	obs	calc	obs
5p π , v = 5	128015.70±0.05	0.69	0.00	0.0±0.2	3.39	3.7±0.5	2.10	
9p σ , v = 3	128080.7±1.0	-0.7	0.22		1.27	0.9±0.4	0.00	
4p π , v = 7	128140.17±0.07	1.31	0.00	0.1±0.2	8.68	11.0±1.7	0.67	
4p σ , v = 9	128242.7±1.0	-0.3	0.00		0.02		7.23	9.0±2.0
9p π , v = 3	128254.48		7.37		0.14		1.51	
10p3, v = 3	128356.7±1.0	-0.2	0.62		1.13	1.1±0.4	0.56	
5p σ , v = 6	128439.70±0.07	-0.23	0.01	0.2±0.3	3.58	5.3±0.8	5.22	3.8±2.4
7p σ , v = 4	128462.83		0.88		0.32		0.11	
11p3, v = 3	128516.1±1.0	-0.4	4.53		2.89	2.2±1.2	0.46	
10p5, v = 3	128573.10		0.98		0.02		1.40	
12p3, v = 3	128668.50		2.83		0.31		0.44	
11p5, v = 3	128736.3±1.0	0.1	1.56	2.2±1.5	1.08	1.6±0.7	0.00	
7p π , v = 4	128750.37		1.61		0.99	tb	2.61	
13p3, v = 3	128795.08		0.53		0.44		0.13	
14p3, v = 3	128865.59		3.01		0.13		0.13	
12p5, v = 3	128903.00		0.60		0.41		0.32	
6p σ , v = 5	128914.4±1.0	-0.6	0.18	0.0±0.5	4.11	4.3±0.8	4.77	6.8±2.0
15p3, v = 3	128950.97		0.97		0.51		0.00	
16p3, v = 3	128995.35		2.03		0.01		0.33	
13p5, v = 3	129022.4±1.0	0.5	0.11		0.35	0.3±0.3	0.38	
4p σ , v = 10	129028.3±1.0	-0.3	0.00		4.12	7.1±0.9	1.70	3.1±0.9
17p3, v = 3	129057.84		0.65		0.00		0.03	
8p σ , v = 4	129072.80±0.08	0.71	0.01	0.0±0.2	4.28	2.0±1.4	0.01	
18p3, v = 3	129096.45		1.57		2.05	tb	0.17	
14p5, v = 3	129112.27		0.41		0.11		0.46	
19p3, v = 3	129136.13		0.44		0.35		0.03	
20p3, v = 3	129161.69		1.17		0.40		0.03	
15p5, v = 3	129178.17		0.80		0.04		0.26	
21p3, v = 3	129193.43		0.07		0.14		0.11	
22p3, v = 3	129212.27		0.41		0.23		0.01	
16p5, v = 3	129228.27		0.86		0.14		0.01	
23p3, v = 3	129239.33		0.28		0.02		0.08	
24p3, v = 3	129251.19		0.05		0.16		0.16	
5p π , v = 6	129258.91±0.10	0.11	0.00	0.7±0.3	6.07	8.1±1.5	8.08	
25p3, v = 3	129263.51		0.25		0.07		0.15	
8p π , v = 4	129271.51		0.07		0.00		0.77	
28p3, v = 3	129300.99		0.05		0.08		0.21	
6p π , v = 5	129304.1±1.0	-0.5	0.02		0.01		3.03	2.5±1.4
4p π , v = 8	129336.04±0.05	0.59	0.00	0.00±0.20	2.65	2.8±0.6	4.18	4.6±1.4
9p σ , v = 4	129457.4±1.0	0.30	2.24		1.24	0.9±0.3	0.05	
5p σ , v = 7	129571.8±1.0	0.2	0.02		1.38	2.4±1.1	3.08	
10p3, v = 4	129736.3±1.0	0.3	1.08		1.16	1.2±0.5	0.47	
7p σ , v = 5	129772.7±1.0	0.1	0.10		1.54	1.4±0.4	0.23	
4p σ , v = 11	129809.8±1.0	0.0	0.00		2.42	3.5±0.6	2.72	
11p3, v = 4	129881.78		8.39		1.47	tb	0.55	
10p5, v = 4	129948.15		0.54		0.24		1.03	
7p π , v = 5	130035.5±1.0	-0.3	1.60	1.6±0.6	4.23	3.1±0.8	0.27	
6p σ , v = 6	130166.6±1.0	-0.7	0.10	0.0±0.4	1.44	1.9±0.3	5.15	8.0±4.0
13p3, v = 4	130175.65		1.31		1.82	bl	0.38	
14p3, v = 4	130240.83		4.59		0.26		0.59	
12p5, v = 4	130279.28		0.40		0.28		0.61	
15p3, v = 4	130329.41		1.70		0.21		0.00	
16p3, v = 4	130362.4±1.0	-0.1	1.09	0.0±0.8	1.03	0.54±0.15	0.22	
8p σ , v = 5	130392.94		1.18		5.74	bl	0.05	
4p π , v = 9	130400.07±0.12	0.52	0.02	0.1±0.3	4.78	5.7±1.0	2.75	2.5±0.6
13p5, v = 4	130403.42		0.29		0.02		0.91	
17p3, v = 4	130439.11		1.61		0.83		0.00	
5p π , v = 7	130454.65±0.04	0.05	0.00	0.10±0.20	2.01	3.1±0.5	1.75	
14p5, v = 4	130469.54		2.25		0.26		0.33	
18p3, v = 4	130489.15		0.05		0.07		0.23	
19p3, v = 4	130515.82		1.01		0.32		0.01	
4p σ , v = 12	130536.9±1.0	0.2	0.00	0.0±0.5	0.71	1.0±0.2	1.14	2.1±0.7
20p3, v = 4	130538.45		1.56		0.11		0.03	
6p π , v = 6	130552.8±1.0	0.3	0.03		0.41	bl	1.73	2.9±1.5
15p5, v = 4	130555.15		0.20		0.02		0.05	
21p3, v = 4	130572.88		0.28		0.20		0.28	
8p π , v = 5	130584.31		0.11		0.06		1.47	
22p3, v = 4	130596.21		0.52		0.06		0.68	
23p3, v = 4	130609.37		1.66		0.03		0.98	
16p5, v = 4	130618.01		0.07		0.05		0.23	

Table 5: Photoabsorption transitions of D₂ involving $N' = 4$ upper levels (cont'd)

state	$\frac{E}{hc}$ (cm ⁻¹)		$\frac{\Gamma}{hc}$ (cm ⁻¹)		$A(R3)$ (10 ⁶ s ⁻¹)		$A(P5)$ (10 ⁶ s ⁻¹)	
	obs ^{a,b}	o-c ^a	calc	obs	calc	obs	calc	obs
24p3, v = 4	130631.76		0.30		0.10		0.00	
25p3, v = 4	130645.09		0.77		0.06		0.00	
26p3, v = 4	130654.4±1.0	-0.4	0.33		0.62		2.84	
5pσ, v = 8	130656.4±1.0	-0.1	0.85		0.81	1.1±0.3	4.36	
17p5, v = 4	130663.47		0.24		0.01		0.33	
9pσ, v = 5	130766.27		0.02		0.09		0.03	
46p3, v = 4	130768.53		0.01		0.09		0.01	
46p3, v = 4	130770.73		0.01		0.08		0.01	
47p3, v = 4	130772.82		0.02		0.07		0.00	
48p3, v = 4	130774.80		0.03		0.08		0.00	
7pσ, v = 6	131017.5±1.0	0.0	0.14		0.20	1.3±0.3	0.15	
63p5, v = 4	131018.16		0.02		0.12		0.12	
63p5, v = 4	131018.92		0.05		0.05		0.08	
10p3, v = 5	131054.97		2.50		1.24	bl	0.33	
4pσ, v = 13	131136.5±1.0	-0.2	0.00		1.15	1.5±0.2	0.59	
11p3, v = 5	131189.79		1.11		0.47		0.39	
6pσ, v = 7	131257.41±0.14	-0.32	0.18	0.4±0.4	4.85	4.7±0.7	0.09	
10p5, v = 5	131266.6±1.0	-0.3	0.60		0.32	0.3±0.2	0.64	
12p3, v = 5	131355.12		1.66		0.10		0.70	
7pπ, v = 6	131384.9±1.0	0.7	2.47		1.04	0.9±0.8	3.15	7.0±6.0
11p5, v = 5	131429.58		4.86		0.00		1.88	
4pπ, v = 10	131451.18±0.06	-0.12	0.49	0.3±0.2	3.55	4.3±0.6	2.87	3.9±2.7
13p3, v = 5	131493.20		2.00		0.56		0.03	
12p5, v = 5	131551.23		9.81		0.00		0.45	
5pπ, v = 8	131561.21±0.07	0.68	0.00	0.0±0.2	3.40	3.5±1.3	0.03	
14p3, v = 5	131595.4±1.0	-0.4	0.13		0.66	1.1±0.3	0.37	
8p3, v = 6	131629.58		0.09		1.50	bl	0.00	
15p3, v = 5	131653.07		2.53	2.1±2.0	1.75	tb	0.06	
13p5, v = 5	131689.32		1.92		0.12		0.95	
5pσ, v = 9	131697.0±1.0	-0.3	1.77		0.68	bl	3.62	3.4±3.4
16p3, v = 5	131719.76		0.15		0.18		0.23	
6p5, v = 7	131751.64		0.10		0.56	bl	1.96	
17p3, v = 5	131757.26		2.56		0.27		0.24	
14p5, v = 5	131783.45		1.89		0.06		0.16	
18p3, v = 5	131807.92		0.14		0.16		0.16	
19p3, v = 5	131827.57		0.69		0.04		1.38	
8pπ, v = 6	131841.96		0.53		0.11		0.94	
20p3, v = 5	131860.41		2.38		0.06		1.40	
15p5, v = 5	131873.37		0.06		0.08		0.20	
7pσ, v = 7	132213.22		2.05		0.10		0.38	
9pπ, v = 6	132219.18		2.14		0.05		0.25	
4pσ, v = 15	132377.0±1.0	-0.9	0.00		2.54	2.0±0.4	0.09	
6pσ, v = 8	132392.8±1.0	-0.6	0.17	0.0±0.5	1.75	2.1±0.5	0.16	
4pπ, v = 11	132422.28±0.06	-0.46	0.11	0.0±0.2	3.08	1.5±0.2	1.72	
11p3, v = 6	132441.79		16.20		1.27	tb	0.36	
5pσ, v = 10	132522.9±1.0	-1.1	0.19		1.50	1.5±0.5	0.14	
7pπ, v = 7	132574.7±1.0	-1.5	0.10		1.69	2.1±0.4	3.26	
10p5, v = 6	132621.48		10.00		0.92	tb	0.69	
11p5, v = 6	132682.39		2.60		0.07		0.96	
5pπ, v = 9	132736.5±1.0	-0.2	0.01		0.81	1.2±0.5	2.93	
8pσ, v = 7	132839.7±1.0	0.4	3.69	3.7±1.0	2.46	2.1±0.5	0.12	
7pσ, v = 8	133200.21		0.06		0.16		0.01	
4pπ, v = 12	133310.8±1.0	-30.3	0.02		1.40	2.2±0.5	0.70	
6pσ, v = 9	133531.9±1.0	-1.3	0.20		3.41	6.8±1.4	0.63	

E/hc , upper state level energy. Γ/hc , calculated ionization width and observed total width (FWHM). $A(R3)$, $A(P5)$, emission probability to the ground state for $R(3)$ and $P(5)$ transitions, respectively. The transition energies for the $R(3)$ and $P(5)$ transitions are obtained by subtracting the ground-state rotational energies 357.30 cm⁻¹ ($N'' = 3$) and 881.21 cm⁻¹ ($N'' = 5$), respectively, from the upper state energy.

^a When no observed-calculated value is given, the energy corresponds to the calculated value.

^b Transition energies with uncertainties = 1 cm⁻¹ are based on the NIM spectra.

^c Value based on the FT spectrum.

^d Complex resonance. The A value given corresponds to the sum over all components.

^e from Ref. [32].

tb, too broad to be detected. *bl*, blended line. *tl*, too low intensity to be measured.

Table 6: Photoabsorption transitions of D₂ involving $N' = 5$ upper levels

state	$\frac{E}{hc}$ (cm ⁻¹)		$\frac{\Gamma}{hc}$ (cm ⁻¹)		$A(R4)$ (10 ⁶ s ⁻¹)	
	obs ^{a,b}	o-c ^a	calc	obs	calc	obs
4pσ, v = 0	117599.6±0.2	-0.6		0.0±0.2	2.2	4.1±1.9 ^c
4pπ, v = 0	118611.2±0.3	0.4		0.0±0.2	2.9	2.0±1.7 ^c
4pσ, v = 1	119081.3±0.3	-1.0		1.0±0.6	8.2	17±17 ^c
4pπ, v = 1	120170.6±0.3	0.3		0.3±0.2	8.8	8±5 ^c
5pσ, v = 0	120416.3				0.8	
4pσ, v = 2	120499.7±0.3	-1.0		0.0±0.2	8.2	10±5 ^c
5pπ, v = 0	120966.4				0.6	
4pπ, v = 2	121655.4±0.3	0.1		0.4±0.2	16.5	21±12 ^c
4pσ, v = 3	121844.7				1.5	
6pσ, v = 0	121873.6				0.4	
5pσ, v = 1	121971.6±0.4	-1.0		0.5±0.4	9.0	12±9 ^c
6pπ, v = 0	122272.2				0.0	
5pπ, v = 1	122524.5				1.9	
7pσ, v = 0	122760.5				0.6	
4pσ, v = 4	123027.6±0.3	-0.4		0.3±0.2	20.1	24±11 ^c
7pπ, v = 0	123063.7				0.0	
4pπ, v = 3	123184.0				0.8	
8pσ, v = 0	123313.2				0.0	
5pσ, v = 2	123359.1				1.2	
6pσ, v = 1	123486.3±0.3	0.2		0.0±0.2	10.9	7±4 ^c
8pπ, v = 0	123584.7				0.8	
9pσ, v = 0	123696.5				0.4	
6pπ, v = 1	123826.8				0.1	
10p4, v = 0	123911.4				0.3	
9pπ, v = 0	123992.8				0.1	
5pπ, v = 2	124019.4±0.4	0.6		0.0±0.2	3.3	2.7±2.7 ^c
11p4, v = 0	124123.3±1.0	0.1		0.2±0.5	0.2	0.4±0.1
10p6, v = 0	124227.6				0.0	
4pσ, v = 5	124256.1±0.4	-0.3		0.2±0.2	14.4	19±2
7pσ, v = 1	124282.2±1.0	-0.3		0.1±0.3	2.6	2.8±0.4
12p4, v = 0	124318.0				0.0	
13p4, v = 0	124379.4±1.0	-0.5			0.4	0.2±0.1
11p6, v = 0	124434.3				0.0	
14p4, v = 0	124479.1				0.0	
4pπ, v = 4	124528.7±0.4	0.2		0.0±0.3	6.2	7.2±1.0
7pπ, v = 1	124613.4				0.0	
5pσ, v = 3	124759.8±1.0	-0.5		0.1±0.2	3.1	4.6±1.1
8pσ, v = 1	124874.9±1.0	-0.3			0.4	0.4±0.1
6pσ, v = 2	124959.8±1.0	-0.9		0.0±0.2	6.0	16.3±2.0
38p4, v = 0	124961.7±0.3	0.5		0.0±0.2	6.3	8.0±6.0 ^c
8pπ, v = 1	125135.2±1.0	-1.3	1.25	4.8±0.6	0.8	1.1±0.2
34p6, v = 0	125258.8		0.56		0.3	
9pσ, v = 1	125260.2±1.0	0.0	0.69	0.5±0.2	0.8	1.1±0.1 ^d
6pπ, v = 2	125318.5		0.00		0.3	bl
4pσ, v = 6	125386.1±0.3	-1.0	0.00	0.0±0.2	10.5	12.2±1.6
5pπ, v = 3	125450.5±1.0	-0.5	0.00	0.0±0.6	4.9	6.2±1.4
10p4, v = 1	125469.4±1.0	0.5	2.55	1.3±1.6	0.6	0.6±0.4
9pπ, v = 1	125551.1		0.22		0.1	
11p4, v = 1	125685.7±1.0	0.0	1.18	1.7±0.8	0.5	0.3±0.2
10p6, v = 1	125775.4		0.75		0.5	
7pσ, v = 2	125817.2±0.3	0.0	0.38	0.5±0.4	3.4	3.2±0.6
4pπ, v = 5	125834.7±0.3	-0.7	0.00	0.0±0.2	7.3	9.1±2.1
12p4, v = 1	125846.2±1.0	0.0	0.24		0.4	0.4±0.1
13p4, v = 1	125942.0		1.10		0.6	bl
11p6, v = 1	125990.8		0.86		0.0	
14p4, v = 1	126043.2		0.27		0.4	
5pσ, v = 4	126080.8		0.00		0.8	
15p4, v = 1	126099.5		0.20		2.4	
7pπ, v = 2	126111.7±1.0	0.4	0.55	0.2±1.0	0.1	0.2±0.2
12p6, v = 1	126139.2		0.30		0.1	
16p4, v = 1	126175.2±1.0	-0.3	0.17		0.2	0.2±0.1
17p4, v = 1	126219.2		0.47		0.1	
13p6, v = 1	126247.4		0.47		0.0	
18p4, v = 1	126268.1		0.56		0.1	
19p4, v = 1	126298.2		0.20		0.1	
20p4, v = 1	126324.6		0.39		0.0	
14p6, v = 1	126340.4		0.17		0.0	
21p4, v = 1	126355.4		0.04		0.3	
8pσ, v = 2	126356.0±1.0	-1.3	0.01		0.8	0.9±0.4
22p4, v = 1	126376.2		0.11		0.0	

Table 6: Photoabsorption transitions of D₂ involving $N' = 5$ upper levels (cont'd)

state	$\frac{E}{hc}$ (cm ⁻¹)		$\frac{\Gamma}{hc}$ (cm ⁻¹)		$A(R4)$ (10 ⁶ s ⁻¹)	
	obs ^{a,b}	o-c ^a	calc	obs	calc	obs
6pσ, v = 3	126390.7±1.0	-0.3	0.04	0.0±0.3	5.8	8.3±1.2
23p4, v = 1	126395.4±1.0	-0.3	0.13	0.9±1.1	3.1	4.0±1.4
24p4, v = 1	126410.0±1.0	0.3	0.28	0.0±0.6	0.6	0.6±0.1
15p6, v = 1	126418.4		0.11		0.1	
25p4, v = 1	126428.9		0.02		0.0	
4pσ, v = 7	126438.5±1.0	0.1	0.00	0.2±0.4	10.8	16.3±2.5
8pπ, v = 2	126621.8		3.90		0.8	
20p6, v = 1	126633.5		2.15		0.1	
6pπ, v = 3	126743.4±1.0	-0.1	0.01	0.3±0.6	1.5	1.6±0.3
9pσ, v = 2	126763.0		0.12		0.7	bl
5pπ, v = 4	126821.1±1.0	0.0	0.00	0.0±1.1	4.3	5.0±2.6
10p4, v = 2	126959.5		5.10		0.7	
9pπ, v = 2	127045.8		0.24		0.6	
4pπ, v = 6	127082.9±0.4	-0.4	0.00	0.0±0.2	8.1	9.5±1.7
11p4, v = 2	127180.3		2.40		0.3	
7pσ, v = 3	127228.6±0.4	-0.3	0.04	0.0±0.2	3.6	3.8±2.1
10p6, v = 2	127283.3±1.0	-1.0	2.29		0.8	0.5±0.3
5pσ, v = 5	127341.7		0.01		0.7	bl
12p4, v = 2	127345.6		0.66		1.0	bl
4pσ, v = 8	127418.6±0.4	-1.2	0.00	0.1±0.2	5.0	7.7±0.9
13p4, v = 2	127437.8		2.53		1.0	
11p6, v = 2	127483.8		0.48		0.0	
7pπ, v = 3	127515.8±1.0	-0.1	0.06		1.5	1.2±0.5
14p4, v = 2	127544.3		0.80		0.2	
15p4, v = 2	127603.6		1.75		0.1	
12p6, v = 2	127633.2		0.25		0.2	
16p4, v = 2	127675.4		0.56		0.3	
17p4, v = 2	127717.1		1.30		0.0	
6pσ, v = 4	127727.9±1.0	-1.0	0.04	0.0±0.8	6.4	5.8±1.7
13p6, v = 2	127741.0		0.51		0.2	
18p4, v = 2	127767.7		0.18		0.3	
19p4, v = 2	127797.3		0.51		0.1	
8pσ, v = 3	127810.6±1.0	0.1	0.02		4.6	3.2±3.0
20p4, v = 2	127826.5±1.0	-0.2	0.76	0.1±0.6	2.3	1.7±0.7
14p6, v = 2	127838.6		0.06		0.2	
21p4, v = 2	127856.8		0.16		0.2	
22p4, v = 2	127877.0		0.40		0.3	
18p6, v = 2	128041.5		0.01		0.2	
8pπ, v = 3	128043.8		0.01		0.2	
6pπ, v = 4	128110.2		0.64		2.7	bl
5pπ, v = 5	128131.6±1.0	0.4	0.01	0.0±0.5	3.1	4.6±1.0
9pσ, v = 3	128196.7		0.06		1.3	bl
4pπ, v = 7	128226.7±1.0	-0.7	0.00	0.3±0.3	8.7	10.9±1.2
4pσ, v = 9	128350.1±1.0	-1.0	0.00		0.1	0.1±0.1
9pπ, v = 3	128478.7±1.0	-0.3	0.20	0.0±0.5	0.8	0.9±0.2
5pσ, v = 6	128552.9±0.4	-0.6	0.00	0.0±0.2	3.4	4.9±1.1
7pσ, v = 4	128583.8		0.44		0.7	bl
11p4, v = 3	128628.0±1.0	1.0	4.21	4.4±0.7	3.0	3.9±0.7
10p6, v = 3	128709.0		3.17		0.2	
12p4, v = 3	128781.6		1.53		1.1	
7pπ, v = 4	128858.9±1.0	-0.1	1.47	1.2±0.5	2.1	2.4±0.6
13p4, v = 3	128879.5		4.07		0.2	
11p6, v = 3	128917.0		0.42		0.3	
14p4, v = 3	128980.0		1.59		0.3	
6pσ, v = 5	129028.3±1.0	-1.0	0.76	0.6±0.2	2.3	2.7±1.0
15p4, v = 3	129037.4±1.0	-1.6	2.24	1.6±0.7	2.6	3.3±0.8
12p6, v = 3	129066.9		0.09		0.3	
4pσ, v = 10	129106.4±1.0	-0.4	0.00	0.1±0.2	5.2	7.0±0.8
16p4, v = 3	129112.1		1.18		0.3	
17p4, v = 3	129171.9±1.0	0.2	0.04	0.0±0.6	1.6	2.2±0.7
8pσ, v = 4	129188.5±1.0	-0.4	0.32	0.4±0.4	3.6	4.9±0.9
18p4, v = 3	129205.1		0.58		0.6	
5pπ, v = 6	129369.8±0.4	0.2	0.01	0.0±0.2	6.6	7.1±1.3
8pπ, v = 4	129402.5		0.19		0.2	
6pπ, v = 4	129427.7		0.15		0.1	
4pπ, v = 5	129444.6±1.0	1.9	0.02	0.0±0.3	1.5	1.7±0.4
9pσ, v = 4	129569.0		2.47		1.2	bl
5pσ, v = 7	129681.9±1.0	-0.6	0.00	0.0±0.4	1.4	1.9±0.4
9pπ, v = 4	129743.5		0.03		0.1	
10p4, v = 4	129850.9±1.0	0.6	0.35	0.6±0.6	1.5	1.8±0.4

Table 6: Photoabsorption transitions of D₂ involving $N' = 5$ upper levels (cont'd)

state	$\frac{E}{hc}$ (cm ⁻¹)		$\frac{\Gamma}{hc}$ (cm ⁻¹)		$A(R4)$ (10 ⁶ s ⁻¹)	
	obs ^{a,b}	o-c ^a	calc	obs	calc	obs
4pσ, v = 11	129886.1±1.0	-0.9	0.01	0.1±0.4	3.4	4.4±0.9
7pσ, v = 5	129891.9±1.0	0.4	0.20	0.0±0.7	0.4	0.4±0.1
11p4, v = 4	129994.0		7.24		1.8	tb
10p6, v = 4	130075.5		3.16		0.0	
7pπ, v = 5	130146.1±1.0	-0.5	0.66	0.7±0.4	4.5	4.0±1.0
12p4, v = 4	130159.3		1.75		0.0	
11p6, v = 4	130238.1		4.50		0.0	
6pσ, v = 6	130286.3±1.0	-0.8	0.15	0.0±0.3	2.3	2.3±0.5
13p4, v = 4	130291.7±1.0	-0.8	0.77	0.0±0.8	1.0	0.7±0.4
14p4, v = 4	130354.6		3.02		0.6	
12p6, v = 4	130402.7		3.83		0.0	
15p4, v = 4	130440.6		0.16		0.5	
8pσ, v = 5	130480.5		0.93		1.1	bl
4pπ, v = 9	130490.1±0.4	1.3	0.09	0.0±0.2	6.5	9.9±1.7
16p4, v = 4	130495.3±1.0	0.2	0.74	0.7±1.0	1.2	1.1±0.4
13p6, v = 4	130528.0		2.81		1.2	bl
5pπ, v = 7	130549.1±1.0	-0.6	0.00	0.1±0.2	2.3	1.7±0.2
17p4, v = 4	130580.7±1.0	0.2	1.26		0.4	0.4±0.1
4pσ, v = 12	130622.9±1.0	0.2	0.00	0.0±0.3	0.6	0.9±0.1
6pπ, v = 6	130664.1±1.0	-0.1	0.11	0.2±0.7	0.3	0.3±0.2
8pπ, v = 5	130714.7		0.05		0.1	
5pσ, v = 8	130767.2±1.0	0.9	0.10	0.0±0.6	1.0	0.6±0.5
9pσ, v = 5	130883.8		0.03		1.6	bl
9pπ, v = 5	131033.6		0.14		0.0	
7pσ, v = 6	131130.0±1.0	0.8	0.40	0.9±0.6	0.6	1.2±0.3
10p4, v = 5	131131.3		0.04		0.4	
4pσ, v = 13	131244.6±1.0	7.8	0.00	0.1±1.5	1.8	2.4±0.4
11p4, v = 5	131301.7		11.14		1.0	
6pσ, v = 7	131355.7±1.0	-1.3	0.09	0.0±0.2	4.6	5.3±0.7
10p6, v = 5	131383.2		5.60		0.0	
12p4, v = 5	131467.6		3.11		0.3	
7pπ, v = 6	131497.1±1.0	-1.6	0.37		0.8	0.8±0.3
4pπ, v = 10	131543.8±0.6	-0.5	0.04	0.3±0.3	3.6	3.5±0.5
13p4, v = 5	131551.8		11.78		0.5	
11p6, v = 5	131602.5		0.16		0.4	
5pπ, v = 8	131643.8±1.0	-3.0	0.00	0.0±0.2	3.4	1.4±0.2
14p4, v = 5	131665.5		4.58		0.2	
12p6, v = 5	131705.2		1.14		0.7	
8pσ, v = 6	131746.6±1.0	0.6	1.47	1.0±1.3	2.8	3.3±2.3
15p4, v = 5	131755.7		0.31		0.1	
16p4, v = 5	131801.5		2.84		0.5	
5pσ, v = 9	131808.0		0.92		0.5	bl
13p6, v = 5	131835.2		3.22		0.2	
6pπ, v = 7	131856.9±1.0	-1.6	0.05	0.0±1.4	0.3	0.5±0.4
17p4, v = 5	131863.0		0.19		0.1	
18p4, v = 5	131894.1		2.49		0.3	
96p6, v = 5	132487.7		0.10		0.3	
6pσ, v = 8	132487.0±1.0	-0.8	0.02	0.1±0.7	1.1	2.2±1.0 ^d
97p6, v = 5	132488.0		0.11		0.2	
4pπ, v = 11	132526.8±1.0	11.9	0.00	0.0±0.3	3.2	2.3±0.4
11p4, v = 6	132548.5		13.60		1.2	tb
5pσ, v = 10	132613.4±1.0	-1.8	0.01	0.0±0.2	1.9	2.4±0.4
10p6, v = 6	132633.4		2.08		0.6	
7pπ, v = 7	132685.3		0.29		1.2	bl
12p4, v = 6	132727.3		9.00		0.9	
11p6, v = 6	132795.4		9.00		0.0	
5pπ, v = 9	132847.5±1.0	4.0	0.02		0.5	0.7±0.2
13p4, v = 6	132857.5		0.41		0.4	
8pσ, v = 7	132902.7		2.79		0.4	
14p4, v = 6	132935.4		3.05		2.2	bl
12p6, v = 6	132972.9		4.37		0.5	
6pπ, v = 8	132996.0		0.41		0.0	
15p4, v = 6	133011.1		1.44		0.3	
16p4, v = 6	133053.9		5.80		0.4	
4pπ, v = 12	133423.8±1.0	-2.0	0.05	0.1±0.9	1.0	1.0±0.4
10p4, v = 7	133612.9±1.0	0.7	1.31	0.7±0.2	2.7	3.7±0.9
9pπ, v = 7	133616.3±1.0	-0.6	1.56	1.0±0.2	0.9	1.3±0.9
6pσ, v = 9	133622.7±1.0	-1.3	0.17	0.3±0.5	1.0	2.1±0.5
30p4, v = 6	133625.0		1.96		0.6	
5pπ, v = 10	133850.3		0.09		0.6	

Table 6: Photoabsorption transitions of D₂ involving $N' = 5$ upper levels (cont'd)

state	$\frac{E}{hc}$ (cm ⁻¹)		$\frac{\Gamma}{hc}$ (cm ⁻¹)		$A(R4)$ (10 ⁶ s ⁻¹)	
	obs ^{a,b}	o-c ^a	calc	obs	calc	obs
12p4, v = 7	133918.1		11.63		0.4	
11p6, v = 7	133977.7		5.84		0.2	
6pπ, v = 9	134036.7±1.0	-1.4	1.40	1.1±0.3	1.8	1.9±0.3
4pπ, v = 13	134272.2±1.0	-24.0	0.06		0.4	0.4±0.1
5pπ, v = 11	134798.9		0.02		0.7	
6pπ, v = 10	135063.2±1.0	-2.5	3.23	3.5±1.2	2.2	2.3±0.4
4pπ, v = 14	135093.1				0.0	

E/hc , upper state level energy. Γ/hc , calculated ionization width and observed total width (FWHM). $A(R4)$, emission probability to the ground state for $R(4)$ transitions. The $R(4)$ transition energies are obtained by subtracting the ground-state rotational energy 593.72 cm⁻¹ ($N'' = 4$) from the upper state energy.

^a When no observed-calculated value is given, the energy corresponds to the calculated value.

^b Transition energies with uncertainties = 1 cm⁻¹ are based on the NIM spectra.

^c Value based on the FT spectrum.

^d Complex resonance. The A value given corresponds to the sum over all components.

tb, too broad to be detected. *bl*, blended line. *tl*, too low intensity to be measured.

Table 7: Photoabsorption transitions of D₂ involving $N' = 6$ upper levels

state	$\frac{E}{hc}$ (cm ⁻¹)		$A(R5)$ (10 ⁶ s ⁻¹)	
	obs ^{a,b}	o-c ^a	calc	obs
4pσ, v = 5	124380.3±1.0	-2.3	18.3	23±4
4pπ, v = 4	124679.8±1.0	-2.0	5.5	bl
6pσ, v = 2	125101.4±1.0	-2.7	12.1	20±3
4pσ, v = 6	125510.6±1.0	1.9	11.2	10.6±2.1
5pπ, v = 3	125605.3±1.0	0.6	4.0	9±5
12p5, v = 1	125967.0		3.5	bl
4pπ, v = 5	125979.4±1.0	1.3	6.8	bl
8pσ, v = 2	126524.6±1.0	0.3	4.2	6.2±4.3
23p5, v = 1	126532.7±1.0	0.2	2.9	1.7±1.1
4pσ, v = 7	126556.9±1.0	0.4	13.8	bl
4pπ, v = 6	127213.8±1.0	-0.3	6.6	bl
7pσ, v = 3	127369.7±1.0	-1.4	3.4	2.8±1.1
4pσ, v = 8	127538.6±1.0	-0.7	5.7	bl
6pσ, v = 4	127870.2±1.0	-1.9	7.6	17±3
8pσ, v = 3	127952.5		4.5	bl
5pπ, v = 5	128262.6		4.8	bl
4pσ, v = 9	128331.5±1.0	-0.1	8.2	8.4±1.3
5pσ, v = 6	128686.4±1.0	-2.6	2.2	43±29
4pσ, v = 10	129199.7±1.0	-2.4	6.8	9.0±3.6
8pσ, v = 4	129309.2±1.0	-1.4	2.8	5.0±1.7
4pσ, v = 11	129978.5±1.0	-0.5	2.9	3.5±4.6
5pπ, v = 6	129499.4±1.0	2.4	6.5	bl
4pσ, v = 12	130740.9		0.3	
7pσ, v = 5	130279.8±1.0	0.5	4.2	3.1±0.7
4pπ, v = 9	130588.4±1.0	-2.5	6.5	6.1±1.5
17p5, v = 4	130660.9±1.0	0.6	3.5	bl
6pσ, v = 8	131475.8		4.3	bl
4pσ, v = 10	131656.8		2.8	
4pσ, v = 13	131318.9±1.0	1.7	2.3	1.7±0.6
5pσ, v = 9	131749.6		3.2	bl
6pσ, v = 9	133721.0		4.3	bl
4pσ, v = 14	131924.3±1.0	2.1	0.3	6.9±1.1

E/hc , upper state level energy. $A(R5)$, emission probability to the ground state for $R(5)$ transitions. The $R(5)$ transition energies are obtained from the upper state energy by subtracting the ground-state rotational energy 887.21 cm⁻¹ ($N'' = 5$).

^a When no observed-calculated value is given, the energy corresponds to the calculated value.

^b Transition energies with uncertainties = 1 cm⁻¹ are based on the NIM spectra.

bl, blended line.

Table 8: List of unassigned lines observed in the vacuum ultraviolet excitation spectra of D₂, most likely pertaining to *f*-Rydberg states. It is indicated what lines were observed in dissociation (Lyman- α , the optical probe for the dissociation channel) or in fluorescence.

Frequency (cm ⁻¹)	Lyman- α	Fluorescence
123516.0	x	x
123582.0	x	x
124031.4	x	x
124085.4	x	x
124534.7	x	x
124728.7	x	x
125120.1	x	x
125368.8		x
125383.0		x
125562.8		x
125732.2		x
126496.6		x
126530.5		x
126995.9		x
127046.8		x
127180.7		x
127404.4		x
127637.0		x
128329.1		x
129396.5		x
130084.8		x
130419.9		x
133189.0		x
133671.4		x
133819.0		x
133852.0		x
133999.1		x

Table 9: Cases of different line identifications in the VUV absorption spectrum of D_2 between the present study and that of Ref. [35]. In the first four columns the presently observed line is given with its transition frequency; in the next column the transition frequency of this first line is given as observed in [35]; in the final three columns the new assignment of that previously observed line is provided. Numbers in italic refer to calculated values.

Present line				Previous	New assignment		
State	Line	ν	Transition Freq.	Transition Freq. [35]	State	Line	ν
$7p\pi$	R(0)	0	122594.13	122601.2	$4p\sigma$	P(2)	4
$4p\sigma$	R(0)	4	122779.92	122799.7	$8p\sigma$	P(2)	0
$5p\sigma$	R(0)	2	123008.33	123162.2	$6p\sigma$	R(0)	1
$8p\pi$	R(0)	0	123104.94	123117.6	$8p\pi$	R(1)	0
$6p\sigma$	R(0)	1	123161.71	123009.2	$5p\sigma$	R(0)	2
$9p\sigma$	R(0)	0	123370.20	123392.6	$6p\pi$	R(0)	1
$14p0$	R(0)	0	<i>124192.17</i>	124178.3	$7p\pi$	R(1)	1
$5p\sigma$	R(0)	3	124410.89	124644.5	$6p\sigma$	R(0)	2
$8p\sigma$	R(0)	1	124545.2	124573.8	$6p\sigma$	R(2)	2
$6p\sigma$	R(0)	2	124643.89	124411.3	$5p\sigma$	R(0)	3
$9p\sigma$	R(0)	1	124944.01	124963.3	$9p\pi$	Q(1)	1
$11p0$	R(0)	1	125409.34	125405.8	$7p\sigma$	F(1)	2
$7p\sigma$	R(0)	2	125496.79	125540.9	$12p\pi$	Q(1)	1
$12p0$	R(0)	1	125560.79	<i>125554.4</i>	$7p\pi$	Q(2)	2
$13p0$	R(0)	1	125674.65	125608.7	$5p\sigma$	F(1)	4
$5p\sigma$	R(0)	4	125752.07	126099.4	$6p\sigma$	R(0)	3
$8p\sigma$	R(0)	2	126010.92	126092.9	$22p0$	R(0)	1
$6p\sigma$	R(0)	3	126104.31	125752.4	$5p\sigma$	R(0)	4
$25p0$	R(0)	1	126146.54	126142.3	$28p1$	R(1)	1
$15p0$	R(0)	2	127356.48	127343.0	$3p\pi$	Q(1)	11
$23p0$	R(0)	2	127636.87	127627.8	$5p\pi$	F(2)	5
$6p\pi$	R(1)	0	<i>121821.41</i>	121812.7	$3p\pi$	Q(1)	6
$7p\pi$	R(1)	0	<i>122606.11</i>	122594.9	$7p\pi$	R(0)	0
$8p\sigma$	R(1)	0	<i>122963.58</i>	122954.5			
$8p\pi$	R(1)	0	123116.52	123123.1	$8p\pi$	R(2)	0
$9p\sigma$	R(1)	0	123346.72	123371.3	$6p\pi$	R(2)	1
$9p\pi$	R(1)	0	<i>123481.04</i>	123505.9	$7p\sigma$	F(4)	1
$11p1$	R(1)	0	123831.41	123812.7			
$7p\sigma$	R(1)	1	123974.71	123971.0	$4p\sigma$	R(0)	5
$9p\sigma$	R(1)	1	124924.3	124954.8	$5p\pi$	Q(2)	3
$10p1$	R(1)	1	125188.48	125189.7	$3p\pi$	F(2)	9
$10p1$	R(1)	2	126696.98	126698.6	$4p\pi$	R(2)	6
$5p\sigma$	R(1)	2	122995.95	123153.1	$6p\sigma$	R(1)	1
$6p\sigma$	R(1)	1	123152.68	122996.7	$5p\sigma$	R(1)	2
$5p\sigma$	R(1)	3	124401.31	124625.6	$6p\sigma$	R(1)	2
$6p\sigma$	R(1)	2	124625.12	124401.7	$5p\sigma$	R(1)	3
$5p\sigma$	R(1)	4	125741.17	126075.7	$6p\sigma$	R(1)	3
$6p\sigma$	R(1)	3	126075.15	125741.6	$5p\sigma$	R(1)	4
$6p\pi$	R(2)	0	121802.51	121789.0			
$5p\sigma$	R(2)	2	122951.36	123122.6	$8p\pi$	R(2)	0
$6p\sigma$	R(2)	1	123084.90	122951.9	$5p\sigma$	R(2)	2
$9p\sigma$	R(2)	0	123292.6	123295.6			
$10p2$	R(2)	0	123562.06	123524.8	$5p\pi$	R(3)	2
$5p\sigma$	R(2)	3	124357.0	124573.1	$6p\sigma$	R(2)	2
$6p\sigma$	R(2)	2	124572.57	124357.5	$5p\sigma$	R(2)	3
$5p\sigma$	R(2)	4	125695.26	126017.3	$6p\sigma$	R(2)	3
$6p\sigma$	R(2)	3	126016.87	125695.6	$5p\sigma$	R(2)	4
$6p\sigma$	R(3)	0	<i>121387.07</i>	121378.4			
$5p\sigma$	R(3)	2	122874.62	123046.2	$6p\pi$	Q(4)	1
$5p\sigma$	R(3)	3	124279.40	124486.6	$6p\sigma$	R(3)	2
$6p\sigma$	R(3)	2	124486.38	124278.9	$5p\sigma$	R(3)	3
$4p\pi$	R(3)	8	128978.79	128989.8	$5p\pi$	R(2)	6
$4p\pi$	R(4)	8	128851	128860.7	$4p\sigma$	R(1)	10